論文 / 著書情報
Article / Book Information

題目(和文)	
Title(English)	Design and control of the metal-molecule interface for highly conductive single molecular junctions
著者(和文)	金子哲
Author(English)	Satoshi Kaneko
出典(和文)	学位:博士（理学）, 学位授与機関:東京工業大学, 報告番号:乙第4127号, 授与年月日:2016年4月30日, 学位の種別:論文博士, 審査員:木口　学,河内　宣之,腰原　伸也,大島　康裕,河合　明雄,西野　智昭
Citation(English)	Degree:, Conferring organization: Tokyo Institute of Technology, Report number:乙第4127号, Conferred date:2016/4/30, Degree Type:Thesis doctor, Examiner:,,,,,
学位種別(和文)	博士論文
Type(English)	Doctoral Thesis

Thesis

Design and control of the metal-molecule interface for highly conductive single molecular junctions

Submitted to the Tokyo Institute of Technology
for the degree of Doctor of Science

Satoshi Kaneko

Department of Chemistry
Graduate School of Science and Engineering
Tokyo Institute of Technology

January 2016

Contents

1 Introduction

1.1 Single molecular junctions

With the increasing concern regarding the limited amount of fossil fuel, there have been many attempts to realize a more effective utilization of existing supplies. Dennard proposed that the scaling down of semiconductors would lead to energy savings and improved performance of the electronic devices (*1*). Dennard's scale theory has had a significant impact on the electric industry, and has contributed towards the miniaturization of electronic devices. Recently developed micro-fabrication techniques have accelerated the miniaturization of electronic devices. Up to now, the integration ratio has been increasing, as predicted by Moore (*2*). According to Moore's law, the size of electronic components has decreased to the order of a few nanometers. In the near future, it is expected that the size of devices will further decrease to the atomic scale; however, it is impossible to fabricate sufficient insulator layers on the atomic scale. It is believed that we have approached practical limits with respect to the top-down method for fabricating electronic devices. Therefore, the use of single atoms and molecules has attracted much attention as a bottom-up method for the fabrication of minimum size electronic devices. Aviram and Ratner predicted a single-molecule rectifier in 1974 (*3*), which triggered a variety of studies to fabricate a "metal/single molecule/metal structure" called a single molecular junction, and to investigate electron transport on the single molecular junction.

In the 1990s, van Ruitenbeek successfully measured the electric conductance of a single gold atomic junction utilizing the break-junction method with an elastic metal substrate (*4*). This research accomplished the measurement of the quantum conductance of 1 G_0 ($2e^2/h$ = 13 kΩ). This is very different from the figure of the bulk metal that obeys Ohm's law. Further investigation has been done with respect to a single hydrogen molecule that is placed between platinum electrodes. Reed also measured the conductance of a single 1,4-benzenedithiol via gold-sulfur connection by using scanning tunneling micro spectroscopy (STM) (*5*). Their method, which uses sulfur atoms, enables us to fabricate the metal-molecular junction: The sulfur atom works as an anchoring group and enables us to form a rigid bond between the molecular backbone and metal electrodes. The concept of the anchoring group and synthesis technique led to the development of a variety of single molecular junctions that have properties such as negative differential conductance (*6, 7*), rectification (*8, 9*), and switching (*10, 11*). Recently, not only the conductance value, but also a variety of physical quantities has been investigated for many single molecular junctions. Current-voltage (*I*-*V*) characteristics have

revealed molecular level position (*12, 13*). Thermopower measurements (*14-16*) were performed considering the concept that a single molecular junction has potential for application in thermoelectric materials. Thermopower in a single molecular junction revealed the carriers and the energy difference between the molecular orbital and the fermi level of 1,4-benzene dithiol and 4-4' bipyridine, and fullerene (*15-17*). The differential conductance measurement addressed the effect of the electron-vibration coupling on the current in a single molecular junction (*18-20*). Shot-noise measurements revealed the transmission probability of the hydrogen single molecular junction (*21*) and the magnetic state in the Pt atomic chain (*22*). These efforts made single molecular junctions more attractive from a scientific perspective as a system that provides fundamental physical phenomena in nanoscale systems in addition to the potential that is realized.

This research flow indicates that the high conductive single molecular junction is an attractive system in the science and engineering fields. It is clear that high conductivity is a practical benefit for electric compounds. Highly conductive single molecular junctions reduce energy consumption in the on-states, and they produce strong signals to be extracted. In addition to its engineering benefit, a highly conductive single molecular junction is attractive because of the manifestation of its novel property as a meta-molecule system because molecular orbital and metal atomic states are effectively hybridized in highly conductive molecular junctions.

1.2 Electron transport depending on metal species and molecule species

In order to discuss the electron transport of the single molecular junction, the contribution from each part of the single molecular junctions is separated into several parts, namely, the molecular backbone, interfaces, and metal electrodes. The molecular backbone determines the size of the energy gap between the highest occupied molecular orbital (HOMO) and lowest unoccupied molecular orbital (LUMO). Because the Fermi energy gap is located between the HOMO and LUMO in a usual single molecular junction, a smaller energy gap between the HOMO and LUMO results in a smaller energy difference between the molecule's orbital energy and E_F, leading to higher conductivity. A simple way of reducing the HOMO-LUMO energy gap is to use π-conjugated molecules for the molecular backbone. The π-conjugated molecule has a smaller HOMO-LUMO gap compared with a single molecular junction with a saturated hydrocarbon system. However, recent studies have revealed that increasing aromatic property does not always result in an increased conductivity of the single molecular junction (*23, 24*).

The effective energy difference between the molecular orbital and E_F is important for high conductivity. The type of metal used for electrodes also affects the conductivity. The Fermi energy positions, the density of states at the Fermi energy, and the number of channels involved in the transport are different from the metal types. For example, transition metals such as Pt have large density of states at the Fermi energy, and these metals tend to have multiple channels, which lead to high conductivity compared with gold, silver, and copper.

1.3 Role of interface in electron transport of single molecular junctions

Another area that contributes to electron transport is the interface between molecules and metals. The effect of the metal-molecule interface is also discussed in bulk-sized organic conductors such as light emitting diodes, because the interface structure determines the charge injection of the organic conductor. Briefly, the charge injection depends on the dipole on the metal surface, electric affinity, and ionic potential of the adsorbed molecule (*25-27*). In a single molecular junction, configuration of a molecule between electrodes, as well as the adsorption site, plays a decisive role in the electron conductance. Even when we keep the same molecules between metal electrodes, the conductance value drastically changes depending on the molecular configuration. For example, it is reported that 1,4'-benzenedithiol molecular junction, which is one of the most widely investigated molecular junctions, showed a conductance value in the range of 0.0001-0.1 G_0 (*5, 28-32*). It was reported that the variability of the conductance values originate from the variable configuration that molecules have in the single molecular junction.

Previous studies have revealed that changes in the molecular configuration change reduce the energy level of the molecules that are bridged between electrodes (*7, 33*). The energy shift of the molecule induced the conductance change of the molecular junction. The molecular configuration changes the orbital coefficients at the connecting point. The large orbital confidents induce the effective hybridization between the metal and molecule, leading to a large electric coupling. The effect of configurational change on the anisotropic orbital distribution was investigated utilizing an H_2TPP molecule (*7*). The H_2TPP molecule had two conductance states depending on the orbital configuration of the HOMO-2 orbital (*7*). Heiss *et al.* precisely investigated the electron-coupling effect on the conductance using STM. The tilt angle of the molecule affects the coupling between the phenyl ring and metal electrodes (*34*). Kitaguchi similarly investigated the metal-molecule interaction between the phenoxy molecule and Cu substrate (*35*). A strong interaction via oxygen atom forms a strong bond between phenoxy and

Cu. On the other hand, there is a somewhat weak interaction between the phenyl ring and the tip compared to that of the substrates. The interaction between the phenyl ring and tip is precisely controlled by the tilt angle of the phenyl ring. The conductance value is also affected by the electric states of the metal atom near the oxygen atom. Queck *et al.* observed a mechanical switch using bipyrizine molecule (*11*).

The single molecular junction shows a variety of conductance values depending on the connecting points. A theoretical study showed that the benzene molecule connected with the para position has a different conductance value from benzene with a meta position because of the quantum-interface effects (*36*), which are based on the property of the electron as waves. When electron waves propagate through the two terminal ring-shaped mesoscopic structures, the partial electron wave at each branch interferes with each other destructively or constructively depending on the phase of the electron waves. A theoretical study gives a simple example for the benzene molecule. The wave functions constructively interfere in the para position; however, they interfere destructively in the meta position. In order to realize constructive interference, it is important to have the same sign for C and C* in Eq. (2.42) (*37*). The molecules that have a cross-conjugated system are expected to exhibit the destructive effect by their conductance values. Compounds that have cross-conjugated systems showed distractive quantum-interference effects (*38*).

As mentioned above, single molecular junctions tend to have a variety of conductance values for specific single molecular junction, and most studies have not determined the molecular configuration in the single molecular junction. Uncertainty about the molecular configuration, and not the fixed conductance value, is an obstacle to discussing the electron transport of the single molecular junction and fabrication of electronic components.

1.4 Anchoring groups and direct-binding technique

In order to fabricate single molecular junctions with fixed conductance values, many attempts have been made to determine how to connect the molecular backbone to metal electrodes. In a single molecular junction, the molecular backbone is connected to metal electrodes using a part called an anchoring group. The main role of anchoring groups is to connect the molecular backbone to metal electrodes. The other roles of anchoring groups are to separate the molecular backbone from metal electrodes, and to protect the property of an isolated molecule in a single molecular junction. One of the most famous anchoring groups is thiol. The strength of the gold-thiol bond is about 1 eV, which enables it to form stable bonds, and we can fabricate photo

switches, rectifiers and other electronic components by protecting the original molecule's property.

With respect to anchoring groups, systematic studies about the benzene derivatives revealed that the amine, cyano, and carboxyl groups showed well-defined conductance values (*39-41*). The hybridized states originating from the lone pair in amine helps the single molecular junction to maintain fixed conductance value with different tilt angles (*39, 41*). Recent synthesizing techniques have been developed to fabricate single molecular junctions having three anchoring groups at each side, and an anchoring group containing fullerene molecules.

Actually, these anchoring groups enabled us to successfully fabricate a single molecular junction with fixed conductance values and to reproduce the function of an isolated molecule in a single molecular junction; however, some issues still need to be overcome. The observed phenomena are similar to those in isolated states with reduced performance. For example, the fabricated photo switching utilizing diarylethene derivatives showed a conductance value of 0.001 G_0, resulting in a low on-off ratio (*10*). Because anchoring groups prevent hybridization between the molecular backbone and metal electrodes in order to protect the intrinsic property of the molecular backbone, they also function as obstacles to electron transport (*42*). As long as we use the anchoring group in a single molecular junction, there remain limitations in terms of our ability to improve the electron transport.

In this study, I eliminated the concept of the anchoring group, and aimed to hybridize the molecular orbital with metal electric states. Kiguchi *et al.* demonstrated that benzene molecules showed high conductance values with Pt electrodes (*43*). The direct binding via the π orbital in aromatic molecules enables molecular orbitals to be effectively hybridized with the orbitals of metals, leading to not only improvements in the conductance value, but also makes the single molecular junction a novel material. However, it is difficult to fabricate the single molecular junction with a well-defined conductance value without anchoring groups. In highly conductive single molecular junctions, molecular orbitals are hybridized with metal electric states. Highly conductive single molecular junctions have potential as novel materials whose properties are different from those of isolated molecules and metal species.

1.5 Purpose of this thesis

The purpose of this thesis is to fabricate a highly conductive single molecular junction with a well-defined conductance value, and to control its electric property by designing the interface structure between a metal and molecule. In order to clarify the molecular configuration and

electric states of a single molecular junction, I investigated the fabricated single molecular junction by performing inelastic tunneling electron spectroscopy or using current-voltage characteristics as well as conductance measurements.

In this thesis, I focused on the direct-binding technique utilizing a π-conjugated molecule with the aim of fabricating a highly conductive single molecular junction. In chapter 4, I present details regarding the fabrication of a benzene molecular junction with a well-defined conductance value, focusing on the interaction between benzene and metal. By designing the interface to have proper interaction between metal and benzene, the molecular configurational change can be limited. Proper interaction enables us to form a single molecular junction only in the most stable configuration, which leads to a well-defined conductance value. On the other hand, the metal-molecule interface is designed such that it maintains the conductance value even when the molecular configuration changes, as discussed in chapter 5. Fullerene, which has a spherical shape, is expected to have a fixed conductance value with configurational changes. In chapters 6 and 7, the anchoring part is enclosed in the π-conjugated system in order to control the electric property of the single molecular junctions. The nitrogen atom in the π-conjugated system is expected to maintain a high conductivity with a fixed molecular configuration. The lone pair on the nitrogen atom is orthogonal to the π system, which is expected to have two stable configurations, a π-connected one and a lone-pair-connected one. By controlling the interface structure, it is expected to control the electric property of the single molecular junction. In chapter 6, the use of the nitrogen molecule is investigated as the simplest π-conjugated system that includes nitrogen atoms. The formation and electric transport of nitrogen molecules are investigated for each metal species. In chapter 7, the pyrazine molecular junction is investigated using Pt electrodes. By controlling the metal-molecule distance, the molecular configuration can be controlled, as well as the electrical properties. The two conductance states are fabricated depending on the configuration of the pyrazine molecule. The configuration of the pyrazine molecule is investigated by the *dI/dV* spectrum to determine the configuration of the benzene molecule. The high and low conductance states were assigned to the configuration with its *p* orbital being both parallel and vertical to the binding direction. Finally, the electrical properties of the single molecular junction are controlled by controlling the interface structure, and the two atomic configurations were successfully switched using an external force. The ability to control the electrical property using a mechanical force is a unique property of the single molecular junction because it is difficult to change the electrical property of a conductor using an external force. The tiny structural change in the interface induced the drastic change in the conductance value of the single molecular junction. The observed behavior may enable us to

apply the single molecular junction as a novel material whose molecular orbital strongly correlates with metal orbitals.

References

1. R. H. Dennard, Gaenssle. Fh, H. N. Yu, V. L. Rideout, E. Bassous *et al.*, Design of ion-implanted mosfets with very small physical dimensions. *Ieee J. Solid-St. Circ.* Sc. **9**, 256-268 (1974).
2. G. E. Moore, Cramming more components onto integrated circuits (Reprinted from Electronics, pg 114-117, April 19, 1965). *Proc. IEEE* **86**, 82-85 (1998).
3. A. Aviram, M. A. Ratner, Molecular rectifiers. *Chem. Phys. Lett.* **29**, 277-283 (1974).
4. A. I. Yanson, G. R. Bollinger, H. E. van den Brom, N. Agrait, J. M. van Ruitenbeek, Formation and manipulation of a metallic wire of single gold atoms. *Nature* **395**, 783-785 (1998).
5. M. A. Reed, C. Zhou, C. J. Muller, T. P. Burgin, J. M. Tour, Conductance of a molecular junction. *Science* **278**, 252-254 (1997).
6. M. L. Perrin, R. Frisenda, M. Koole, J. S. Seldenthuis, J. A. C. Gil *et al.*, Large negative differential conductance in single-molecule break junctions. *Nat. Nanotechnol.* **9**, 830-834 (2014).
7. S. Sakata, K. Yoshida, Y. Kitagawa, K. Ishii, K. Hirakawa, Rotation and anisotropic molecular orbital effect in a single H2TPP molecule transistor. *Phys. Rev. Lett.* **111**, 246806 (2013).
8. B. Capozzi, J. L. Xia, O. Adak, E. J. Dell, Z. F. Liu *et al.*, Single-molecule diodes with high rectification ratios through environmental control. *Nat. Nanotechnol.* **10**, 522-U101 (2015).
9. I. Diez-Perez, J. Hihath, Y. Lee, L. P. Yu, L. Adamska *et al.*, Rectification and stability of a single molecular diode with controlled orientation. *Nat. Chem.* **1**, 635-641 (2009).
10. D. Dulic, S. J. van der Molen, T. Kudernac, H. T. Jonkman, J. J. D. de Jong *et al.*, One-way optoelectronic switching of photochromic molecules on gold. *Phys. Rev. Lett.* **91**, 207402 (2003).
11. S. Y. Quek, M. Kamenetska, M. L. Steigerwald, H. J. Choi, S. G. Louie *et al.*, Mechanically controlled binary conductance switching of a single-molecule junction. *Nat. Nanotechnol.* **4**, 230-234 (2009).

12. S. Y. Guo, J. Hihath, I. Diez-Perez, N. J. Tao, Measurement and statistical analysis of single-molecule current-voltage characteristics, transition voltage spectroscopy, and tunneling barrier height. *J. Am. Chem. Soc.* **133**, 19189-19197 (2011).
13. S. Y. Guo, G. Zhou, N. J. Tao, Single molecule conductance, thermopower, and transition voltage. *Nano Lett.* **13**, 4326-4332 (2013).
14. P. Reddy, S. Y. Jang, R. A. Segalman, A. Majumdar, Thermoelectricity in molecular junctions. *Science* **315**, 1568-1571 (2007).
15. T. Kim, P. Darancet, J. R. Widawsky, M. Kotiuga, S. Y. Quek *et al.*, Determination of energy level alignment and coupling strength in 4,4 '-bipyridine single-molecule junctions. *Nano Lett.* **14**, 794-798 (2014).
16. S. K. Yee, J. A. Malen, A. Majumdar, R. A. Segalman, Thermoelectricity in fullerene-metal heterojunctions. *Nano Lett.* **11**, 4089-4094 (2011).
17. Y. Kim, W. Jeong, K. Kim, W. Lee, P. Reddy, Electrostatic control of thermoelectricity in molecular junctions. *Nat. Nanotechnol.* **9**, 881-885 (2014).
18. R. H. M. Smit, Y. Noat, C. Untiedt, N. D. Lang, M. C. van Hemert *et al.*, Measurement of the conductance of a hydrogen molecule. *Nature* **419**, 906-909 (2002).
19. D. Djukic, K. S. Thygesen, C. Untiedt, R. H. M. Smit, K. W. Jacobsen *et al.*, Stretching dependence of the vibration modes of a single-molecule Pt−H_2−Pt bridge. *Phys. Rev. B* **71**, 161402(R) (2005).
20. O. Tal, M. Krieger, B. Leerink, J. M. van Ruitenbeek, Electron-vibration interaction in single-molecule junctions: from contact to tunneling regimes. *Phys. Rev. Lett.* **100**, 196804 (2008).
21. D. djukic, J. M. van Ruitenbeek, Shot noise measurements on a single molecule. *Nano Lett.* **6**, 789-793 (2006).
22. M. Kumar, O. Tal, R. H. M. Smit, A. Smogunov, E. Tosatti *et al.*, Shot noise and magnetism of Pt atomic chains: Accumulation of points at the boundary. *Phys. Rev. B* **88**, 245431, (2013).
23. W. B. Chen, H. X. Li, J. R. Widawsky, C. Appayee, L. Venkataraman *et al.*, Aromaticity decreases single-molecule junction conductance. *J. Am. Chem. Soc.* **136**, 918-920 (2014).
24. A. Mahendran, P. Gopinath, R. Breslow, Single molecule conductance of aromatic, nonaromatic, and partially antiaromatic systems. *Tetrahedron Lett.* **56**, 4833-4835 (2015).
25. X. Crispin, V. Geskin, A. Crispin, J. Cornil, R. Lazzaroni *et al.*, Characterization of the

interface dipole at organic/metal interfaces. *J. Am. Chem. Soc.* **124**, 8131-8141 (2002).

26. O. T. Hofmann, P. Rinke, M. Scheffler, G. Heimel, Integer versus fractional charge transfer at metal(/insulator)/organic interfaces: Cu(/NaCl)/TCNE. *Acs Nano* **9**, 5391-5404 (2015).
27. N. Koch, S. Duhm, J. P. Rabe, A. Vollmer, R. L. Johnson, Optimized hole injection with strong electron acceptors at organic-metal interfaces. *Phys. Rev. Lett.* **95**, (2005).
28. X. Y. Xiao, B. Q. Xu, N. J. Tao, Conductance titration of single-peptide molecules. *J. Am. Chem. Soc.* **126**, 5370-5371 (2004).
29. M. Tsutsui, Y. Teramae, S. Kurokawa, A. Sakai, High-conductance states of single benzenedithiol molecules. *Appl. Phys. Lett.* **89**, 163111 (2006).
30. C. Bruot, J. Hihath, N. J. Tao, Mechanically controlled molecular orbital alignment in single molecule junctions. *Nat. Nanotechnol.* **7**, 35-40 (2012).
31. S. Ghosh, H. Halimun, A. K. Mahapatro, J. Choi, S. Lodha *et al.*, Device structure for electronic transport through individual molecules using nanoelectrodes. *Appl. Phys. Lett.* **87**, 233509 (2005).
32. Y. Kim, T. Pietsch, A. Erbe, W. Belzig, E. Scheer, Benzenedithiol: A broad-range single-channel molecular conductor. *Nano Lett.* **11**, 3734-3738 (2011).
33. R. Stadler, Fermi level alignment in single molecule junctions and its dependence on interface structure. *J. Phys. Conf. Ser.* **61**, 1097-1101 (2007).
34. W. Haiss, C. S. Wang, I. Grace, A. S. Batsanov, D. J. Schiffrin *et al.*, Precision control of single-molecule electrical junctions. *Nat. Mater.* **5**, 995-1002 (2006).
35. Y. Kitaguchi, S. Habuka, H. Okuyama, S. Hatta, T. Aruga *et al.*, Controlling single-molecule junction conductance by molecular interactions. *Sci. Rep.* **5**, 11796, (2015).
36. D. Darau, G. Begemann, A. Donarini, M. Grifoni, Interference effects on the transport characteristics of a benzene single-electron transistor. *Phys. Rev. B* **79**, 235404, (2009).
37. M. Taniguchi, M. Tsutsui, R. Mogi, T. Sugawara, Y. Tsuji *et al.*, Dependence of single-molecule conductance on molecule junction symmetry. *J. Am. Chem. Soc.* **133**, 11426-11429 (2011).
38. C. M. Guedon, H. Valkenier, T. Markussen, K. S. Thygesen, J. C. Hummelen *et al.*, Observation of quantum interference in molecular charge transport. *Nat. Nanotechnol.* **7**, 304-308 (2012).
39. Y. S. Park, A. C. Whalley, M. Kamenetska, M. L. Steigerwald, M. S. Hybertsen *et al.*, Contact chemistry and single-molecule conductance: A comparison of phosphines,

methyl sulfides, and amines. *J. Am. Chem. Soc.* **129**, 15768- 15769 (2007).

40. R. Frisenda, S. Tarkuc, E. Galan, M. L. Perrin, R. Eelkema *et al.*, Electrical properties and mechanical stability of anchoring groups for single-molecule electronics. *Beilstein J. Nanotech.* **6**, 1558-1567 (2015).

41. L. Venkataraman, J. E. Klare, I. W. Tam, C. Nuckolls, M. S. Hybertsen *et al.*, Single-molecule circuits with well-defined molecular conductance. *Nano Lett.* **6**, 458-462 (2006).

42. J. Ferrer, V. M. Garcia-Suarez, Tuning the conductance of molecular junctions: Transparent versus tunneling regimes. *Phys. Rev. B* **80**, 085426 (2009).

43. M. Kiguchi, O. Tal, S. Wohlthat, F. Pauly, M. Krieger *et al.*, Highly conductive molecular junctions based on direct binding of benzene to platinum electrodes. *Phys. Rev. Lett.* **101**, 046801 (2008).

2 Theoretical background

2.1 Electric states in one-dimensional conductor

One-dimensional conductors have different conductance states when compared with three-dimensional conductors (*1*, *2*). Here, we consider a one-dimensional conductor that has a nanoscale in the x and y directions, but is infinite in the z direction. The Schorödinger equation can be expressed as in Eq. (2.1).

$$\left[-\frac{\hbar^2}{2m}\nabla^2 + V(R)\right]\varphi(R) = E\varphi(R) \quad \ldots(2.1)$$

Because the potential in the z direction is zero, the system can be described as a free electron model. The three-dimensional potential $V(R)$ can be described as $V(x, y)$. The wave function in the z direction can be described as $\varphi = \varphi(x,y)exp(ik_z z)$, and the Schorödinger equation is expressed as in Eq. (2.2) and Eq. (2.3).

$$\left[-\frac{\hbar^2}{2m}\left(\frac{\partial^2}{\partial x^2}+\frac{\partial^2}{\partial y^2}+\frac{\partial^2}{\partial z^2}\right)+V(x,y)\right]\varphi(x,y)\exp(ik_z z) = E\varphi(x,y)\exp(ik_z z) \ldots(2.2)$$

$$\left[\frac{\hbar^2 k_z^2}{2m}-\frac{\hbar^2}{2m}\left(\frac{d^2}{dx^2}+\frac{d^2}{dx^2}\right)+V(x,y)\right]\varphi(x,y)\exp(ik_z z) = E\varphi(x,y)\exp(ik_z z) \ldots(2.3)$$

The wave function is satisfied by Eq. (2.4).

$$\left[\frac{\hbar^2 k_z^2}{2m}\right]\exp(ik_z z) = E_z\exp(ik_z z) \ldots(2.4)$$

Therefore, $E_z=\frac{\hbar^2 k_z^2}{2m}$ in the z direction. On the other hand, the wave function is satisfied by Eq. (2.5) in the x and y directions.

$$\left[-\frac{\hbar^2}{2m}\left(\frac{d^2}{dx^2}+\frac{d^2}{dx^2}\right)+V(x,y)\right]\varphi(x,y) = E_{x,y}\varphi(x,y) \ldots(2.5)$$

When we assume a rectangular conductor, $\varphi(x,y)$, $E_{x,y}$, are the same as the eigen function and

eigen energy, respectively, in quantum wells. Hence, the eigen energy of a one-dimensional conductor can be expressed as follows:

$$E = E_{i,j} + \frac{\hbar^2 k_z^2}{2m} \ldots (2.6)$$

$$\varphi = exp(ik_z z) \ldots (2.7)$$

Figure 2.1(a) is the band distribution based on Eq. (2.6) (*1*). The parabola for each index notation i, j is called an electric sub band. The density of states of the sub band D_{ij} is expressed as follows, and the density of states can be described as in Figure 2.1(b) (*1*).

$$D_{ij} = \frac{dN_{i,j}}{dk}\frac{dk}{dE} \ldots (2.8)$$

$$D_{ij} = \frac{4L}{h v_{i,j}} \quad (E > E_{i,j}) \ldots (2.9)$$

$$D_{i,j} = 0 \quad (E < E_{i,j}) \ldots (2.10)$$

where $v_{i,j}$ is the velocity of the electron in the i, j sub band. When we have different sub bands, the sub bands can be called “modes” and “channels”.

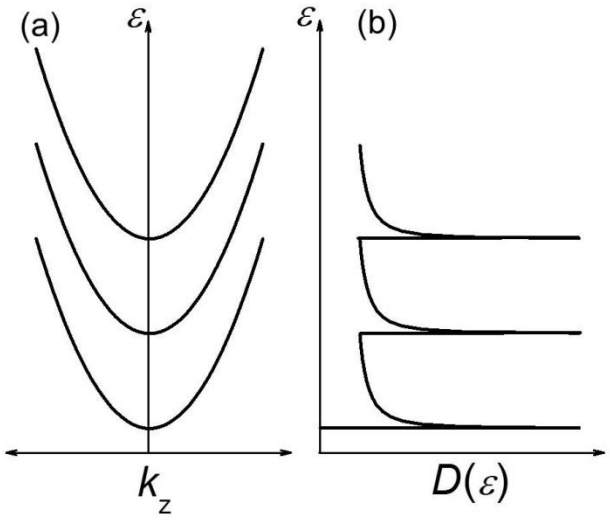

Figure 2.1: Schematic image showing (a) electric states and (b) density of states of one-dimensional conductor.

2.2 Electron transport in nano-sized conductor

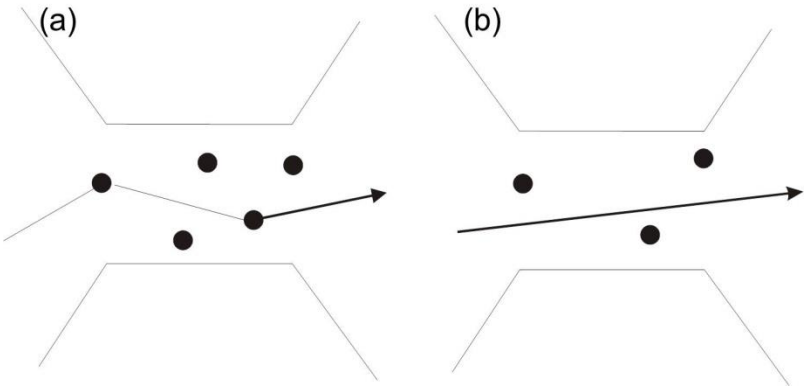

Figure 2.2: Schematic image of (a) diffusive and (b) ballistic electron transport.

The electron transport of an atomic-sized conductor is different from that of a bulk-sized conductor. In a bulk-sized conductor, the electron transport is diffusive, as shown in Figure 2.2(a). The electrons scatter at scattering point such as impurities and defects. The conductance of the bulk-sized conductor obeys Ohm's law, and it is proportional to the area S and electric conductivity σ, as shown in Eq. (2.11).

$$G = \sigma S / L \qquad \cdots(2.11)$$

When the size of the conductor reaches an atomic scale, electron transport is influenced by the conductor size compared with the mean free path (l) and phase-coherence length ($l_{\varphi.}$). The mean free path, which represents the distance travelled by an electron between collisions, is about 100 nm. On the other hand, l_{φ} represents the distance within which the phase information is preserved. For gold, l_{φ} is of the scale of 1 μm. Therefore, the single atomic and molecular junctions discussed in this thesis are smaller than l, l_{φ}. In this region, electrons travel ballistically though the conductor, as shown in Figure 2.2 (b).

2.3 Landauer-Büttiker formula

Here, we consider the electron transport through an atomic-sized conductor utilizing the scattering approach. In this approach, the sample works as a scattering point, which connects to the left (L) and right (R) electrodes over which the electron scattering is negligible, as shown in Figure 2.3 (*3*).

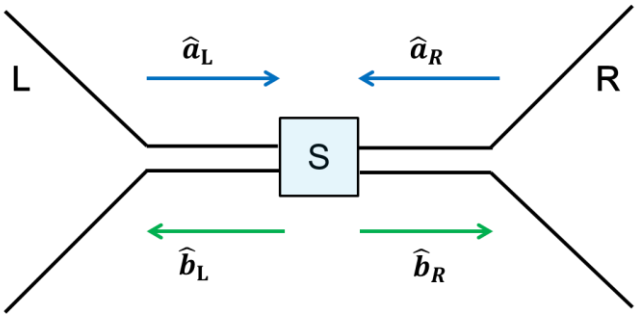

Figure 2.3: Schematic view of scattering approach for two terminal conductors.

The electrodes work as a reservoir that is the source of carriers, which are determined by the Fermi-Dirac distribution function. The Fermi-Dirac distribution function is described as follows:

$$f_\alpha = \frac{1}{\exp\left[\frac{E-\mu_\alpha}{k_B T_\alpha}\right]+1} \quad \ldots(2.12)$$

where the parameter μ_α and T_α, represents the chemical potential and temperature of the left and right electrodes, respectively. k_B is the Boltzmann constants. As discussed in the previous section, the wave function can be expressed separately in the longitudinal and transverse directions, and its energy is expressed as in Eq.(2.6). The electron transport can be separated into incoming and outgoing states depending on the sample for each electrode. In order to express incoming and outgoing states, we introduced creation and annihilation operators. For the outgoing states, we expressed the creation and annihilation operators as $\hat{a}_{\alpha n}(E)$, $\hat{a}^{\dagger}_{\alpha n}(E)$. For incoming states, we expressed the operators as $\hat{b}_{\alpha n}(E)$, $\hat{b}^{\dagger}_{\alpha n}(E)$. The index, n represents the quantum number to describe the quantum channels. The two operators were connected via the scattering matrix *S*,

$$\begin{pmatrix} \hat{\mathrm{b}}_{\mathrm{L1}}(\mathrm{E}) \\ \cdots \\ \hat{\mathrm{b}}_{\mathrm{RN_R}}(\mathrm{E}) \end{pmatrix} = \boldsymbol{S} \begin{pmatrix} \hat{\mathrm{a}}_{\mathrm{L1}}(\mathrm{E}) \\ \cdots \\ \hat{\mathrm{a}}_{\mathrm{RN_R}}(\mathrm{E}) \end{pmatrix} \quad \ldots (2.13)$$

The scattering matrix *S* is described using the transmitting (*t*) and reflecting states (*r*) as follows:

$$S = \begin{pmatrix} r & t' \\ t & r' \end{pmatrix} \quad \ldots (2.14)$$

The dimensions of each element are characterized by the quantum number of each electrode, which is related to the number of channels. The dimensions of each element are $\mathrm{N_L} \times \mathrm{N_L}$, $\mathrm{N_R} \times \mathrm{N_R}$, $\mathrm{N_R} \times \mathrm{N_L}$, and $\mathrm{N_L} \times \mathrm{N_R}$, for *r, r', t,* and *t'*, respectively. In total, the dimensions of the scattering matrix are $(\mathrm{N_L} + \mathrm{N_R}) \times (\mathrm{N_L} + \mathrm{N_R})$. The flux conservation and time-reverse symmetry leads to the unique character of unitarily and symmetricity of the scattering matrix. The current operator in the left electrodes can be described using the field operator Ψ_{L}.

$$\hat{I}_{\mathrm{L}}(\mathrm{z.t}) = \frac{\hbar e}{2im} \int \mathrm{d}\boldsymbol{r}_{\mathbf{T}} \left[\hat{\Psi}_{\mathrm{L}}^{\dagger}(\boldsymbol{r}, \mathrm{t}) \frac{\partial}{\partial \mathrm{z}} \hat{\Psi}_{\mathrm{L}}(\boldsymbol{r}, \mathrm{t}) - \left(\frac{\partial}{\partial \mathrm{z}} \hat{\Psi}_{\mathrm{L}}^{\dagger}(\boldsymbol{r}, \mathrm{t}) \right) \hat{\Psi}_{\mathrm{L}}(\boldsymbol{r}, \mathrm{t}) \right] \quad \ldots (2.15)$$

$$\hat{\Psi}_{\mathrm{L}}(\boldsymbol{r}, \mathrm{t}) = \int \mathrm{d}E \mathrm{e}^{-\mathrm{i}E\mathrm{t}/\hbar} \sum_{\mathrm{n}=1}^{\mathrm{N_L}} \frac{\chi_{\mathrm{Ln}}(\boldsymbol{r}_{\mathbf{T}})}{\sqrt{2\pi\hbar\upsilon_{\mathrm{Ln}}(E)}} \left[\hat{\mathrm{a}}_{\mathrm{Ln}} \mathrm{e}^{\mathrm{i}k_{\mathrm{Ln}}\mathrm{z}} + \hat{\mathrm{b}}_{\mathrm{Ln}} \mathrm{e}^{-\mathrm{i}k_{\mathrm{Ln}}\mathrm{z}} \right] \quad \ldots (2.16)$$

$$\hat{\Psi}_{\mathrm{L}}^{\dagger}(\boldsymbol{r}, \mathrm{t}) = \int \mathrm{d}E \mathrm{e}^{\frac{\mathrm{i}E\mathrm{t}}{\hbar}} \sum_{\mathrm{n}=1}^{\mathrm{N_L}} \frac{\chi *_{\mathrm{Ln}}(\boldsymbol{r}_{\mathbf{T}})}{\sqrt{2\pi\hbar\upsilon_{\mathrm{Ln}}(E)}} \left[\hat{\mathrm{a}}_{\mathrm{Ln}}^{\dagger} \mathrm{e}^{-\mathrm{i}k_{\mathrm{Ln}}\mathrm{z}} + \hat{\mathrm{b}}_{\mathrm{Ln}}^{\dagger} \mathrm{e}^{\mathrm{i}k_{\mathrm{Ln}}\mathrm{z}} \right] \ldots (2.17)$$

$\boldsymbol{r}_{\mathbf{T}}$ is the transverse coordination and *z* is the coordination along the leads. $\chi_{\mathrm{Ln}}(\boldsymbol{r}_{\mathbf{T}})$ are the transverse wave functions. Because the observable values do not change drastically, especially near the Fermi energy, we can neglect the energy dependence of the quantities. For the condition where the physical quantity does not depend on the energy, the current operator is expressed as follows:

$$\hat{I}_{\mathrm{L}}(\mathrm{t}) = \frac{e}{2\pi\hbar} \sum\nolimits_{\mathrm{n}} \int \mathrm{d}E \mathrm{d}E' \mathrm{e}^{\mathrm{i}(E-E')\mathrm{t}/\hbar} \left[\hat{\mathrm{a}}_{\mathrm{Ln}}^{\dagger}(E') \hat{\mathrm{a}}_{\mathrm{Ln}}(E) - \hat{\mathrm{b}}_{\mathrm{Ln}}^{\dagger}(E') \hat{\mathrm{b}}_{\mathrm{Ln}}(E) \right] \quad \ldots (2.18)$$

where $\hat{\mathrm{n}}_{\mathrm{Ln}}^{+}(\mathrm{E})$ is the operator of the occupation number of the incident electrons in the left leads, $\hat{\mathrm{n}}_{\mathrm{Ln}}^{-}$ is the operator of the occupation number of the out-going electrons in lead *L* in channel *n*, and $\hat{\mathrm{n}}_{\mathrm{Ln}}^{+}(\mathrm{E}), \hat{\mathrm{n}}_{\mathrm{Ln}}^{-}$ is expressed as Eq. (2.19) and (2.20).

$$\hat{n}^{+}_{Ln}(E) = \hat{a}_{Ln}(E')\,\hat{a}^{\dagger}_{Ln}(E) \ldots (2.19)$$
$$\hat{n}^{-}_{Ln}(E) = \hat{b}_{Ln}(E')\,\hat{b}^{\dagger}_{Ln}(E) \ldots (2.20)$$

Now, $E' = \hbar\Omega + E$, and the integral over Ω gives

$$\hat{I}_{L}(t) = \frac{e}{2\pi\hbar}\sum\nolimits_{n}\int dE[\hat{n}^{+}_{Ln}(E,t) - \hat{n}^{-}_{Ln}(E,t)] \quad \ldots (2.21)$$

$\hat{n}^{\pm}_{Ln}(E,t)$ are the time-dependent occupation numbers. Eq. (2.21) shows that the current can be expressed as the difference in the occupation number in the electrodes. Eq. (2.21) is then re-expressed using the scattering matrix ***s***,

$$\hat{I}_{L}(t) = \frac{e}{2\pi\hbar}\sum_{\alpha\beta}\sum_{mn}\int dE dE'\, e^{\frac{i(E-E')t}{\hbar}}\hat{a}^{\dagger}_{\alpha m}(E)A^{mn}_{\alpha\beta}(L;E,E')\hat{a}_{\beta n}(E') \ldots (2.22)$$
$$A^{mn}_{\alpha\beta}(L;E,E') = \delta_{mn}\delta_{\alpha L}\delta_{\beta L} - \sum\nolimits_{k} S^{\dagger}_{L\alpha;mk}(E)S_{L\beta;kn}(E') \quad \ldots (2.23)$$

Note, that α and β represent the electrodes R and L,respectively. $S_{L\alpha;mk}(E)$ is the element of the scattering matrix that relates $\hat{b}_{Lm}(E)$ to $\hat{a}_{\alpha k}(E)$. At the equilibrium, the mean square of the annihilation operator is

$$\langle \hat{a}^{\dagger}_{\alpha m}(E)\hat{a}_{\beta n}(E')\rangle = \delta_{\alpha\beta}\delta_{mn}\delta(E-E')f_{\alpha}(E) \quad \ldots (2.24)$$

The mean current in the junction is derived from Eq. (2.22).

$$\langle I_L\rangle = \frac{e}{2\pi\hbar}\int dE Tr\left[t^{\dagger}(E)t(E)\right][f_L(E) - f_R(E)] \quad \ldots (2.25)$$

The matrix *t* is the off-diagonal block of the scattering matrix, and $t_{mn} = S_{RL;mn}$. At the limit of zero temperature and small voltage, the electric conductance *G* is

$$G = \frac{e^2}{h}Tr\left[t^{\dagger}(E_F)t(E_F)\right] \qquad \ldots (2.26)$$

The matrix $\left[t^{\dagger}(E)t(E)\right]$ can be diagonalized. The eigenvalues of $t^{\dagger}(E)t(E)$ give the transmission probability, T_n, and the mean current and conductance are expressed as follows:

$$\langle I_L \rangle = \frac{e}{2\pi\hbar} \int T_n dE[f_L(E) - f_R(E)] \quad \ldots (2.27)$$

$$G = \frac{e^2}{h} \sum T_n \quad \ldots (2.28)$$

When we consider the spin degeneracy, the Landauer-Büttiker expression is derived as

$$G = \frac{2e^2}{h} \sum T_{\mathrm{n}} \quad \ldots (2.29)$$

The conductance is expressed using only the transmission probability. Note that the conductance of the bulk metal depends on the temperature. $2e^2/h$ is referred to as the quantum unit, and is expressed as $G_{0,}$ which has a conductance of about 77 μS or 13 kΩ. If the transmission probability of all transmission channels is 1, the conductance is an integer multiple value of G_0.

2.4 Electron transport in molecular junction

The model for molecular conductors was proposed by Paulsson. In this model, a molecule behaves like a quantum dot (*4*). We assume that the electron tunneling with double barriers (*5*) is as shown in the upper panel of Figure 2.4.

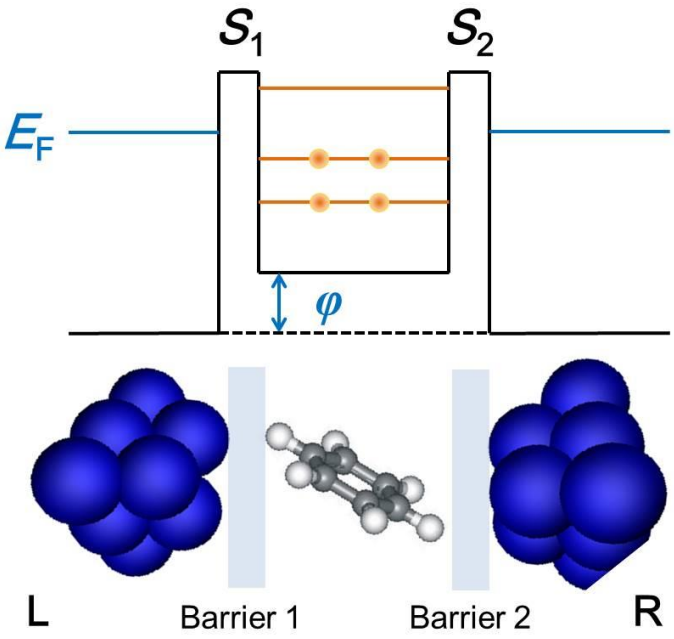

Figure 2.4: Schematic image of resonant-tunneling model with double barrier and schematic image of single molecular junction.

The scattering matrix for barriers 1 and 2 are expressed as follows:

$$S_1 = \begin{pmatrix} r_1 & t'_1 \\ t_1 & r'_1 \end{pmatrix}, \qquad S_2 = \begin{pmatrix} r_2 & t'_2 \\ t_2 & r'_2 \end{pmatrix} \ldots (2.30)$$

Both S_1 and S_2 are unitary, and the amplitude A of the wave function is given by Eq. (2.31).

$$A = \frac{t_1 t_2 e^{ikW}}{1 - r_2 r'_1 e^{2ikW}} \ldots (2.31)$$

W is the distance between two barriers, and k is the momentum of the electron. The transmission probability T_0 is given by the square of the amplitude.

$$T_0 = \frac{T_1 T_2}{1 - 2\sqrt{R_1 R_2}\cos(2kW + \delta) + R_1 R_2} \ldots (2.32)$$

T_γ and R_γ are the transmission and reflection at barriers 1 and 2, respectively. δ is the declination of r_2 and r'. T_0 is a maximum at

$$2kW + \delta = 2\pi l \text{ } (l \text{ is an integer}) \qquad \ldots (2.33)$$

Eqs. (2.32) and (2.33) imply that the energy in the quantum dot is discrete. When the energy of the incident electron is equal to the discrete energy level, T_0 has a maximum at the resonance position. Now, T_1 and T_2 are small, and the resonant position shift from $\varphi = \varphi_0$ to $\varphi = \varphi_0 + \delta$. The momentum k is expressed by $k = [2m(E+\varepsilon\varphi)/\hbar^2]^{1/2}$, and k is shifted to $k + (\varepsilon/v_F\hbar)$. The transmission probability T_0 is expressed by

$$T_0 \approx \frac{T_1 T_2}{\left(1 - \sqrt{R_1 R_2}\right)^2 + \sqrt{R_1 R_2}\left(\frac{2W\varepsilon}{\hbar v_F}\right)^2} \ldots (2.34)$$

$$T_0 \approx \frac{\Gamma_1 \Gamma_2}{\varepsilon^2 + \frac{(\Gamma_1 + \Gamma_2)^2}{4}} \ldots (2.35)$$

$$\Gamma_i = \frac{\hbar v_F T_i}{2R} \ldots (2.36)$$

Here, Γ_i is the transition probability for the transition when an electron travels from the discrete level to the electron reservoir. The resonance is expressed by the Lorenz curve. The width Γ is expressed as the summation of the transition probabilities, Γ_1 and Γ_2. Considering the single transmission channel, the conductance value is given by

$$G = \frac{2e^2}{h} \frac{\Gamma_1\Gamma_2}{\varepsilon^2 + (\Gamma_1+\Gamma_2)^2/4} \qquad \ldots (2.37)$$

In single molecular junction systems, the double barriers are comparable to tunnel barriers between the molecule and electrodes. The discrete energy level is comparable to the energy level of the molecule. In the molecular junction, Γ_1 is described by the relaxation time (*4*) as

$$\Gamma_i = e\hbar/\tau_i \quad \ldots(2.38)$$

Γ represents the line width of the energy level after interacting with metals, as shown in Figure 2.5. When the electric coupling increases, the relaxation time decreases, leading to a larger Γ, which means that Γ represents the electric coupling between the metal and molecule (*4*).

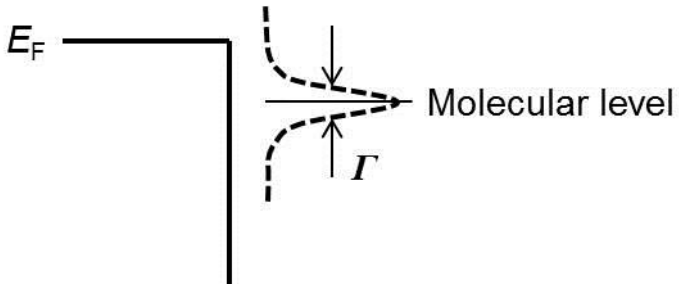

Figure 2.5: Schematic image metal electric states and molecular level.

The Fermi energy is located between HOMO and LUMO. Because the energy level near the Fermi level plays an important role in electron transport, the discrete level that we refer to is HOMO or LUMO. When the energy difference between HOMO and E_F is smaller than that between LUMO and E_F, the carrier is a hole. Otherwise, the carrier is electron. Eq. (2.37) indicates that the smaller energy difference between the molecule's orbital and E_F, as well as the larger coupling Γ result in a large conductance value in the molecular junction.

Although the scattering approach explains physical quantities such as the conductance, thermopower, and shot noise, it is difficult to express the properties of an individual single molecular junction. In the scattering approach, it is difficult to contain the intrinsic physical property of a molecule and metal electrodes. In most cases, the transmission probability of the

single molecular junction is expressed using advanced and retarded non-equilibrium green function $G^{R/A}$.

$$T(\mathrm{E}) = Tr\left[\Gamma_L(E)G^R(E)\Gamma_R(E)G^A(E)\right] \quad \cdots(2.39)$$

$$G^{R/A}(E) = \left[EI - H - \Sigma_L^{R/A}(E) - \Sigma_R^{R/A}(E)\right]^{-1} \quad \cdots(2.40)$$

where I and H are the unit matrix and Hamiltonian matrix of the molecule, respectively. Γ is expressed by the self-energy $\Sigma_{\mathrm{L(R)}}{}^{\mathrm{R/A}}$.

$$\Gamma_{L(R)} = i\left[\Sigma_{L(R)}^R - \Sigma_{L(R)}^A\right] \quad \cdots(2.41)$$

The real part of the self-energy gives the energy shift of the resonance position in Figure 2.5, and the imaginary part gives the broadening of the energy level. $\Gamma_{\mathrm{L(R)}}$ represents the broadening function. For a weak coupling system, Green's function can be obtained from the zeroth Green's functions that are calculated separately for the electrodes and the molecule.

$$G_{RL}^{(0)R/A}(E) = \sum_k \frac{C_{R,k}C_{L,k}^*}{E - \varepsilon_k \pm i\eta} \quad \cdots(2.42)$$

where $C_{\mathrm{R,k}}$, ε_{k}, and η represent the *k*-th molecule's orbital coefficient at site *R*, the *k*-th molecule's orbital energy, and the infinitesimal value, which is determined by the relationship between Green's function and the DOS. The term *CC** represents the orbital distribution of a molecule that is bridged between metal electrodes. The NEGF method explained the conductance of graphene, the single molecular junction, and many nano-sized conductors (*6*). Eqs. (2.39) – (2.42) express the physical effects expressed by scattering models. The transmission probability derived by the Green function explained the effects of the orbital alignments and DOS of the metal electrodes.

2.5 Coupling between electron transport and vibration

2.5.1 Inelastic electron tunneling spectroscopy

In single molecular junctions, it is important to evaluate the interface structure. Although scanning electron microscopy (SEM) images are successfully observed for gold atomic contacts, their observation is limited to fullerene molecules in studies regarding single molecular junctions (*7*). To identify a single molecule, Stipe demonstrated the differential conductance measurement of acetyl molecule on the Cu surface. The injected electron excites the vibration of the C-H stretching mode of the acetylene molecule (*8*), as shown in Figure 2.6. The first derivative of the differential conductance dependence is called IETS (inelastic electron tunneling spectroscopy). In this section, the differential conductance behavior in an atomic-sized conductor is discussed.

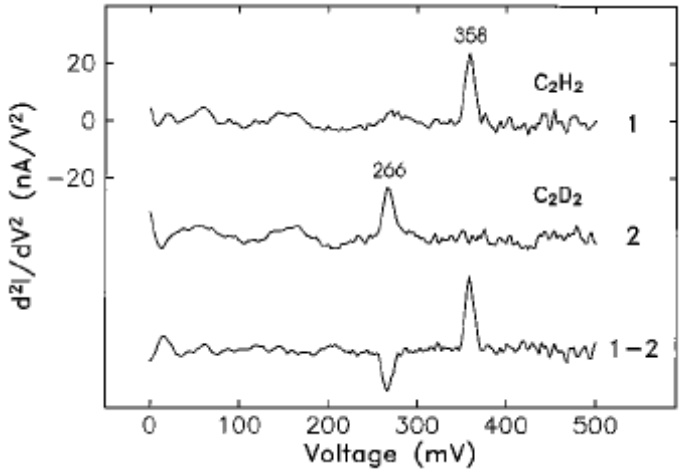

Figure 2.6: IETS of acetylene molecule on Cu surface (*8*). Copyright (1998) by the American Association for the Advancement of Science.

The electron-vibration coupling in the tunneling regime is described, as shown in Figure 2.7. When $V < V_k$, the electron tunnels are from the left electrode (L) to the right electrode (R). When the electron obtains sufficient energy to excite the vibration ($eV_k > \hbar\omega$), the inelastic tunneling channel opens. The opening of the additional channel slightly increases the conductance of the junction. Therefore, the peak structure is observed in the d^2I/dV^2 spectrum in the tunneling regime.

In order to excite the vibration by tunneling electrons, the vibration should be coupled with the molecular orbital, which mainly contributes to the transport of electrons. The tunneling current that is enhanced by electron-vibration coupling is expressed as Eq. (2.43).

$$I_{\text{tunnel}} = \langle \Psi_{in} | M | \Psi_{fm} \rangle \cdots \quad (2.43)$$

Ψ_{in} and Ψ_{fm} are the initial and final states of inelastic scattering. M represents the electron-vibration coupling matrix.

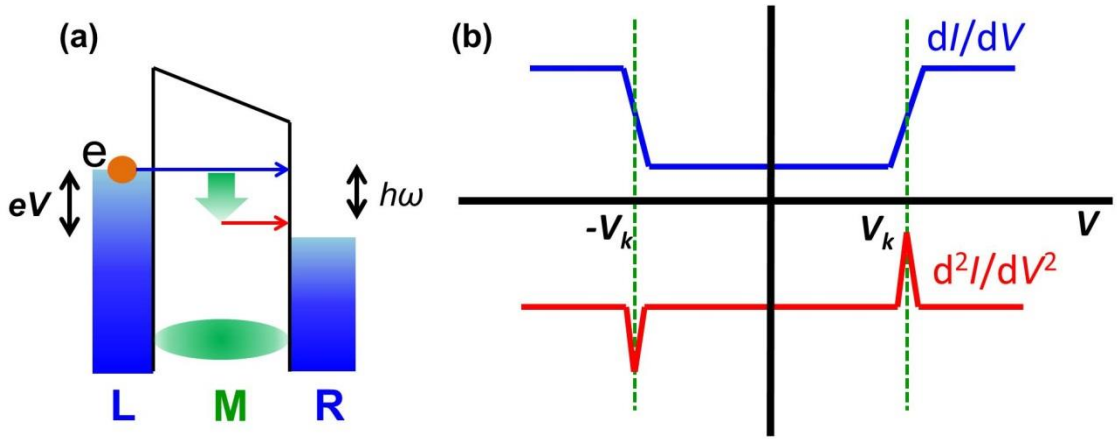

Figure 2.7: (a) Schematic image of electron transport in tunneling regime. (b) Typical *dI/dV spectrum* in the tunneling regime.

2.5.2 Point-contact spectroscopy

In the case of nano-sized conductors with ballistic electron transport, the *dI/dV* spectrum is called point-contact spectroscopy (PCS). In the ballistic transport regime, energy dispersion is described using a free electron model, as shown in Figure 2.8(a). In the ballistic regime, an electron occupies the states having momentum from $-k_z$ to $+k_z$ without a bias voltage. Note, that k_z is the momentum in the direction that is parallel to the atomic junction. At the bias voltage of V_k, the electron obtains sufficient energy to excite the vibration mode. Then, the electron transits from the occupied states having a momentum of k_z to the unoccupied states having a momentum of $-k_z$, which means that electrons are back-scattered, leading to a reduction in the conductance value. Therefore, a dip structure is observed at the vibration energy in the d^2I/dV^2 spectrum in the ballistic regime, as shown in Figure 2.8(b).

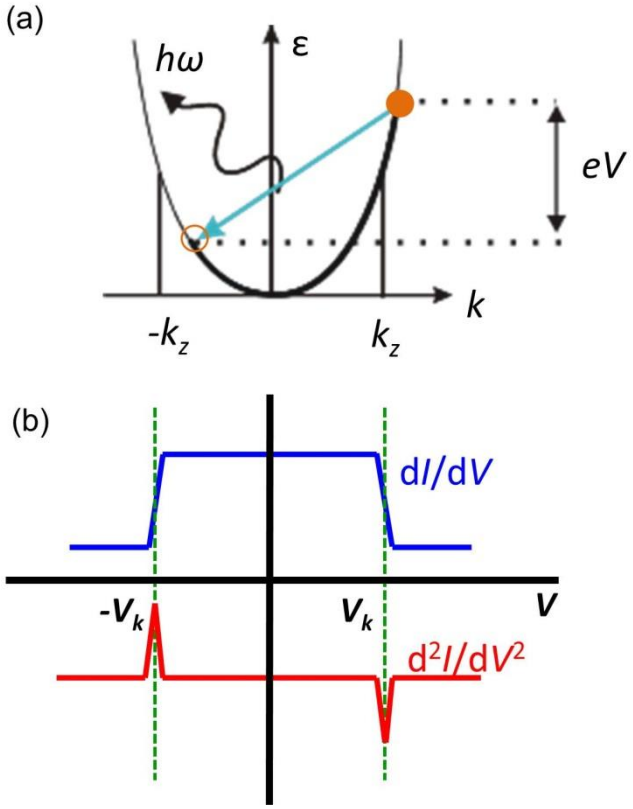

Figure 2.8: (a) Energy dispersion in the ballistic regime. (b) Typical *dI/dV* spectrum in the ballistic regime.

2.5.3 d^2I/dV^2 spectrum behavior

In a realistic single molecular junction, the differential conductance spectrum behavior is governed by the transmission probability *T, w*here we assume a single channel. The scattering approach also explains the limited understanding of the *dI/dV* spectrum behavior. In the ballistic regime, the ongoing states are fully occupied because almost all electrons travel from the left to right electrodes. At V_k, the only states to which the electrons can transit are the unoccupied incoming states, leading to a reduction of the conductance. On the other hand, in the tunneling regime, almost all electrons are reflected, and the incoming states are occupied. At V_k, the only states to which electrons can transit are unoccupied outgoing states, leading to an increase in the conductance value. Paulsson et al. explained the d^2I/dV^2 spectrum behavior depending on the symmetricity (α) of the junction and transmission (*9, 10*), as shown in Figure 2.9. When we have the symmetric junction (α = 1), the dI/dV response behavior changes from the peak to dip at T = 0.5. This theory was experimentally verified with an H_2O molecule and 1,4-benzenedithiol molecule, which have single channels (*11, 12*).

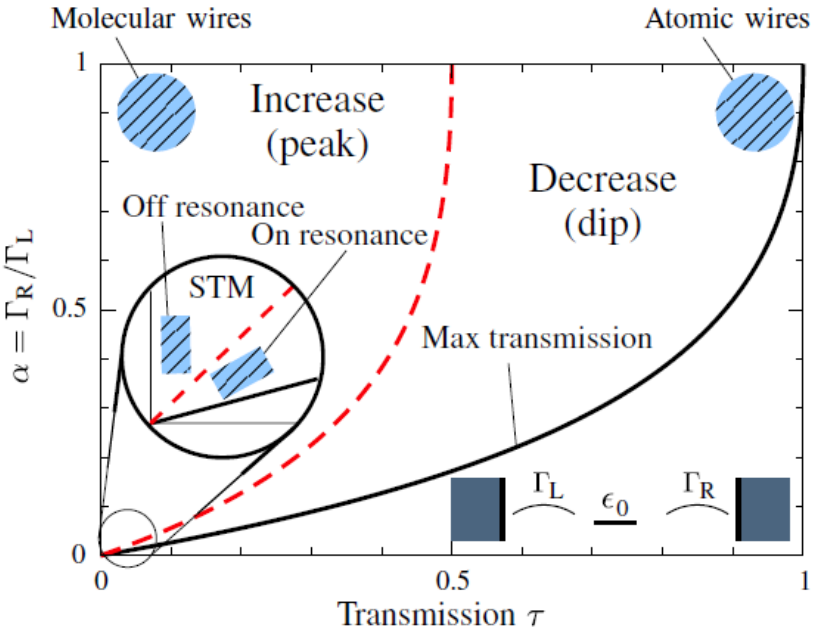

Figure 2.9: d^2I/dV^2 spectrum behavior depending on the symmetry and transmission (*10*). Copyright (2008) by the American Physical Society.

The *dI/dV* curve also shows a characteristic structure when the tunneling electron induces elementary process of reaction triggered by the vibration excitation (*13-16*). When the vibration coordination is the same as the reaction coordination, the reaction is induced by vibration with a larger energy than the reaction barrier. The hydrogen dissociation reaction of the trans-2-butene molecule on Pd (110) was observed (*14*). When the vibration coordination is not equal to the reaction coordination, the reaction is induced by the coupling between tunneling electrons and vibration modes along the reaction coordination. In this mechanism, the CO molecule diffuses on the Cu substrate by the injection of the tunneling electrodes (*15*). In a single molecular junction, the transition between two meta-stable structures is observed by the injection of the tunneling electrons. The peak structure was observed in the *dI/dV* spectrum.

It has been reported that when a magnetic impurity exists in the nano-contacts, a peak or dip is observed at $V = 0$, which is due to the Kondo effect. The Kondo effects is explained in terms of the many-body scattering problem. In a metallic atomic contact, this zero bias anomaly is also observed for Pt atomic junctions.

References

1. C. Kittel, *Introduction to Solid State Physics*. (Wiley, US, ed. 8, 2004).

2. J. H. Davies, *The Physics of Low-dimensional Semiconductors An Introduction.*

(Camgridge university press, Cambridge, UK, 1997).

3. Y. M. Blanter, M. Buttiker, Shot noise in mesoscopic conductors. *Phys. Rep.* **336**, 1-166 (2000).
4. M. Pausson, F. Zahid, S. Datta, *Handbook of Nanoscience, Engineering, and Technology*. (CRC Press US, 2003).
5. H. Fukuyama, *シリーズ物性物理の新展開「メゾスコピック系の物理」*. (maruzen, 1996).
6. T. Tada, K. Yoshizawa, Quantum transport effects in nanosized graphite sheets. *Chemphyschem* **3**, 1035-1037 (2002).
7. M. Yoshida, Y. Kurui, Y. Oshima, K. Takayanagi, In-situ observation of the fabrication process of a single shell carbon fullerene nano-contact using transmission electron microscope-scanning tunneling microscope. *Jpn. J. Appl. Phys.* **46**, L67-L69 (2007).
8. B. C. Stipe, M. A. Rezaei, W. Ho, Single-molecule vibrational spectroscopy and microscopy. *Science* **280**, 1732-1735 (1998).
9. T. Shimazaki, Y. Asai, Theoretical study of the lineshape of inelastic electron tunneling spectroscopy. *Phys. Rev. B* **77**, 5428 (2008).
10. M. Paulsson, T. Frederiksen, H. Ueba, N. Lorente, M. Brandbyge, Unified description of inelastic propensity rules for electron transport through nanoscale junctions. *Phys. Rev. Lett.* **100**, 226604 (2008).
11. O. Tal, M. Krieger, B. Leerink, J. M. van Ruitenbeek, Electron-vibration interaction in single-molecule junctions: from contact to tunneling regimes. *Phys. Rev. Lett.* **100**, 196804 (2008).
12. Y. Kim, T. Pietsch, A. Erbe, W. Belzig, E. Scheer, Benzenedithiol: A broad-range single-channel molecular conductor. *Nano Lett.* **11**, 3734-3738 (2011).
13. K. Motobayashi, Y. Kim, H. Ueba, M. Kawai, STM を用いた表面吸着分子のアクションスペクトル. *表面科学* **9**, 597-602 (2011).
14. Y. Kim, T. Komeda, M. Kawai, Single-molecule reaction and characterization by vibrational excitation. *Phys. Rev. Lett.* **89**, 126104 (2002).
15. T. Komeda, Y. Kim, M. Kawai, B. N. J. Persson, H. Ueba, Lateral hopping of molecules induced by excitation of internal vibration mode. *Science* **295**, 2055-2058 (2002).
16. Y. Sainoo, Y. Kim, T. Okawa, T. Komeda, H. Shigekawa *et al.*, Excitation of molecular vibrational modes with inelastic scanning tunneling microscopy processes: Examination through action spectra of cis-2-butene on Pd(110). *Phys. Rev. Lett.* **95**, 246102 (2005).

3 Experimental concepts and techniques

3.1 Fabrication of single molecular junction

In order to investigate the electron transport of a single molecular junction, a single molecule should be trapped in the metal nanogap. Metal nanogaps are commonly fabricated using the break-junction technique. The metal electrodes are broken down and the nanogap can be formed just after the break-down of the metal electrodes. The molecule around the nanogap can move to the nanogap, and then a single molecule is placed between the metal atoms. The metal nano contacts are broken by the tip movement of the STM, bending of the elastic substrate, electric bias, and electro-static gate. The applied bias at the nano contact induces the movement of metal atoms in the electron-migration method, and the external force was applied by electro static gating. With the STM-break-junction method, the lateral movement of the STM-tip fabricates the nanogap. In this thesis, mechanically controllable break-junction (MCBJ) technique is applied (*1*). In this MCBJ technique, the nano contact is broken by mechanical bending, as shown in Figure 3.1. The advantage of the MCBJ technique is the stability of the molecular junction because it is free from thermal drift.

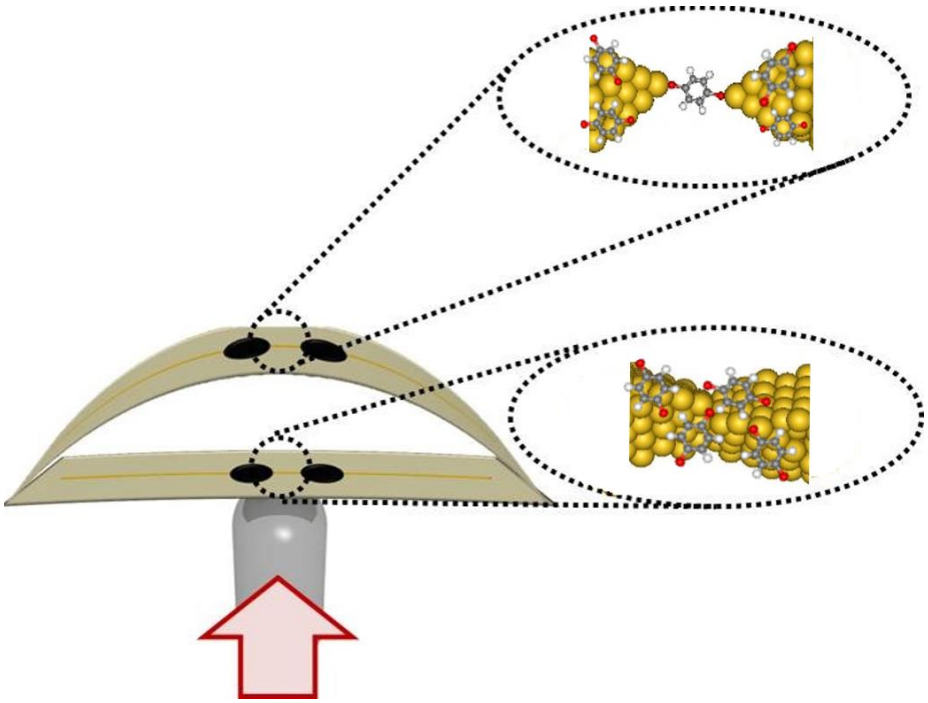

Figure 3.1: Schematic image of the MCBJ technique.

3.2 Break-down and re-formation of the metal nano contact

Yanson *et al*. demonstrated the MCBJ technique using Au electrodes (*2*), and showed the electric conductance behavior during the breaking process of Au nano contacts. Figure 3.2(a) shows the time course of the electric conductance of the Au nano contact during the breaking process, which is called the conductance trace. The electric conductance is gradually reduced in a step-wise fashion. The plateaus are observed at a conductance value that is the integer multiple of the quantum unit of G_0 ($2e^2/h$). Figure 3.2(b) shows the conductance histogram, which was constructed from seveal thousand traces. The peaks in the conductance histogram represent the preferred conductance states that are formed during the breaking process. Because the Au atomic contact has only one channel and perfect transmission, the conductance values of 3, 2, and 1 G_0 correspond to the atomic junctions made of 3, 2, and 1 atoms, respectively.

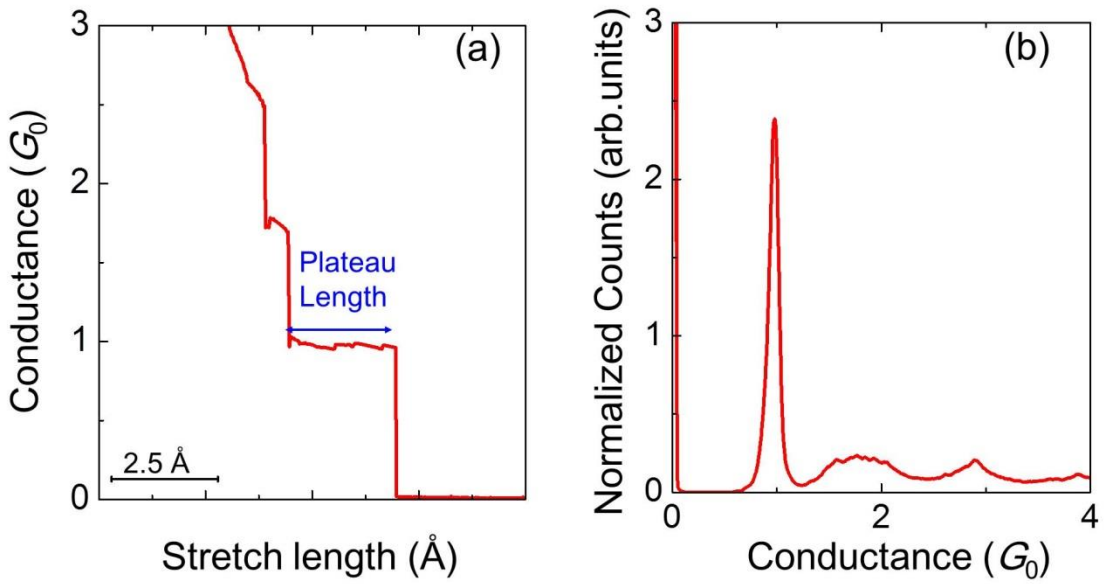

Figure 3.2: (a) Conductance trace, (b) Conductance histogram of the Au nano contact with the bias voltage of 100 mV.

Note that the Au atomic junction forms the linear atomic chain, while the other metals such as Ag and Cu do not form the linear atomic chain (*3*). Yanson *et al*. also showed the formation of the Au linear atomic chain by constructing a histogram of the plateau length. As shown in Figure 3.3(a), the peak represents the atomic contact with a length of 1, 2, and 3 atoms (*2*). Ohnishi also verified the formation of a linear atomic chain with a length of a few atoms (*4*), as shown in Figure 3.3(b). The Au atomic junction is composed of two parts; the linear atomic

chain and the atomic electrodes. The inter-atomic distance is about 2.5 Å. This property of the tendency to form a linear atomic chain is limited to 5d metals such as Au, Pt, and Ir. On the other hand, 4d metals do not form linear atomic chains (*3*, *5-8*). Figure 3.3(c) is a plateau length histogram measured by Ag electrodes (*5*). In 5d metals, the relative effects increase the effective coupling of the *s* states and *d* states, leading to the stabilization of the low-dimensional states (*3*, *8*).

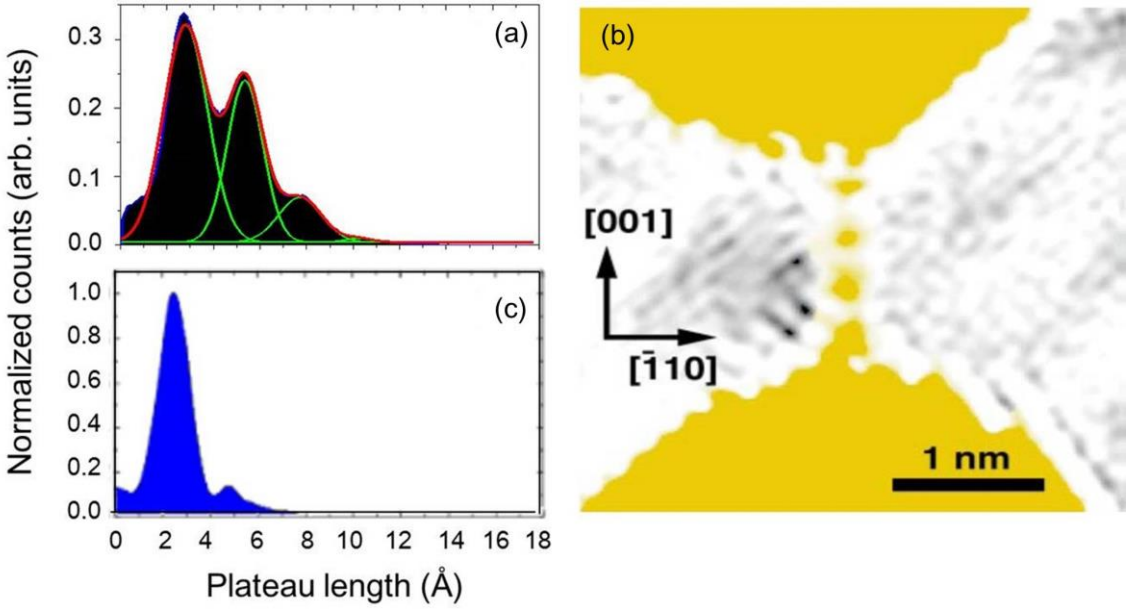

Figure 3.3: (a) Plateau length histogram obtained from over 10000 traces for the Au atomic junction. (b) TEM image of the Au atomic chain (*4*). Copyright (1998) by the Nature Publishing Group. (c) Plateau length histogram for Ag atomic junction (*5*). Copyright (2006) by the American Physical Society.

Figure 3.4(a) is a trace of the breaking process and re-formation process. After the break down of the atomic chain, the atomic electrodes also shrink. The gap size is estimated to be a few Angstroms. When the bias supply to the piezo is stopped, the elastic substrate return to the initial states, leading to the re-formation of the nano contacts. The separation, which is required to reform the nano contacts, equals the size of the nanogap, which is the summation of the length of the linear atomic chain and that of the shrinkage of the atomic electrodes. The relation between the return length and the plateau length is shown in Figure 3.4(b). The shrinkage of the electrodes is estimated to be 5 Å. Even though no linear atomic chain is not formed, a nanogap with a size of 5 Å is formed.

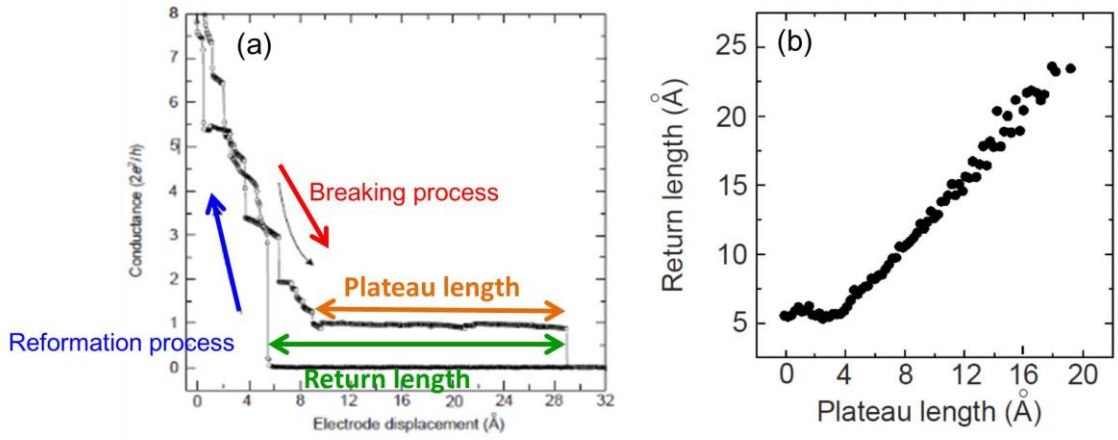

Figure 3.4: (a) Conductance trace observed during breaking and formation processes. (b) Correlation of the plateau length and return length (*2*). Copyright (1998) by the Nature Publishing Group.

In the presence of a molecule, the plateau is observed the after the break-down of the metal atomic contact, as shown in Figure 3.5(a) (*9*). The plateau originates from the rearrangements of the gold electrodes at the atomic electrodes, as well as the configurational change of the molecule. The change in the conductance of the single molecular junction was also studied by Bruot *et al.* with 1,4-benzenedithiol (*10*). Figure 3.5(b) shows the variation in conductance of the benzene molecular junction. In the region of 2-7, the conductance is decreases with the decrease of the electric coupling between the molecule and gold electrodes. At points 1 and 8, the conductance value increases as the HOMO energy of benzenedithiol approaches the Fermi energy of the Au electrodes (*10*).

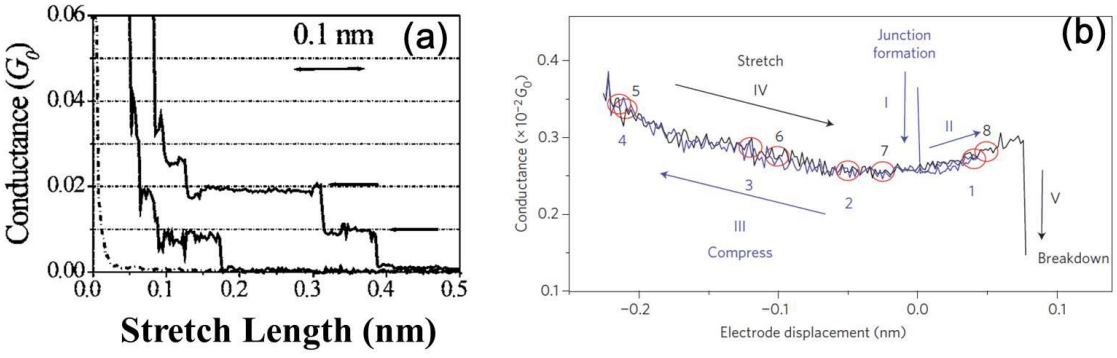

Figure 3.5: Conductance trace observed in the presence of molecule. (a) Benzene diamine (*9*) Copyright (2008) by the American Chemical Society. (b) Benzenedithiol (*10*). Copyright (2012) by the American Chemical Society.

3.3 Experimental setup

3.3.1 MCBJ setup

MCBJ sample was fabricated by typical procedure. The notched metal wire (φ = 0.1) is placed on the elastic substrate (phosphor blond, t = 1 mm). The sample was mounted on sample stage at a three-point bending configuration. The substrate is roughly bent by pushing using the driving shaft. The mechanical vibration is decoupled at the fork blade part by disconnecting the driving shaft, and the mechanical bending is precisely controlled by a piezo element. The vertical movement of the piezo is converted to the horizontal movement of the metal wire at the center part. The conversion ratio r_d is expressed as follows (*1*, *11*):

$$r_{\mathrm{d}} = \frac{\delta d}{\delta z} = \frac{3uh}{h^2} \quad \ldots (3.1)$$

where each parameter is described as in Figure 3.6 (f). The conversion factor r_d is estimated to be ~10^{-3}, which is sufficient to control the separation on a sub-nanometer scale.

For low-temperature measurements, I used the measurement system that is described in Figure 3.2(a)-(f). The custom-made chamber was evacuated and dipped in the liquid helium chamber. The temperature of the MCBJ substrate reached 10 K. The target molecule was introduced via a heated capillary.

For room-temperature measurements, I used the measurement system described in Figure 3.6(e). The chamber was evacuated with a turbo molecular pump (TMP: 250l/s) or sputter-ion pump (IP: 270l/s). Because the mechanical vibration from the TMP affected the conductance measurements of the single molecular junctions, the chamber was evacuated by only IP during the conductance measurements. The base pressure reached 2×10^{-7} Pa.

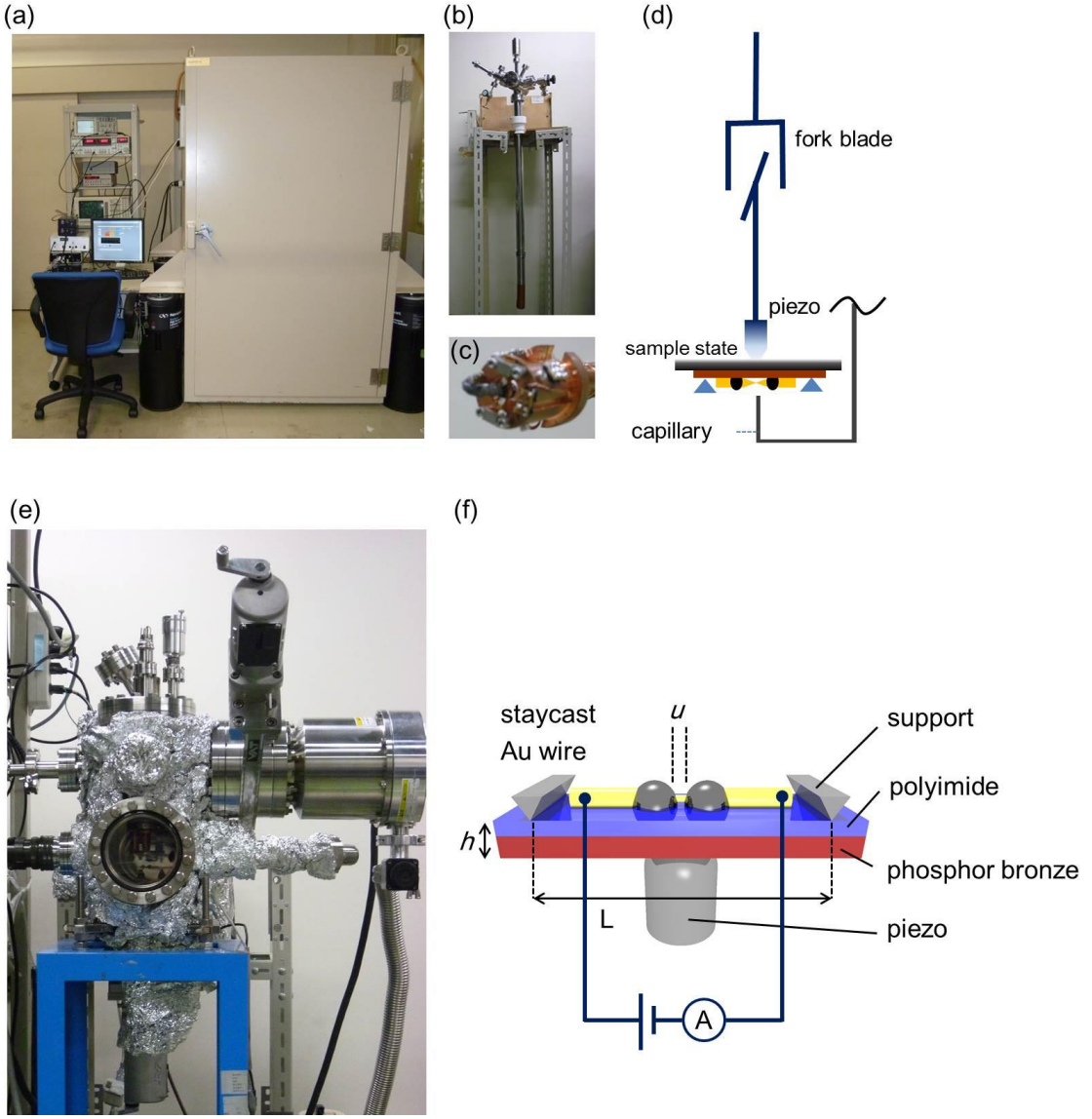

Figure 3.6: (a) Image of MCBJ system for low-temperature measurement. (b) Custom-made chamber for low-temperature measurement. (c) Image of the chamber around the sample. (d) Schematic image of the MCBJ system. (e) Custom-made chamber for room-temperature measurement. (f) Schematic image for MCBJ substrate and two-terminal conductance measurement.

3.3.2 Two-terminal conductance measurements

The metal wire was connected to the copper wire using silver paste, and the copper wire was connected to the measurement devices via coaxial cable. Electric conductance was measured with the given DC bias voltage. The bias voltage was sourced by a PCI-MIO-16XE-10 AD converter (National Instrument) and the current was measured using a Keithley 428 picoammeter. In this setup, the electric noise level was below 2×10^3 G_0 under an applied bias voltage. Typically, the metal contact was repeatedly formed and broken at 6 Hz. In a single conductance trace, 2500 data points were recorded in 80 ms. At least 1000 traces were recorded for each sample. Artificial selection of a specific trace was not performed during the construction of the histogram.

3.3.3 *dI/dV* measurements

dI/dV measurements were performed using the lock-in techniques, as shown in Figure 3.7. The differential conductance was measured using the lock-in technique with an AC modulation with a 1-mV amplitude and a 7.777-kHz frequency. The conductance was monitored for a fixed contact configuration during a sweep of the DC bias.

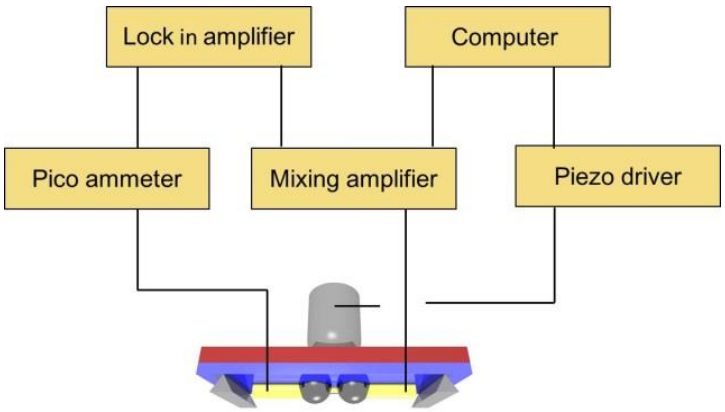

Figure 3.7: Schematic image for *dI/dV* measurement.

References

1. N. Agrait, A. L. Yeyati, J. M. van Ruitenbeek, Quantum properties of atomic-sized conductors. *Phys. Rep.* **377**, 81-279 (2003).
2. A. I. Yanson, G. R. Bollinger, H. E. van den Brom, N. Agrait, J. M. van Ruitenbeek, Formation and manipulation of a metallic wire of single gold atoms. *Nature* **395**, 783-785 (1998).
3. R. H. M. Smit, C. Untiedt, A. I. Yanson, J. M. van Ruitenbeek, Common origin for surface reconstruction and the formation of chains of metal atoms. *Phys. Rev. Lett.* **87**, 266102 (2001).
4. H. Ohnishi, Y. Kondo, K. Takayanagi, Quantized conductance through individual rows of suspended gold atoms. *Nature* **395**, 780-783 (1998).
5. W. H. A. Thijssen, D. Marjenburgh, R. H. Bremmer, J. M. van Ruitenbeek, Oxygen-enhanced atomic chain formation. *Phys. Rev. Lett.* **96**, 026806 (2006).
6. R. H. M. Smit, C. Untiedt, G. Rubio-Bollinger, R. C. Segers, J. M. van Ruitenbeek, Observation of a parity oscillation in the conductance of atomic wires. *Phys. Rev. Lett.* **91**, 076805 (2003).
7. S. R. Bahn, K. W. Jacobsen, Chain formation of metal atoms. *Phys. Rev. Lett.* **87**, 266101 (2001).
8. B. Hammer, J. K. Norskov, Why gold is the noblest of all the metals. *Nature* **376**, 238-240 (1995).
9. M. Kiguchi, S. Miura, T. Takahashi, K. Hara, M. Sawamura *et al.*, Conductance of single 1,4-benzenediamine molecule bridging between Au and Pt electrodes. *J. Phys. Chem. C* **112**, 13349-13352 (2008).
10. C. Bruot, J. Hihath, N. J. Tao, Mechanically controlled molecular orbital alignment in single molecule junctions. *Nat. Nanotechnol.* **7**, 35-40 (2012).
11. J. C. Cuevas, E. Scheer, *Molecular Electronics: An Introduction to Theory and Experiment* World Scientific Series in Nanotechnology and Nanoscience (World Scientific Publishing Co. Pte. Ltd., Singapore, 2010).

4 Design of the interaction on single benzene molecular junction

In this chapter, I focused on the interaction between the molecule and metal, which enabled the fabrication of a single molecular junction with a well-defined conductance value utilizing a π-conjugated molecule. To do this, it is important to limit the molecule's configuration. Here, I fabricated a benzene molecular junction with a well-defined electric conductance value by choosing an appropriate metal-molecule interaction. Ag and Au are expected to interact more with the benzene molecule compared to Pt. By choosing an appropriate interaction, I fabricated a single benzene molecular junction with a high and well-defined conductance value using Ag electrodes.

The contents in this chapter have been published in: Satoshi Kaneko, Tomoka Nakazumi, Manabu Kiguchi, "Fabrication of the well-defined single benzene molecule junction using Ag electrodes" *The Journal of Physical Chemistry Letters 1*, 3520–3523 (2010).

4.1 Introduction

As mentioned in chapter 1, highly conductive single molecular junctions have attracted widespread attention because of the potential in the development of novel materials, as well as their application to electronic devices. Recent studies revealed that a highly conductive single benzene molecular junction can be prepared by direct binding to Pt electrodes without using an anchoring group (*1, 2*). The conductance of the Pt/benzene/Pt junction was 0.1-1 G_0, which was comparable to that of the metal atomic contact. The direct binding of a π-conjugated molecule to metal electrodes is a promising technique for obtaining a conducting molecule wire in molecular electronic devices. Although the single Pt/benzene/Pt junction is highly conductive, it does not show a fixed conductance value. The variance of the conductance of the Pt/benzene/Pt junction was a factor of 10 (*1*). In order to develop the single molecular electronics, it is strongly desired to fabricate well-defined single molecular junctions showing high and fixed conductance values. In the case of the Pt/benzene/Pt junction, the junction can take various atomic configurations during stretching because of the strong metal-molecule interaction. In this chapter, I focus on the less reactive metals Au and Ag. I investigated the conductance of the Au and Ag contacts in benzene atmosphere at 10 K. A single benzene molecular junction was formed for the Ag electrode, but there was negligible formation of a benzene molecular junction for the Au electrodes. The single Ag/benzene/Ag junction was characterized by inelastic electron tunneling spectroscopy (IETS) (*1, 3*), which provides information on the vibration mode between the benzene molecule and the Ag electrode.

4.2 Experiments

A single benzene molecular junction was fabricated utilizing the MCBJ technique at 10 K, as mentioned in chapter 3. The benzene molecule was introduced via a heated capillary. The electric conductance of the Au and Ag nano contacts were measured in the presence of the benzene molecule at 10 K.

4.3 Results and discussion

4.3.1 Conductance value and configuration

Figure 4.1 shows a conductance trace and histogram measured during the breaking process of the silver electrode in the presence of the benzene molecule. The conductance trace had a

plateau at 0.25 G_0 (Figure 4.1(a)). The prominent peak at 0.25 G_0 appeared in the corresponding conductance histogram, as shown in Figure 4.1(b). From three different samples, the conductance value was determined to be 0.24 ± 0.08 G_0, which was in agreement with the calculated conductance value (*4*). In order to confirm the presence of the benzene molecule and configuration of the benzene molecule, I measured the *dI/dV* spectra at a conductance value of 0.24 G_0. The observed conductance value agreed with the results of the theoretical calculation study. Figure 4.2 shows the *dI/dV* and d^2I/dV^2 spectrum at the conductance value of 0.2 G_0. I observe an abrupt increase in the conductance at ±42 mV in the *dI/dV* spectrum, and a prominent peak was observed in the d^2I/dV^2 spectrum. The abrupt increase in the conductance originated from the opening of the new conductance channel while exciting the vibration modes in molecular junctions. For clean Ag contacts, the vibration energy was observed around 10 meV and 20 meV in point-contact spectroscopy (*5*). The energy of the internal vibration mode of benzene is higher than 50 meV (*6*). In a previous study, inelastic tunneling spectroscopy was performed for a benzene molecule attached on the surface of Ag (110) (*7*). The vibration mode between benzene and the silver surface was observed at 41 meV when the benzene was absorbed on the kink site. The observed energy agreed with the vibration mode between the silver and benzene molecule. The *dI/dV* spectrum clearly shows that the benzene molecule was placed between silver electrodes.

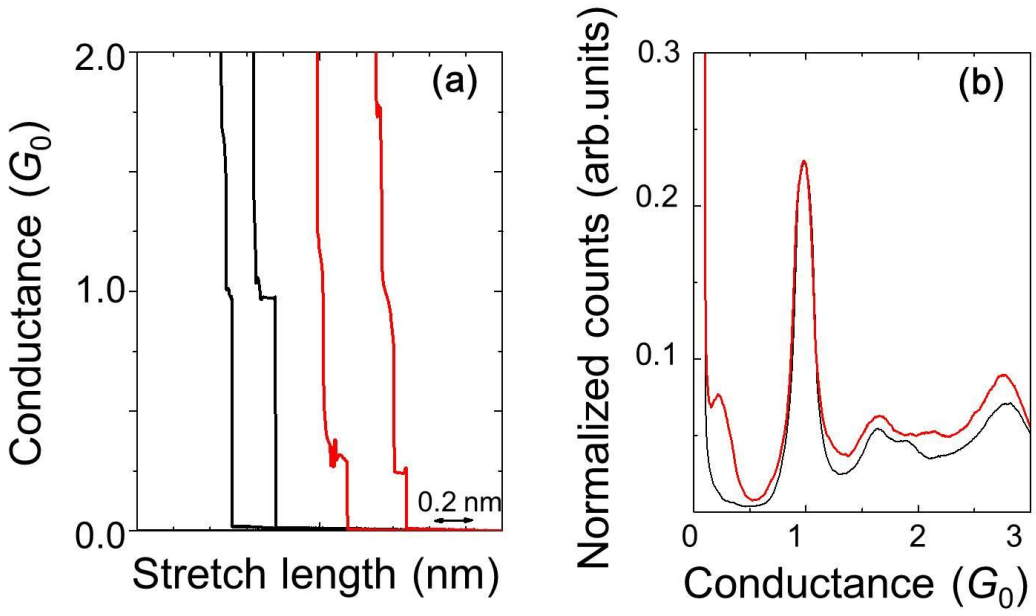

Figure 4.1: (a) Conductance trace measured with the bias voltage of 0.1 V. (b) Conductance histogram constructed from 1000 traces.

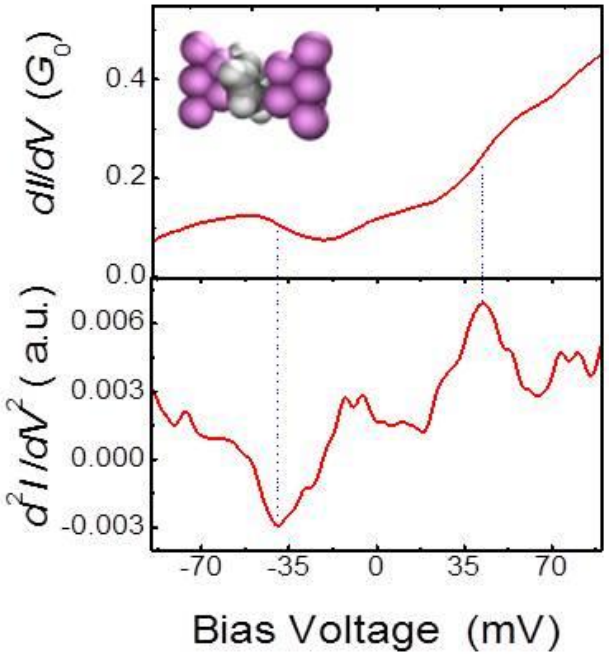

Figure 4.2: *dI/dV* spectrum and d^2I/dV^2 spectrum observed at 0.2 G_0 in the presence of the benzene molecule.

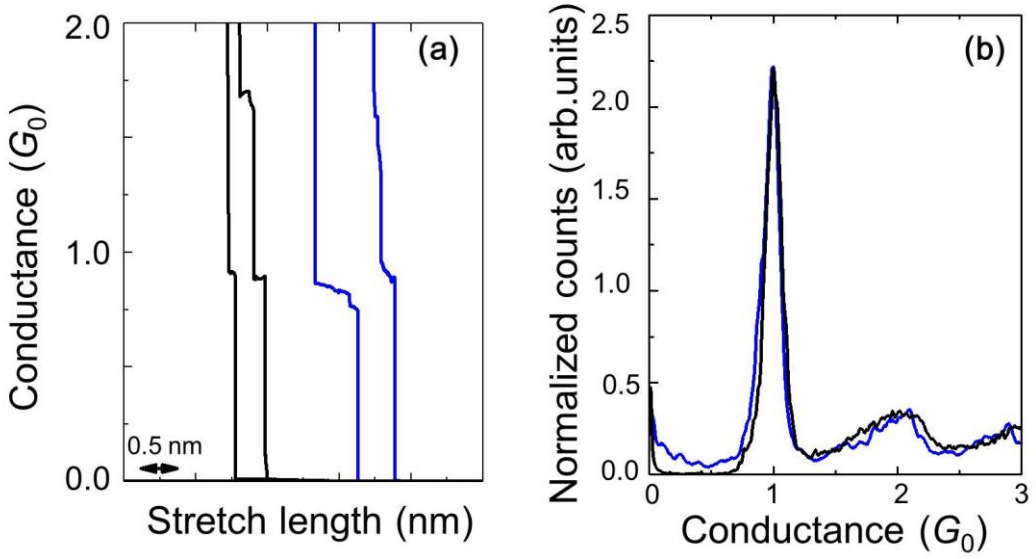

Figure 4.3: Conductance trace and histogram measured for Au electrodes in the presence of benzene. The bias voltage was 100 mV.

On the other hand, neither plateaus nor peaks were observed in the histogram for gold electrodes below 1 G_0 for Au electrodes, which means that a single benzene molecule was not formed using Au electrodes (Figure 4.3). The conductance behavior and *dI/dV* spectra showed that an Ag/benzene/Ag single molecular junction formed with a well-defined conductance value of 0.24 G_0. On the other hand, a single benzene molecular junction was not formed between Au gold electrodes.

4.3.2 High and well-defined conductance value

The observed conductance value of 0.24 G_0 is improved by ten times when compared with an ordinal single molecular junction utilizing anchoring groups. The previous theoretical research revealed the effect of removing the anchoring groups (*8*). In the case of the 1,4-benzenedithiol (BDT) molecule, the BDT molecule is placed between the electrodes with a benzene ring parallel to the electrodes at the most stable configuration. The HOMO mainly contributes to the electron transport in the single molecular junction because the HOMO is located near the Fermi energy (*9*). The HOMO of the BDT molecule consists of a *p* orbital on the sulfur atom, which is perpendicular to the direction of the electron transport. The orbitals that can couple to the *p* orbital on sulfur atoms is limited to the *s* or *p* states of carbon in the molecular back-bone, and these carbon states are not hybridized with sulfur estates, leading to small electron transmission from the benzene ring to the anchoring groups. On the other hand, the benzene molecule is placed between electrodes with a *p* orbital parallel to the bonding direction. In the case of the benzene molecule, LUMO mainly contributes to the electron transport. The geometry at the most stable configuration, as shown in the inset of Figure 4.2, illustrates that the π-conjugated orbitals hybridize directly with the conduction channels at the electrodes. The LUMO of the benzene molecule is effectively hybridized with the orbital on the metal electrodes in a wide energy range. An effective hybridization between the molecule and metal electrodes leads to a high conductance value.

The observed conductance value for the benzene molecule utilizing Ag electrodes was reduced compared with that of benzene between Pt electrodes: The benzene molecule had a conductance value of 1 G_0~0.1 G_0 (*1*). The Pt/benzene/Pt molecular junction was considered, where the benzene molecule showed a conductance value of 1 G_0 at the most stable configuration, and the benzene molecule can take many configurations between Pt electrodes. The interaction between benzene and Pt is considered much stronger than that between benzene and Ag. The bonding energy at the most stable configuration of the benzene molecule to the Pt(111) surface is 1.2 eV (*10*); however, the bonding energy at the most stable configuration of

the benzene molecule to the Ag(111) surface is 0.05 eV(*11*). The larger interaction between the metal and benzene molecule enables benzene to have many configurations between metal electrodes. On the other hand, proper interaction between Ag and benzene formed a single molecular junction only with the most stable configuration. The reason for the difference in the conductance value of Ag/benzene/Ag junction compared with that of the Pt/benzene/Pt junction is explained by the density of the states on the metal atom at the Fermi energy, and the strength of the interaction between the metal and benzene. The density of the states of the Pt at the Fermi energy is larger than that of Ag. The larger density of states and interaction result in a larger Γ in Eq. (2.37), leading to a larger conductance value.

The difference in the formation of the single-molecular junction may have originated from the Au linear atomic chain formation. As mentioned in the previous section, Au tends to form a linear atomic chain, but Ag does not. The benzene molecule was placed between the metal electrodes after the break-down of the Ag atomic contact. On the other hand, when the Au linear atomic chain was formed, a large nanogap was formed for Au electrodes. The benzene molecule was not able to bridge the nanogap after the break-down of the linear atomic chain. As mentioned in the previous paragraph, the benzene should have been attached to the Au electrodes with a benzene ring facing the Au electrodes, as shown in Figure 4.4 (a-b).

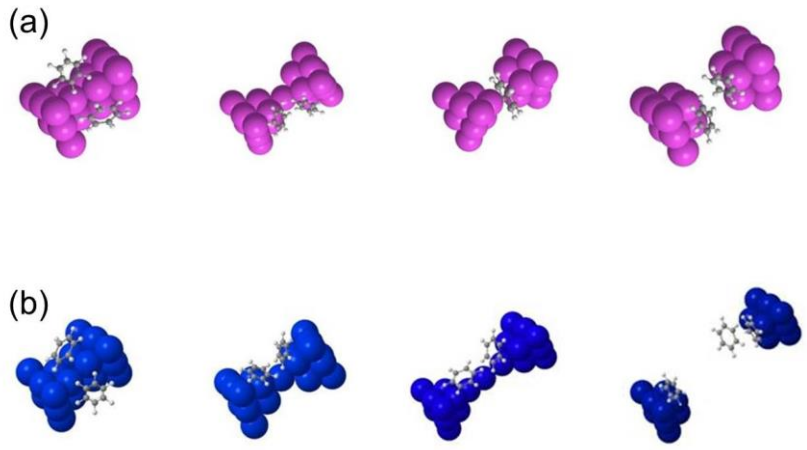

Figure 4.4: Schematic image of the breaking process of the Ag (a) and Au (b) nano contacts.

4.4 Conclusions

I investigated the conductance behavior of the Au and Ag contacts in benzene atmosphere at 10 K. While a single Ag/benzene/Ag junction was formed, there was negligible formation of a single Au/benzene/Au junction. The Ag/benzene/Ag junction showed a fixed conductance value

of 0.24 G_0, indicating the formation of a well-defined single molecular junction. The junction was characterized by IETS, which showed the vibration mode between the benzene molecule and the Ag electrodes. IETS confirmed the formation of a single Ag/benzene/Ag junction. The present study revealed that the moderate metal-molecule interaction is favorable to realizing a well-defined single molecular junction.

References

1. M. Kiguchi, O. Tal, S. Wohlthat, F. Pauly, M. Krieger *et al.*, Highly conductive molecular junctions based on direct binding of benzene to platinum electrodes. *Phys. Rev. Lett.* **101**, 046801 (2008).
2. M. Kiguchi, Electrical conductance of single C_{60} and benzene molecules bridging between Pt electrode. *Appl. Phys. Lett.* **95**, 073301 (2009).
3. M. Kiguchi, R. Stadler, I. S. Kristensen, D. Djukic, J. M. van Ruitenbeek, Evidence for a single hydrogen molecule connected by an atomic chain. *Phys. Rev. Lett.* **98**, 146802 (2007).
4. Y. Li, P. Wei, M. L. Bai, Z. Y. Shen, S. Sanvito *et al.*, Contact geometry and electronic transport properties of Ag-benzene-Ag molecular junctions. *Chem. Phys.* **397**, 82-86 (2012).
5. Y. G. Naidyuk, I. K. Yanson, *Point-contact spectroscopy*. Springer Series in Solid-State Sciences (Springer-Verlag New York, New York, 2005), vol. 145.
6. R. A. Wolkow, M. Moskovits, A comparative study of the electron energy loss spectrum and the surface‐enhance Raman spectrum of benzene adsorbed on silver. *J. Chem. Phys.* **96**, 3966 (1992).
7. J. I. Pascual, J. J. Jackiw, Z. Song, P. S. Weiss, H. Conrad *et al.*, Adsorbate-substrate vibrational modes of benzene on Ag(110) resolved with scanning tunneling spectroscopy. *Phys. Rev. Lett.* **86**, 1050 (2001).
8. J. Ferrer, V. M. Garcia-Suarez, Tuning the conductance of molecular junctions: Transparent versus tunneling regimes. *Phys. Rev. B* **80**, 085426 (2009).
9. H. Song, Y. Kim, Y. H. Jang, H. Jeong, M. A. Reed *et al.*, Observation of molecular orbital gating. *Nature* **462**, 1039-1043 (2009).
10. M. Saeys, M. F. Reyniers, G. B. Marin, M. Neurock, Density functional study of benzene adsorption on Pt (111). *J. Phys. Chem. B* **106**, 7489-7498 (2002).
11. A. Bilic, J. R. Reimers, N. S. Hush, R. C. Hoft, M. J. Ford, Adsorption of benzene on copper, silver, and gold surfaces. *J Chem Theory Comput* **2**, 1093-1105 (2006).

5 Design of interface structure of single molecular junction utilizing spherical endohedral $Ce@C_{82}$ metallofullerenes

In this chapter, I discuss the fabrication of a highly conductive single molecular junction by designing an interface structure. It is expected that the spherical shape would enable us to obtain a well-defined conductance value because the configurational change does not affect the electron transport. Here, I investigate the electron transport of a single endohedral $Ce@C_{82}$ metallofullerene. The endohedral Ce atom modified the electronic states of fullerene and showed the potential for application to electronic devices.

The contents of this chapter have been published in: Satoshi Kaneko, Lu Wang, Guangful Luo, Jing Lu, Shigeru Nagase, Satoru Sato, Michio Yamada, Zdenek Slanina, Takechi Akasaka, Manabu Kiguchi, "Electron transport through single endohedral $Ce@C_{82}$ metallofullerenes" *Physical Review B* 86, 155406 (2012).

5.1 Introduction

Highly conductive molecular junctions have been fabricated by the direct binding of π-conjugated organic molecules to metallic electrodes (Pt, Au, Ag) without the use of anchoring groups (*1-5*).The conductive π orbital directly hybridizes with the orbital of the metal electrodes, resulting in high conductivity. Moreover, the single fullerene molecular junction preferentially shows a fixed conductance value because of its spherical molecular shape in the break-junction process (*3, 5*).

Of the fullerene-related materials, endohedral metallofullerenes (i.e., fullerenes containing metals inside the carbon cage) have received significant attention owing to their remarkable electrical and magnetic properties, and their possible applications in future molecular electronics (*6, 7*). The interaction between the metal and the carbon cage plays an important role in determining their unique properties, which distinguishes them from their counterparts with empty carbon cages. Based on these interests, as well as the unique characteristics of single fullerene molecular junctions, electron transport through a single metallofullerene molecule has been investigated by several groups (*8-12*). Senapati *et al.* investigated the electronic structure and electron transport through a single Gd@C_{82} molecule using theoretical calculations(*8*). The conductance of the single Gd@C_{82} molecular junction was found to be smaller than that of C_{82} because of the reduction of the transmission of the conducting channels caused by the charge localization. Yasutake *et al.* investigated the electron transport through a single Tb@C_{82} molecule on an octanethiol/Au(111) surface via scanning tunneling microscopy (STM) (*9*). Here, the switching of the single Gd@C_{82} molecular orientation caused by the interaction between the electric dipole moment of the Gd@C_{82} molecule and an external electric field was observed. However, to the best of our knowledge, electron transport through the single metallofullerene bridge between metal electrodes has never been directly measured.

In this chapter, I discuss a single metallofullerene molecular junction, and I investigate its electron transport properties using the MCBJ technique in an ultra-high vacuum (UHV). The single Ag/Ce@C_{82}/Ag molecular junction showed a high and fixed conductance value of 0.28 (±0.05) G_0, which was much larger than that of single molecular junctions having anchoring groups (< 0.01G_0), while only half that of the single C_{60} molecular junction of 0.5 G_0. The reduction in the conductance of the single Ce@C_{82} molecular junction compared with that of the single C_{60} molecular junction was explained in terms of the localization of electrons in the C_{82} cage using the *ab initio* quantum transport calculations. In the case of the Au electrodes, the single Ce@C_{82} molecular junction was not formed by the break-junction technique because the

$Ce@C_{82}$ molecule could not be trapped in the large Au nanogap that was formed just after breaking the Au contacts.

5.2 Experiments

Soot containing $Ce@C_{82}$ was prepared according to the reported procedure (*7*) employing the DC arc-vaporization method using a composite anode containing graphite and cerium oxide with the atomic ratio of Ce/C equal to 2.0%. The composite rod was subjected to an arc discharge as an anode under a pressure of 150 Torr He. The raw soot was collected and extracted with 1,2,4-trichlorovenzene solvent for 15 h. The soluble fraction was injected into the HPLC; a PYE column (20 mm × 250 mm i.d.; Cosmosil, Nacalai Tesque Inc.) was used in the first step and a Buckyprep column (20 mm × 250 mm i.d.; Cosmosil, Nacalai Tesque Inc.) in the second step to give pure $Ce@C_{82}$.

A single $Ce@C_{82}$ molecular junction was fabricated by utilizing the MCBJ technique at room temperature, as mentioned in chapter 3. A notched Au or Ag wire was used as electrodes. The MCBJ substrate was placed in the UHV chamber. 1 ML (mono-layer) $Ce@C_{82}$ was deposited on the Au and Ag contacts with a Knudsen cell before stretching the contacts. The distance between the Knudsen cell and the sample was 200 mm. The temperature of the sample was 300 K, and the pressure was kept below 5×10^{-6} Pa during the deposition process. The amount of deposited $Ce@C_{82}$ was monitored with a thickness monitor.

5.3 Results and discussion

5.3.1 Conductance and *I-V* characteristics

Figure 5.1 shows the typical conductance traces and conductance histograms during the breaking of the Au or Ag contacts before and after introduction of $Ce@C_{82}$. The stretch length is the displacement between the stem parts of the metal electrodes that were fixed with epoxy adhesive. Before the introduction of $Ce@C_{82}$, immediately preceding the separation of the Au and Ag electrodes, the conductance was 1 G_0, which corresponded to Au and Ag atomic contacts (*13, 14*). The corresponding conductance histograms showed clear 1 G_0 peaks. Then, after the introduction of $Ce@C_{82}$ to the Ag contacts, the 1 G_0 plateau was elongated in the

conductance traces, and the 1 G_0 peak was enhanced in the conductance histograms. A new sequence of steps appeared in the conductance traces at the lower-conductance region (Figure 5.1(a)). The conductance value of the steps was an integer multiple of 0.2~0.3 G_0. The corresponding conductance histogram showed a peak around 0.3 G_0 (Figure 5.1(b)). There were only a few steps in the conductance traces below 0.1 G_0, and no features were observed in the conductance histograms below 0.1 G_0. These experimental results suggest that the Ce@C_{82} molecule was trapped between the Ag nanogap, and the steps in the traces and peak in the histogram showing values of 1 × and 2 × 0.2~0.3 G_0 could be ascribed to the bridging of one and two Ce@C_{82} molecules between Ag electrodes. From repeated measurements, the conductance of the single Ag/Ce@C_{82}/Ag molecular junctions was determined to be 0.28 (±0.05) G_0, which was much larger than that of single molecular junctions having anchoring groups (< 0.01 G_0) (*15-19*). The appearance of the sharp peak in the conductance histogram also showed the formation of the single molecular junction with a fixed conductance value. The conductance measurements represented a single Ce@C_{82} molecular junction exhibiting a high and fixed conductance value, which was fabricated using direct-binding techniques.

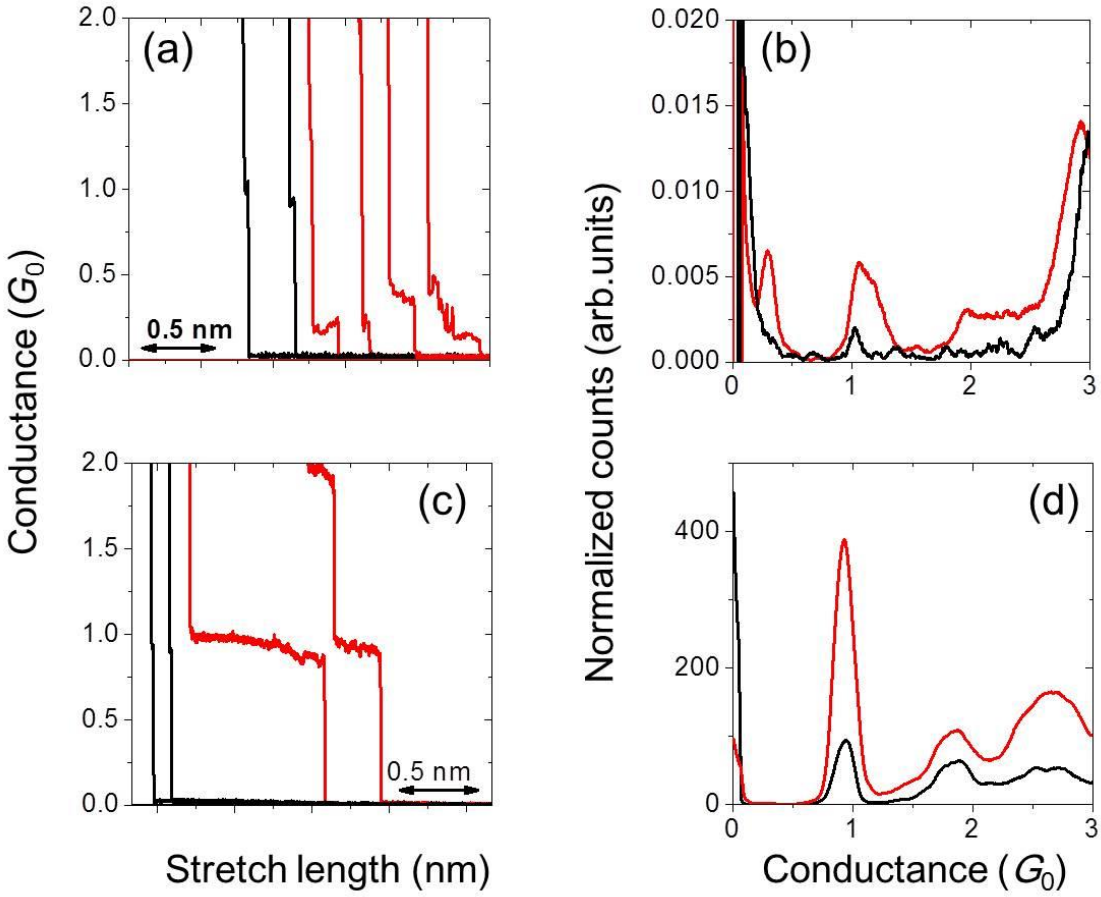

Figure 5.1: Typical conductance traces (a,c) and histograms (b,d) of Ag and Au contacts after the introduction of $Ce@C_{82}$. The black traces and histograms indicate the values obtained for the clean Ag or Au contacts. The metal electrodes were Ag (a,b) and Au (c,d). The intensity of the conductance histograms was normalized with the number of the conductance traces. The bin size was 0.004 G_0.

While the single $Ce@C_{82}$ molecular junctions were formed using Ag electrodes, they were not formed using Au electrodes by the direct-binding technique. No plateaus or features were observed in the conductance traces (Figure 5.1(c)) or histograms (Figure 5.1(d)) below 1 G_0 for Au contacts after the introduction of $Ce@C_{82}$. The elongation of the 1 G_0 plateau in the conductance traces and the enhancement of the 1 G_0 peak in the conductance histogram were observed, as is the case with the Ag contacts after the introduction of $Ce@C_{82}$.

The current-voltage (*I*-*V*) curves were measured for the single $Ag/Ce@C_{82}/Ag$ molecular junctions by a direct current (DC) method, where each curve was recorded at fixed electrodes for a separation at 300 K. The DC voltage was scanned from -0.2 V to +0.2 V (positive scan), or

from +0.2 V to -0.2 V (negative scan) with a step voltage of 0.004 V. In the present study, the *I-V* curves showing similar plots with positive and negative scans were adopted. Figure 5.2 shows the *I-V* curve and the first derivative for the single Ag/Ce@C_{82}/Ag molecular junction, where the *I-V* curves were obtained by averaging the six *I-V* curves. The symmetric upward step in the conductance was observed at ±0.12 V. This conductance enhancement around ±0.12 V was observed for three distinct samples. The conductance enhancement is explained that the Fermi level of the Ag electrode approaches the molecular level of Ce@C_{82} by increasing the bias voltage. Although a simple comparison between the threshold energy and molecular level is not appropriate for a single molecular junction (*20, 21*), there is some relationship between the threshold energy and the energy difference between the molecular orbital and the Fermi level. In the case of a single Au/benzenedithiol/Au molecular junction, a conductance enhancement was observed at a bias voltage of 1 V (*22*). The energy difference between the Fermi level and HOMO (conduction orbital) was 1.2 eV for the Au/benzenedithiol/Au molecular junction, which agreed with the threshold voltage of 1 eV (*23*). Because the energy difference between the Fermi level of the Ag electrode and the conduction orbital of Ce@C_{82} is much smaller than the Au/benzenedithiol/Au molecular junction because of the small energy gap, and the threshold voltage decreased to a low value, which may lead to the appearance of the conductance enhancement at ±0.12 V in *I-V* curves.

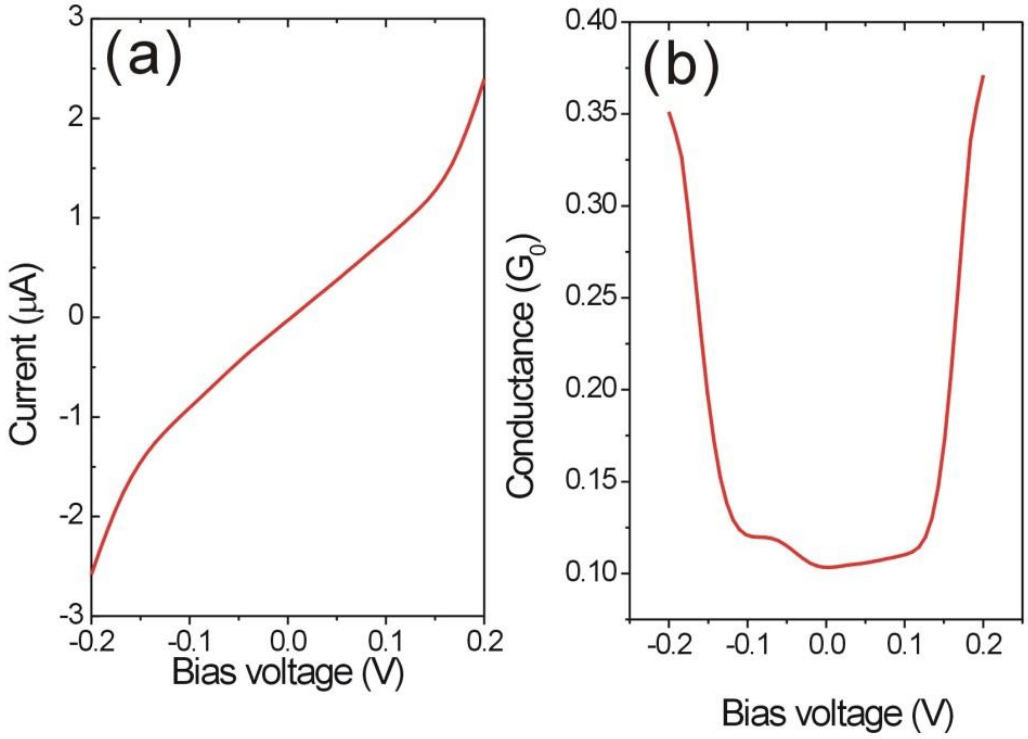

Figure 5.2: (a) *I-V* curve and (b) the first derivative for the single Ag/Ce@C_{82}/Ag molecular junction. The *I-V* curve was measured using a direct current (DC) method at 300 K.

Using a similar direct-binding technique, the conductance of a single C_{60} molecule trapped in the Au and Ag nanogaps has been measured under UHV at 300 K in a previous study (*5*). The conductance values of the single Au/C_{60}/Au junction and Ag/C_{60}/Ag junctions were 0.3(±0.1) and 0.5(±0.1)G_0, respectively. The conductance of the single fullerene molecule was reduced by the introduction of Ce metal, which appeared to be contradictory to the corresponding reduction in the HOMO-LUMO gap (*6*). In the simple-tunneling model (*13, 14*), the conductance of the single molecular junction increases with the decrease in the energy difference between the Fermi level and the conduction orbital related to the HOMO-LUMO gap.

Table 5.1: Summary of the conductance for the single C_{60} and $Ce@C_{82}$ molecular junctions.

System	Conductance
$Au/Ce@C_{82}/Au$	-
$Ag/Ce@C_{82}/Ag$	0.28 (±0.05)G_0
$Au/C_{60}/Au$	0.3(±0.1) G_0
$Ag/C_{60}/Ag$	0.5(±0.1)G_0

5.3.2 Formation process

The $Au/Ce@C_{82}/Au$ junction was not formed, whereas $Au/C_{60}/Au$ and $Ag/Ce@C_{82}/Ag$ junctions were formed. These experimental results can be explained by the difference in the electrode gap distance of the nanogap formed by breaking the metal electrodes. Figure 5.3 shows the length histogram of the 1 G_0 plateau, which corresponds to the Au or Ag atomic contact (*13, 14*). Because the probability of the appearance of the 1 G_0 plateau was very low for a clean Ag contact, the length histograms were not evaluated. For the clean Au, $Au/C_{60}/Au$, and $Ag/Ce@C_{82}/Ag$ junctions, the Au and Ag atomic contacts (1 G_0) broke within 0.3 nm. In contrast, the Au atomic contact could be stretched up to 1.4 nm after the introduction of $Ce@C_{82}$. Most of the junction stretched more than 0.5 nm. Because the Au-Au distance was 0.255 nm, the 1.4-nm stretching breadth indicates the formation of an atomic chain. The theoretical calculation results showed that the interaction between the molecule and the Au electrode was larger for $Ce@C_{82}$ than for C_{60} (see the discussion about the binding energy in the theoretical part). Because of the large interaction between $Ce@C_{82}$ and Au, the Au atomic chain was highly stabilized in the presence of $Ce@C_{82}$ molecules (*24*), while no long atomic chains were formed for the clean Au and Au in the presence of C_{60} at 300 K. After breaking the Au atomic chain, the nanogap was formed between the Au electrodes. The gap size was the sum of the length of the Au atomic chain (< 0.5 nm) and the contraction of the electrode (~0.5 nm) (*25*). The single $Ce@C_{82}$ molecule could not be trapped in the Au nanogap because of its large gap size (~0.9 nm), as shown in Figure 5.3.

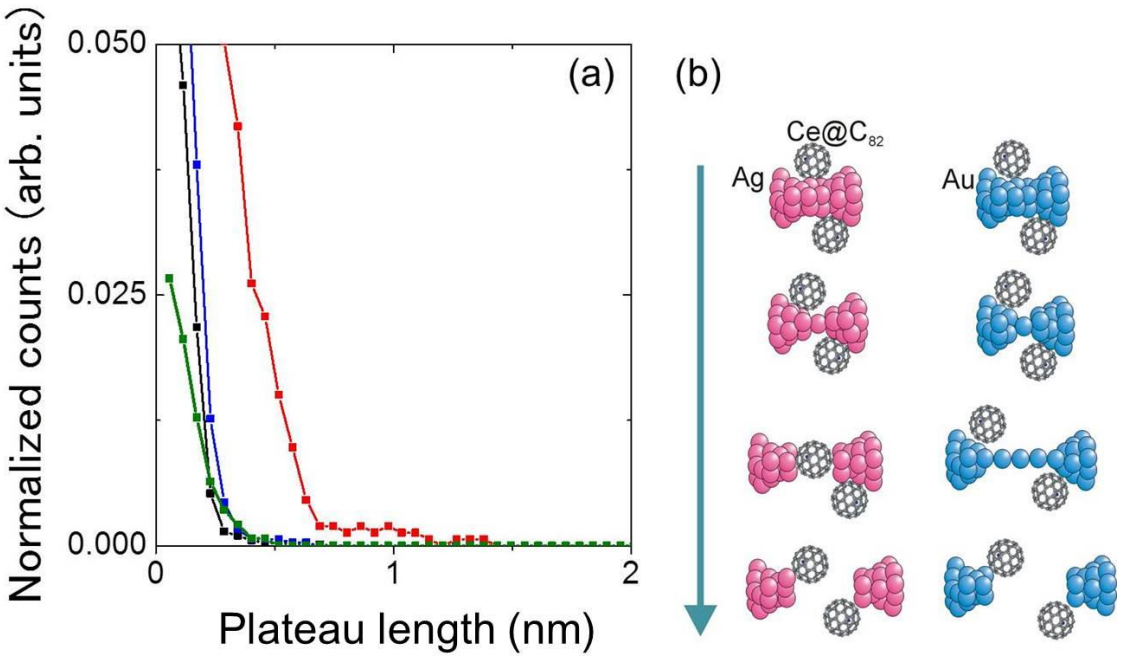

Figure 5.3: (a) Length histogram of the 1 G_0 plateau for the Au and Ag contacts at the bias voltage of 100 mV. The blue, red, green, and black curves are the results of the Au/Ce@C_{82}/Au, Ag/Ce@C_{82}/Ag, Au/C_{60}/Au junction, and clean Au contacts, respectively. The inset shows the typical conductance trace of the Au contacts before the introduction of Ce@C_{82} at a bias voltage of 0.1 V. The intensity of the length histograms was normalized to the number of the conductance traces. The length histograms were constructed without data selection from 1000 conductance traces of breaking metal contacts. (b) Schematic view of the breaking process of the Au and Ag contacts. While a single molecular junction was formed for the Ag contact, no single molecular junction was formed for the Au contact because of the large nanogap.

5.4 Calculations

The following are the first-principle calculations for the single C_{60} and $Ce@C_{82}$ molecular junctions in order to shed light on the experimental observations of single molecular junctions. The structure for free $Ce@C_{82}$ was optimized by employing the density functional theory (DFT) using the B3LYP functional (*26-28*) and the SDD basis (with the SDD effective core potential) for the Ce atom and 3-21G, 6-31G*, 6-31+G*, or 6-311G* basis for the C atom, as implemented in the Gaussian program package (*29*). There was little variation in the structure with the basis set on the C atom, and the optimized free structure was used as a starting geometry in the following conductance calculations. The ground-state structure of $Ce@C_{82}$ has a C2v symmetry, and the Ce atom is located at an off-cage-center position adjacent to a hexagonal ring along the C2 axis of the cage with an average distance of 2.534 Å from the ring carbons at the B3LYP/6-311G*~SDD computational level. The B3LYP functional is the most commonly used DFT functional for fullerene calculations; if it is checked, e.g., at the M06-2X/6-311G*~SDD level (*26, 27*), the shortest Ce-C contact has a similar value of 2.524 Å. In the optimized free $Ce@C_{82}$ structure, more than two electrons are moved from the metal to the cage (measured by the Mulliken atomic charges, although the charge transfer depends on the computational treatment and charge definition (*29*). Transport property calculations were performed using the non-equilibrium Green's function (NEGF) formalism and DFT as implemented in the ATK 2008.10 code (*30, 31*). A single-ζ basis set plus polarization with a mesh cutoff energy of 300 Ry, norm-conserving pseudopotentials, and a local density approximation (LDA) was employed.

In this study, a two-probe model (Figure 5.4) was adopted, where either a C_{60} or $Ce@C_{82}$ molecule was sandwiched between semi-infinite gold or silver electrodes with a (111) surface cross-section. Hexagonal 5 × 5 × 3 unit cells of 14.40 × 14.40 × 7.06 $Å^3$ and 14.45 × 14.45 × 7.08 $Å^3$ containing 75 atoms were used for the Au and Ag electrodes, respectively. The k-points of the electrodes were set to Monkhorst-Pack 1 × 1 × 50. The structures were optimized until the maximum atomic force was less than 0.03 eV/Å. The conductance of the single molecular junction depends on the atomic configuration of the metal electrodes (*13-15*). In the present study, the (111) surface of Au and Ag electrodes was investigated. Although the absolute conductance value depends on the geometry of the surface, the relative conductance value is not sensitive to the geometry of the surface when compared to that of the same geometry of the surface (*32*). Hence, the results obtained from the (111) surface of Au and Ag electrodes should be robust with respect to the geometry of the surface. Two configurations of $Ce@C_{82}$ were considered between electrodes. In configuration-α (Figure 5.4(b)), the C_2 axis of $Ce@C_{82}$

is parallel to the surfaces of the electrodes, whereas in configuration-β (Figure 5.4(c)), the $Ce@C_{82}$ molecule is rotated 90 degrees so that the C_2 axis is perpendicular to the electrode surfaces. The distance between the molecule and the nearest metallic atoms was determined by optimizing the geometry of the molecule on top of the corresponding metallic surface. The relative position of the Ce atom in the carbon cage was also optimized.

The following are the calculations for the binding energy, which is defined as $E_b = (E_s + E_m) - E_{S+M}$, where E_{S+M}, E_S, and E_M are the total energies for the electrode-slabs plus molecule, only the electrode-slabs, and the isolated molecule, respectively. The distance between the molecule and the nearest metallic atoms was determined by optimizing the molecule on top of the corresponding metallic surface. The calculated binding energies of the $Au/C_{60}/Au$, $Au/Ce@C_{82}/Au$ (α), $Au/Ce@C_{82}/Au$ (β), $Ag/C_{60}/Ag$, $Ag/Ce@C_{82}/Ag$ (α), and $Ag/Ce@C_{82}/Ag$ (β) are 1.20 eV, 1.28 eV, 1.31 eV, 1.14 eV, 1.26 eV, and 1.23 eV, respectively. These values were much larger than the physisorption energy, and weak chemical bonds would be formed between $Ce@C_{82}$ and the Au or Ag electrodes.

The electronic properties of electrodes were calculated with periodic conditions using the DFT scheme, and Green's function, together with the self-energy of the central-scattering region, was obtained using the standard NEGF method. An energy criterion of 1×10^{-5} eV was used in all of the self-consistent calculations. Finally, the electric current I under a bias voltage V_{bias} was calculated using the Landauer-Büttiker formula, as shown in Eq. (2.25) (*33*): The molecular-projected self-consistent Hamiltonian (MPSH) energy spectra and the corresponding MPSH orbitals were also calculated to illustrate the mechanism of the electron transport. The calculated conductance values for the $Au/C_{60}/Au$ and $Ag/C_{60}/Ag$ junctions are 0.506 and 0.790 G_0, respectively, compared with the corresponding experimental values of 0.3(±0.1) and 0.5(±0.1) G_0. The calculated conductance of the $Au/Ce@C_{82}/Au$ (α), $Au/Ce@C_{82}/Au$ (β), $Ag/Ce@C_{82}/Ag$ (α), and $Ag/Ce@C_{82}/Ag$ (β) are 0.159, 0.048, 0.212, and 0.063 G_0, respectively. The Mulliken population analysis revealed that 1.10, 1.12, 1.11, and 1.12 electrons were transferred from the Ce atom to the carbon cage in the $Au/Ce@C_{82}/Au$(α), $Au/Ce@C_{82}/Au$(β), $Ag/Ce@C_{82}/Ag$(α), and $Ag/Ce@C_{82}/Ag$(β) configurations, respectively. The conductance histogram of the $Ag/Ce@C_{82}/Ag$ junction showed a single peak at 0.28 G_0, indicating the formation of one stable atomic configuration. The comparison between the calculation and experimental results suggests that the $Ag/Ce@C_{82}/Ag$ (α) junction would be preferentially formed under current experimental conditions. When the $Ag/Ce@C_{82}/Ag$ (β) junction is stretched, the junction would break because of its weak interaction between the benzene

molecule and Ag electrodes at 300 K. Actually, the calculated conductance value (0.212 G_0) of the Ag/Ce@C_{82}/Ag (α) is indeed much closer to the experimental value of 0.28 G_0 than the value of 0.063 G_0 for Ag/Ce@C_{82}/Ag (β). Both the experiments and calculations indicate that the conductance of the Ag/Ce@C_{82}/Ag junction was smaller than that of the Ag/C_{60}/Ag junction; the measured and calculated conductance of the former was smaller than that of the later by 44% and 73%, respectively.

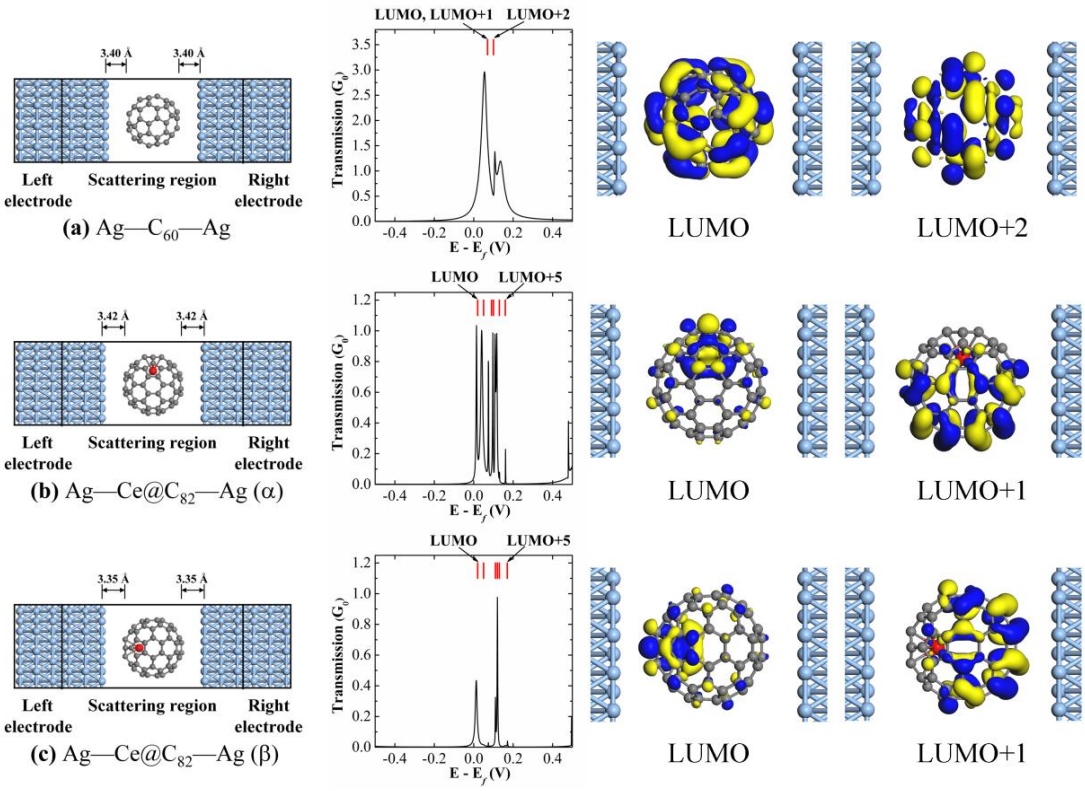

Figure 5.4: Structure models, transmission spectra (black), and MPSH energy spectra (red), and isosurfaces of the MPSH orbitals at zero bias voltage for the systems with (a) Ag/C_{60}/Ag, (b) Ag/Ce@C_{82}/Ag(α), and (c) Ag/Ce@C_{82}/Ag(β). Red ball: Ce; blue ball: Au; grey ball: C.

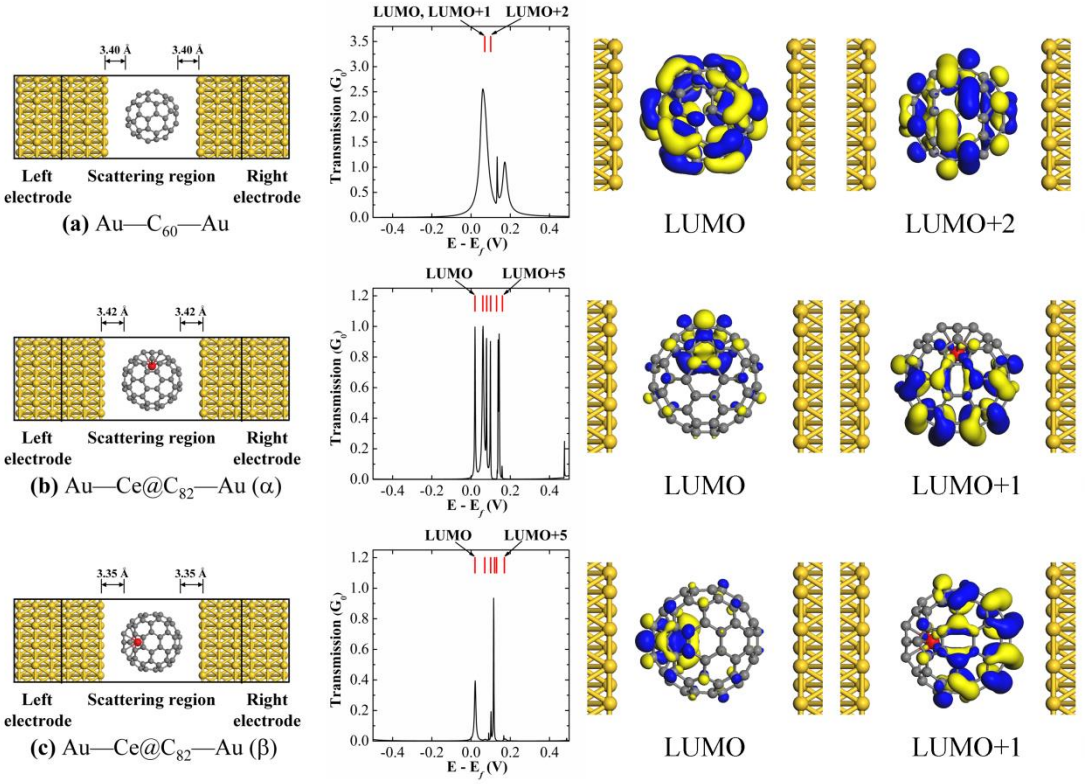

Figure 5.5: Structure models, transmission spectra (black), and MPSH energy spectra (red), and isosurfaces of the MPSH orbitals at zero bias voltage for the systems with (a) Au/C_{60}/Au, (b) Au/Ce@C_{82}/Au(α) , and (c) Au/Ce@C_{82}/Au(β). Red ball: Ce; yellow ball: Au; grey ball: C.

The transmission spectra and MPSH energy spectra of Ag/C_{60}/Ag and Ag/Ce@C_{82}/Ag were investigated, as shown in Figure 5.4. The corresponding results of Au/C_{60}/Au and Au/Ce@C_{82}/Au are shown in Figure 5.5. The electron transmissions are due mainly to contributed by MPSH states above the Fermi level (E_F), which are LUMO – LUMO+2 for C_{60} systems and LUMO – LUMO+5 for Ce@C_{82} systems. The small energy difference between LUMO – LUMO+5 for Ce@C_{82} and the Fermi level may result from the conductance enhancement around ±0.12 V, which was observed for Ag/Ce@C_{82}/Ag (see Figure 5.2). The transmission coefficients of the major peaks in C_{60} systems are about 2.5 times larger than those in the Ce@C_{82} systems. Meanwhile, the transmission peaks in C_{60} systems are also much wider than those of the Ce@C_{82} systems. The transmission coefficients above E_F when C_{60} was used, as opposed to Ce@C_{82}, are attributed to the fact that the electrons are significantly more delocalized in C_{60} than those in Ce@C_{82}. As show, in Figures 5.4 and 5.5, the LUMO and LUMO+1 MPSH of Ce@C_{82} are more localized than those of C_{60}, and this is most likely

because of the interactions between the Ce atoms, which are located at the off-center position of the cage, and the carbon atoms around it. For this reason, the conductance of C_{60} systems was several times larger than that of systems involving Ce@C_{82}. In addition, after performing the rotation of the Ce@C_{82} from configuration-α to configuration-β, it was revealed that the MPSH states contribute less to the connection between the electrodes, and consequently, induce smaller conductance value in configuration-β.

5.5 Conclusions

In this study, I investigated a single Ce@C_{82} molecule bridging between metal electrodes. I fabricated single Ce@C_{82} molecular junctions using the MCBJ technique at 300 K under UHV. The electric conductance of the single Ce@C_{82} molecule bridging between Ag electrodes was 0.28(±0.05) G_0. I successfully fabricated a single metallofullerene molecular junction showing a high and fixed conductance value using the direct-binding technique. The conductance of the single Ce@C_{82} molecule was smaller than that of the single C_{60} molecule bridging between Ag electrodes, which was supported by theoretical calculations. The localization of electrons in the Ce@C_{82} molecule explained the reduction of the conductance of the single Ce@C_{82} molecular junction. While the single Ce@C_{82} molecular junction was formed for the Ag electrodes, it was not formed for the Au electrodes. The Ce@C_{82} molecule could not be trapped in the large nanogap, which was formed after breaking the Au electrodes.

References

1. M. Kiguchi, O. Tal, S. Wohlthat, F. Pauly, M. Krieger *et al.*, Highly conductive molecular junctions based on direct binding of benzene to platinum electrodes. *Phys. Rev. Lett.* **101**, 046801 (2008).
2. M. Kiguchi, T. Takahashi, Y. Takahashi, Y. Yamauchi, T. Murase *et al.*, Electron transport through single molecules comprising aromatic stacks enclosed in self-assembled cages. *Angew. Chem. Int. Ed.* **50**, 5707-5710 (2011).
3. T. Bohler, A. Edtbauer, E. Scheer, Conductance of individual C_{60} molecules measured with controllable gold electrodes. *Phys. Rev. B* **76**, 125432 (2007).

4. C. A. Martin, D. Ding, J. K. Sorensen, T. Bjornholm, J. M. van Ruitenbeek *et al.*, Fullerene-based anchoring groups for molecular electronics. *J. Am. Chem. Soc.* **130**, 13198-13199 (2008).
5. M. Kiguchi, Electrical conductance of single C_{60} and benzene molecules bridging between Pt electrode. *Appl. Phys. Lett.* **95**, 073301 (2009).
6. S. Nagase, K. Kobayashi, T. Akasaka, Endohedral metallofullerenes: New spherical cage molecules with interesting properties. *Bull. Chem. Soc. Jpn.* **69**, 2131-2142 (1996).
7. T. Wakahara, J. Kobayashi, M. Yamada, Y. Maeda, T. Tsuchiya *et al.*, Characterization of Ce@C_{82} and its anion. *J. Am. Chem. Soc.* **126**, 4883-4887 (2004).
8. L. Senapati, J. Schrier, K. B. Whaley, Electronic transport, structure, and energetics of endohedral Gd@C_{82} metallofullerenes. *Nano Lett.* **4**, 2073-2078 (2004).
9. Y. Yasutake, Z. J. Shi, T. Okazaki, H. Shinohara, Y. Majima, Single molecular orientation switching of an endohedral metallofullerene. *Nano Lett.* **5**, 1057-1060 (2005).
10. J. Jiang, B. Gao, Z. P. Hu, W. Lu, Z. Y. Wu *et al.*, Identification of metal-cage coupling in a single metallofullerene by inelastic electron tunneling spectroscopy. *Appl. Phys. Lett.* **96**, 253110 (2010).
11. A. J. Perez-Jimenez, Molecular electronics with endohedral metallofullerenes: The test case of La_2@C_{80} nanojunctions. *J. Phys. Chem. C* **111**, 17640-17645 (2007).
12. A. Strozecka, K. Muthukumar, A. Dybek, T. J. Dennis, J. A. Larsson *et al.*, Modification of the conductance of single fullerene molecules by endohedral doping. *Appl. Phys. Lett.* **95**, 133118 (2009).
13. N. Agrait, A. L. Yeyati, J. M. van Ruitenbeek, Quantum properties of atomic-sized conductors. *Phys. Rep.* **377**, 81-279 (2003).
14. J. C. Cuevas, E. Scheer, *Molecular Electronics: An Introduction to Theory and Experiment* World Scientific Series in Nanotechnology and Nanoscience (World Scientific Publishing Co. Pte. Ltd., Singapore, 2010).
15. F. Chen, X. L. Li, J. Hihath, Z. F. Huang, N. J. Tao, Effect of anchoring groups on single-molecule conductance: Comparative study of thiol-, amine-, and carboxylic-acid-terminated molecules. *J. Am. Chem. Soc.* **128**, 15874-15881 (2006).
16. Y. S. Park, A. C. Whalley, M. Kamenetska, M. L. Steigerwald, M. S. Hybertsen *et al.*, Contact chemistry and single-molecule conductance: A comparison of phosphines, methyl sulfides, and amines. *J. Am. Chem. Soc.* **129**, 15768-15769 (2007).

17. L. Venkataraman, J. E. Klare, I. W. Tam, C. Nuckolls, M. S. Hybertsen *et al.*, Single-molecule circuits with well-defined molecular conductance. *Nano Lett.* **6**, 458-462 (2006).
18. A. Mishchenko, L. A. Zotti, D. Vonlanthen, M. Burkle, F. Pauly *et al.*, Single-molecule junctions based on nitrile-terminated biphenyls: A promising new anchoring group. *J. Am. Chem. Soc.* **133**, 184-187 (2011).
19. W. Haiss, C. S. Wang, I. Grace, A. S. Batsanov, D. J. Schiffrin *et al.*, Precision control of single-molecule electrical junctions. *Nat. Mater.* **5**, 995-1002 (2006).
20. E. H. Huisman, C. M. Guedon, B. J. van Wees, S. J. van der Molen, Interpretation of transition voltage spectroscopy. *Nano Lett.* **9**, 3909-3913 (2009).
21. S. Y. Guo, J. Hihath, I. Diez-Perez, N. J. Tao, Measurement and statistical analysis of single-molecule current-voltage characteristics, transition voltage spectroscopy, and tunneling barrier height. *J. Am. Chem. Soc.* **133**, 19189-19197 (2011).
22. M. A. Reed, C. Zhou, C. J. Muller, T. P. Burgin, J. M. Tour, Conductance of a molecular junction. *Science* **278**, 252-254 (1997).
23. P. Reddy, S. Y. Jang, R. A. Segalman, A. Majumdar, Thermoelectricity in molecular junctions. *Science* **315**, 1568-1571 (2007).
24. H. X. He, C. Shu, C. Z. Li, N. J. Tao, Adsorbate effect on the mechanical stability of atomically thin metallic wires. *J. Electroanal. Chem.* **522**, 26-32 (2002).
25. J. W. Zhao, K. Murakoshi, X. Yin, M. Kiguchi, Y. Guo *et al.*, Dynamic characterization of the postbreaking behavior of a nanowire. *J. Phys. Chem. C* **112**, 20088-20094 (2008).
26. A. D. Becke, Density-functional exchange-energy approximation with correct asymptotic-behavior. *Phys. Rev. A* **38**, 3098-3100 (1988).
27. Y. Zhao, D. G. Truhlar, Density functionals with broad applicability in chemistry. *Acc. Chem. Res.* **41**, 157-167 (2008).
28. M. J. Frisch, G. W. Trucks, H. B. Schlegel, G. E. Scuseria, M. A. Robb *et al.*, *Gaussian 09* (Gaussian, Inc., 2009.).
29. V. Zolyomi, J. Koltai, J. Kuerti, S. Pekker, Theoretical study of the electronic structure of fullerene-cubane cocrystals. *Phys. Rev. B* **78**, 115405 (2008).
30. J. Taylor, H. Guo, J. Wang, Ab initio modeling of quantum transport properties of molecular electronic devices. *Phys. Rev. B* **63**, 245407 (2001).
31. M. Brandbyge, J. L. Mozos, P. Ordejon, J. Taylor, K. Stokbro, Density-functional method for nonequilibrium electron transport. *Phys. Rev. B* **65**, 165401 (2002).

32. Z. Li, D. S. Kosov, Nature of well-defined conductance of amine-anchored molecular junctions: Density functional calculations. *Phys. Rev. B* **76**, 035415 (2007).
33. S. Datta, *Electronic Transport in Mesoscopic Systems*. (Cambridge University Press, Cambridge, 1995).

6 Anchoring groups enclosed in π-conjugated system in N_2 molecule

In the previous chapter, the fabrication of a single molecular junction with a high and well-defined conductance value was discussed by designing the interaction between the molecule and metal and the spherical structure. In order to control the electric property of the single molecular junction, it is important to control the interface structure of single molecular junctions. The anchoring groups enclosed in the π-conjugated system fixed the connecting point with high conductivity. Here, I focus on the π-conjugated system with a connecting part. Nitrogen is one of the promising anchoring groups having a fixed conductance value, as mentioned in the Introduction section. In this chapter, I focus on the nitrogen molecule, which has a π electron and a lone pair. First, I investigate the formation of the molecular junction depending on the interaction between the molecule and metals.

The contents of this chapter have been published in: Satoshi Kaneko, Jinjiang Zhang, Jianwei Zhao, Manabu Kiguchi, "Electronic conductance of platinum atomic contact in a nitrogen atmosphere" *The Journal of Physical Chemistry C* 117, 9903-9907 (2013), and Satoshi Kaneko, Yuuga Nakamura, Jingiang Zhang, Xiongbo Yang, Jianwei Zhao, Manabu Kiguchi, "Formation of single Cu atomic chain in nitrogen atmosphere" *The Journal of Physical Chemistry C* 119, 862–866 (2015).

6.1 Introduction

In the previous section, the highly conductive single molecular junction showed a fixed value utilizing a π-conjugated molecule by properly designing the interface. The next step is to control the electric property of a single molecule by controlling the interface structure. In order to control the interface structure, it is important to fix the anchoring point, which keeps its electric property unless a proper perturbation is applied. It has been reported that nitrogen is one of the most promising anchoring groups that show a fixed conductance value. In this chapter, I focus on the N_2 molecule, which is the simplest molecule that has an anchoring group in the π-conjugated system.

The N_2 molecule is also useful as an impurity in metal linear atomic chains (LACs), and the incorporated or adsorbed molecule modifies the electric property of the metal atomic chain. An interesting interaction and adsorption properties could appear for the metal nanowires, because the atomic and electronic structures of the metal nanowires are different from those of bulk metals. This is because of the decrease in the number of neighboring atoms. A previous study revealed the formation process of the Au atomic wire in a UHV utilizing transmission electron microscopy (TEM). Interestingly, the interatomic distance between Au atoms was extremely long (0.35~0.4 nm) compared with that of bulk (0.25 nm) (*1*). The long interatomic distance has been explained by the formation of a zigzag structure, as well as the presence of impurity atoms, such as C, H, or O in the nanowire. The theoretical calculation showed that the metal nanowire could be stabilized by the adsorption of atoms or molecules on the metal nanowire, or the incorporation of the atoms or molecules into the nanowire. The experimental formation of Ag and Co atomic wires in the presence of hydrogen at 4 K has been reported, although clean silver and cobalt do not form atomic wires (*2-4*). In the case of Pt nanowires, the formation of the single hydrogen molecular junction was revealed by PCS and IETS, shot-noise measurements, and theoretical calculations (*5, 6*). When N_2 molecules interact with transition metals such as Pt, the reactivity of N_2 molecules is enhanced, (e.g., ammonium synthetic reaction (*7*)). The reactivity of N_2 could increase further for metal nanowires because of the decrease in the number of neighboring atoms. It is expected that the electrical property of nitrogen, which is inert in isolated states, will significantly vary. On the other hand, the interaction between Cu nanowire and nitrogen has been investigated using an *ab initio* total energy calculation (*8, 9*). The calculation results predicted a tendency of N and N_2 to make strong bonds in Cu nanowires, leading to the formation of longer Cu atomic wires.

In this chapter, I consider Pt and Cu nanowires in the presence of N_2 molecules. Pt was more

reactive than Cu because of the higher density of states at the Fermi level (*10-14*). The geometry and electronic structures were investigated using an MCBJ technique and theoretical calculation. The conductance and vibration spectroscopy measurement combined with the theoretical study revealed the formation of the single N_2 molecular junction. The conductance of the single N_2 molecular junction was 1 G_0, which was close to that of the metal atomic contact.

6.2 Experiments

Experiments were performed using the MCBJ technique at 10 K, as mentioned in chapter 3. A notched Pt and Cu wire (0.1 mm in diameter, 10 mm in length) were used for the electrode, as mentioned previously. N_2 gas (>99.9995 vol.%, several μmol) was introduced via a heated capillary.

6.3 Results and discussion

6.3.1 Pt electrodes

Figure 6.1(a) shows typical conductance traces representing variations in the conductance of Pt contacts during the breaking process of the metal wire. A stepwise fashion represented the atomic structural transition of the contact. The plateau at 1.5 G_0 corresponded to the conductance of a Pt atomic contact, which agreed with the previous result (*15*). As mentioned in chapter 2, the electrical conductance through the metal atomic contact was expressed by $G = 2e^2 / h\sum T_i$ where T_i is the transmission-coefficient probability of the *i*-th conductance channel. The Pt atomic contact has a conductance of 1.5-2 G_0 (*16*), depending on the atomic configuration of the contact. In the presence of nitrogen, a plateau was observed at 1 G_0 in addition to the plateau at 1.5 G_0. The conductance histogram constructed from one thousand conductance traces showed peaks at both 1 G_0 and 1.5 G_0 (Figure 6.1(b)). The appearance of the 1 G_0 peak indicated that the atomic configuration with conductance of 1 G_0 is more likely to be formed during the breaking process.

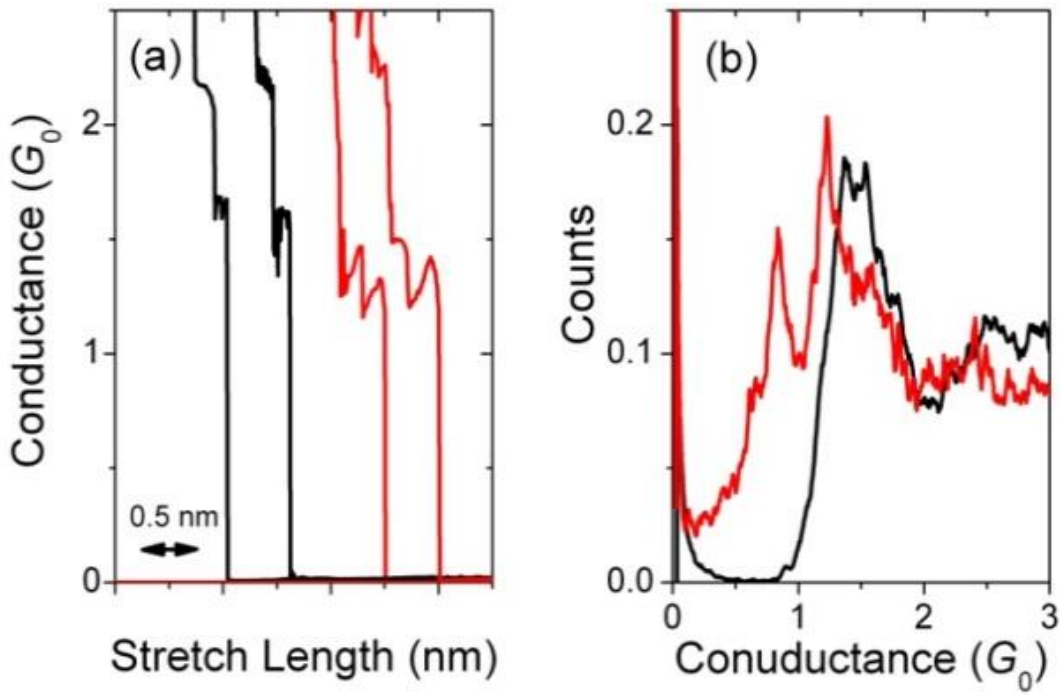

Figure 6.1: (a) Conductance trace before (black) and after (red) the introduction of N_2 gas, measured at the bias voltage of 100 mV. (b) Conductance histogram constructed from 1000 conductance traces before (black) and after (red) introduction of N_2 gas. The bin size was 0.004 G_0. The count was normalized by the number of total breaking processes.

In order to investigate the atomic configuration of the stable atomic contact with 1 G_0, the *dI/dV* and d^2I/dV^2 spectra were measured. Figure 6.2(a) represents a typical *dI/dV* spectrum measured at a conductance value around 1 G_0. A symmetric conductance enhancement was observed around ± 40 meV, which originates from electron-vibration interaction in the contact (*5*, *10*, *11*, *17*).

In order to accurately determine the vibration energy, 41 *dI/dV* spectra were collected for the contact in the conductance regime ranging from 0.05 G_0~1.2 G_0, resulting in the energy histogram presented in Figure 6.2(b). The distribution could be fitted by a Gaussian function, whose peak center was 43 meV and full-width at half maximum was 8 meV. As the energy of 43 meV was larger than the phonon energy of Pt (*18*), and much smaller than the energy of N_2 internal vibration modes (*19*), the vibration mode of 43 meV would correspond to the vibration mode between the Pt electrode and nitrogen. The existence of nitrogen in the Pt contact was revealed by the vibration spectroscopy. Further discussion about the atomic structure and vibration mode are given in the next section related to theoretical calculation part.

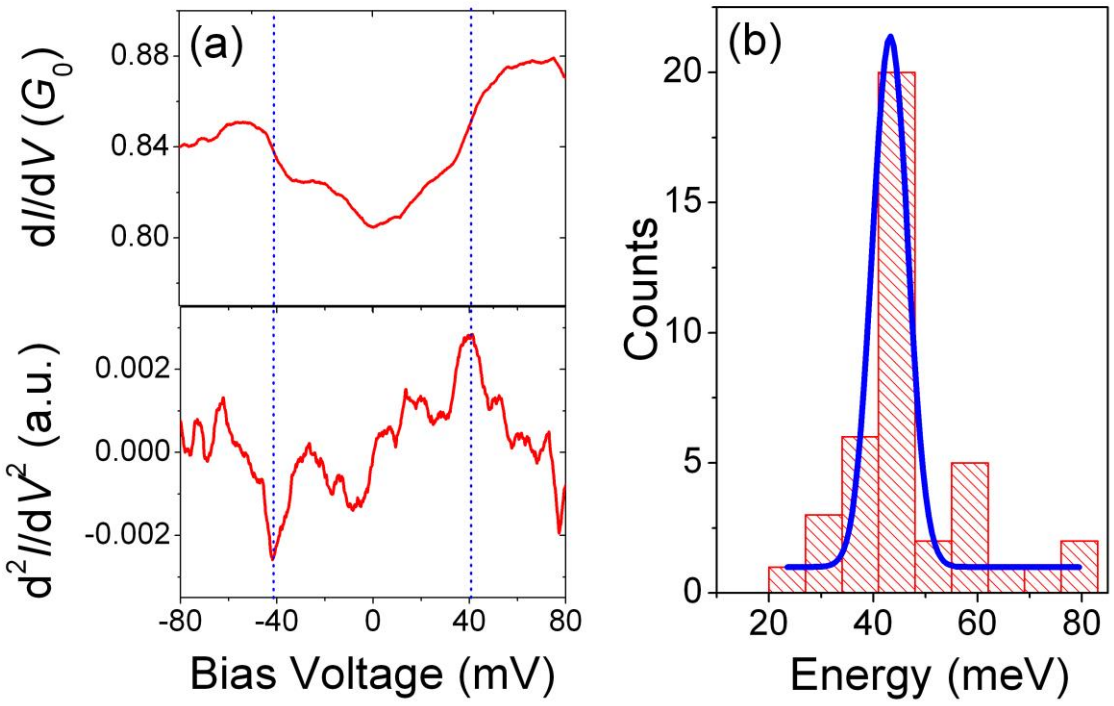

Figure 6.2: (a) Typical *dI/dV* spectrum of the Pt-N_2 system showing a conductance of close to 1 G_0. (b) Histogram of the vibration energy of the Pt-N_2 system constructed from 41 *dI/dV* spectra.

It is worth discussing the shape of the *dI/dV* and d^2I/dV^2 spectra. While the symmetric conductance enhancement was observed in the *dI/dV* spectrum, as in Figure 6.2(a), the conductance suppression was also observed in the *dI/dV* spectrum. Figure 6.3 shows the distribution of the conductance enhancement and suppression in the *dI/dV* spectrum for the Pt-N_2 system as a function of the conductance and energy in the conductance range from 0.05 G_0 to 1.2 G_0. Conductance enhancement was observed more frequently than conductance suppression. There was no correlation between the conductance and shape of the *dI/dV* spectrum. The previous theoretical study predicted that the conductance enhancement is observed if the transmission probability is below 0.5, and conductance suppression is observed otherwise (*20*). This phenomenon was observed in H_2O (*21*) and benzendithiole (*22*). The discrepancy may be explained by the difference in the number of channels. In systems such as H_2O molecules, electron transport occurs through a single channel and the molecule-metal coupling is symmetric (*20-22*). On the other hand, in a Pt-N_2 system, more than one channel contributes to

the electron transport, as shown in Figure 6.6 above. The existence of multi channels may affect the shape of the *dI/dV* spectrum. Based on theoretical calculations conductance enhancement can be induced by nontransmitting *d* channels, which are coupled to the transmitting *s* channel via transverse modes in the Pt-H_2 system (*23*).

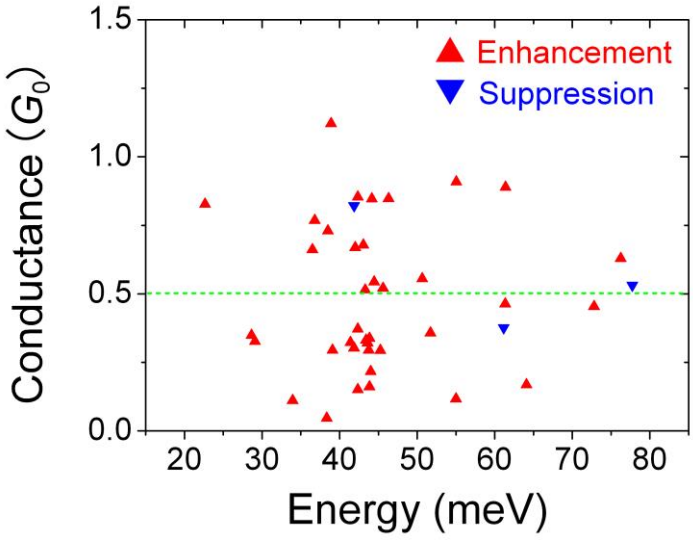

Figure 6.3: Distribution of the conductance enhancement and suppression in the *dI/dV* spectrum for the Pt-N_2 system as a function of the conductance and energy for conductance values ranging from 0.05 G_0 to 1.2 G_0.

In order to investigate the structure of the molecular junction, theoretical calculations were performed for four possible structures (inset in Figure 6.4). The inset of Figure 6.4 shows the structural models investigated in this study. The left and right Pt electrodes were constructed from metal bulk oriented in the (111) direction and an atomically sharp tip. The tips were modeled as 4-atom tetrahedrons. In the model named "atomic" (Pt-N), the atomic nitrogen was placed between Pt electrodes. The other models (Pt-N_2) represent the N_2 molecule placed between the Pt electrodes with its molecular axis vertical ("bridge," "vertical") or parallel ("parallel") to the junction axis. While the N_2 molecule was placed on the line of two top Pt atoms in "vertical," the N_2 molecule was placed above the Pt-Pt bond in "bridge." The geometry of each model was optimized using first-principle computer code Atomistix Toolkit (ATK) software (quantum-wise A/S) (*24*, *25*), during which the bulk of electrodes was fixed while the N atom (or N_2 molecule) and the two tips were relaxed. The total energy of the system was calculated as a function of the distance between electrodes, where the distance was the length between two Pt atoms at the top of the tetrahedrons. The electron-transport behavior of the

models at stable distances was also investigated. During these calculations, double-ξ with a polarization basis set and single-ξ with a polarization basis set were chosen for the N atoms and Pt atoms, respectively.

Models that consist only of an N atom (or N_2 molecule) and two 4-atom Pt tetrahedrons were used for the calculation of the vibration energy, before which geometric optimization was carried out at a b3lyp level using lanl2dz basis set with Gaussian software (*26*). During the geometric optimization, each 4-atom Pt tetrahedron was kept as a group, while the distance between two tetrahedrons and the configuration of the N atom (or N_2 molecule) was relaxed.

Figure 6.4 represents the total energy of the junctions as a function of the distances. The stable states appeared at 3.65 Å, 2.50 Å, 4.29 Å, and 5.03 Å for "atomic," "bridge," "vertical," and "parallel" configurations, respectively. The "bridge" and "parallel" configurations were much more stable than that of "vertical" configuration. The conductance was calculated to be 1.34, 2.91, 1.12, and 0.98 G_0 for "atomic," "bridge," "vertical," and "parallel" configurations, respectively. The vibration energy for each junction was investigated. Table 1 shows a summary of the vibration modes around 40 meV, which was observed in the present study. For the "atomic" and "vertical" configurations, there were no vibration modes around 40 meV. For the "parallel" configuration, there were three vibration modes (42.2, 44.1, and 45.0 meV) around 40 meV. These vibration modes are depicted in Figure 6.5. Based on the experimental and theoretical calculation, the Pt-N_2 system showing a conductance of close to 1 G_0 was assigned to be the "parallel" configuration. Theoretical calculation also revealed that the N-N bond was stretched for the Pt-N_2 junction. While the N-N bond is 1.09 Å for an isolated N_2 molecule, the N-N bond was 1.16 Å in the molecular junction because of the interaction between the molecule and metal electrodes.

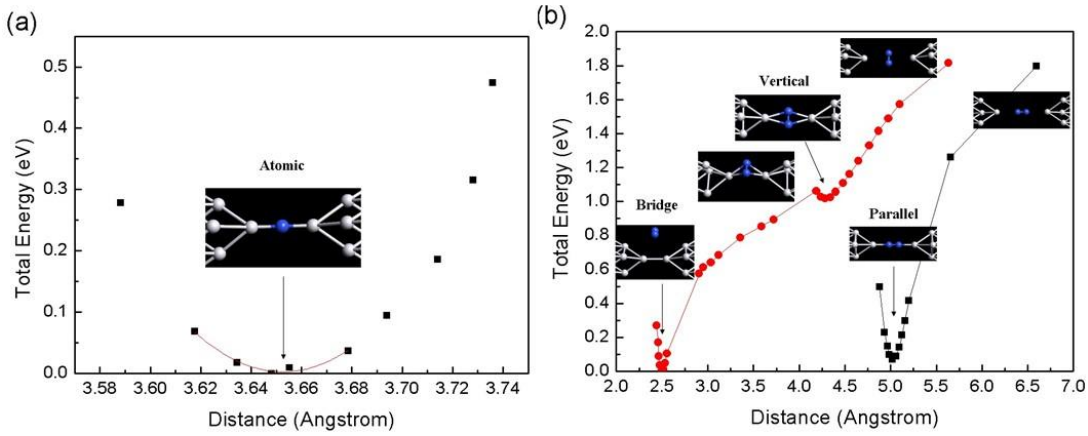

Figure 6.4: Total energy of (a) Pt-N and (b) Pt-N_2 as a function of the distance between electrodes.

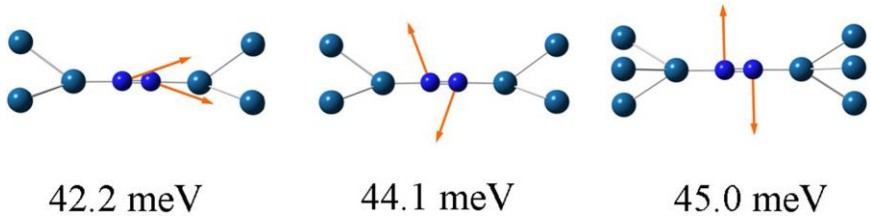

Figure 6.5: Three possible vibration modes having a "parallel" configuration.

Table 6.1: Summary of calculations

Model	Atomic	Bridge	Vertical	Parallel
Most Stable Distance (Å)	3.65	2.50	4.29	5.03
Conductance at 0V (G_0)	1.34	2.91	1.12	0.98
Vibration Modes near 40 meV	-	37.4, 44.1 meV	-	42.2, 44.1, 45.0 meV

In order to obtain a better understanding of the conductance at zero bias, the transmission coefficient at the Fermi level was investigated. It was determined that two dominant channels transfer electrons through the junction, and their transmission probabilities are 0.458 and 0.454, respectively. From the transmission spectrum (Figure 6.6a), It was roughly predicted that these two dominant channels originate from the tail of the broad peak at -0.1 eV. Figure 5b shows the

main channels of -0.1eV; it is determined that these π-type channels are from the coupling between orbitals (d_{xz} and d_{yz}) of the Pt atom and orbitals (p_x and p_y) of the N atom (*27*), which supports the *dI/dV* spectrum behavior.

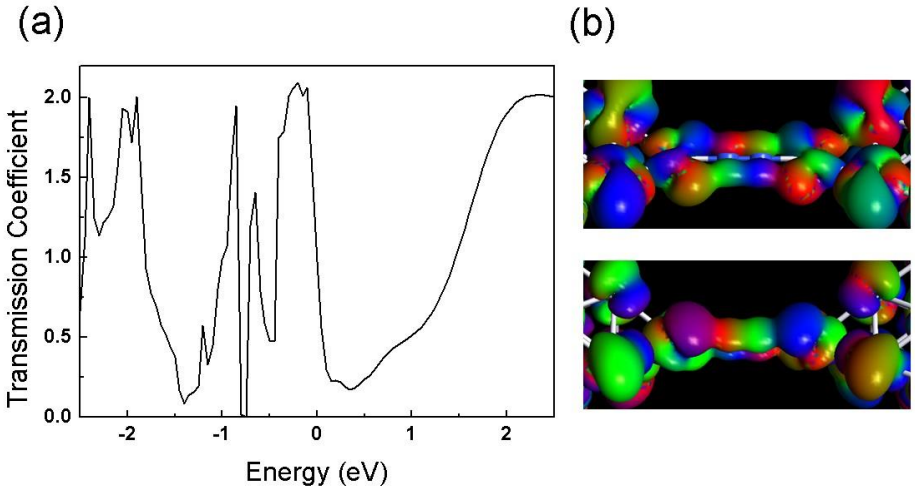

Figure 6.6: (a) Transmission spectrum at zero bias, (b) Two dominant channels of the peak at -0.1 eV.

6.3.2 Cu electrodes

Figure 6.7(a) represents conductance traces of the Cu contacts measured during the breaking process. Before the introduction of nitrogen, a plateau was observed at 1.0 G_0, representing the formation of the Cu atomic contact. The 1.0 G_0 peak was observed in the conductance histogram, as shown in Figure 6.7(b). After the introduction of N_2, a plateau was observed around 0.9 G_0 in the conductance traces, and a prominent peak was observed at 0.9 G_0 in the corresponding histogram. The conductance of the center of the peak was estimated to be 0.86±0.06 G_0 by averaging the conductance values for five distinct samples. The intensity of the 0.86 G_0 peak for the N_2/Cu contacts increased twofold compared with the 1.0 G_0 peak for the Cu contacts. The peak shift and enhancement of the peak intensity in the conductance histogram indicate that the conductance of the Cu atomic junction is reduced and stabilized after the introduction of N_2. Because the plateau length around 1.0 G_0 observed after the introduction of N_2 is elongated in Figure 6.7(a), it is considered that the elongation of the plateau length contributes to the enhancement of the peak intensity in the conductance histogram. In order to estimate the plateau length quantitatively, a plateau length histogram was constructed. The plateau length was defined as the length between the first and last points showing a conductance

of 0.67–1.0 G_0 in the conductance traces. Figure 6.8 shows plateau length histograms obtained before and after the introduction of N_2. Before the introduction of N_2, a single prominent peak is observed, and the plateau length is a maximum of 0.5 nm. This behavior represents Cu form only atomic contact but hardy form atomic chain without molecule, which agrees with previous study (*2, 28*). On the other hand, the plateau was stretched to a maximum of 1.5 nm, and multiple peaks were observed after the introduction of N_2. The plateau length histogram was fitted with four Gaussian functions. The average distance between the peaks is 0.25 ± 0.06 nm, which is close to the interatomic distance of bulk 0.25 nm Cu crystal. The elongation of the plateau length and multiple peaks in the plateau length histogram indicates that Cu forms a single atomic chain with a length of 2–3 atoms.

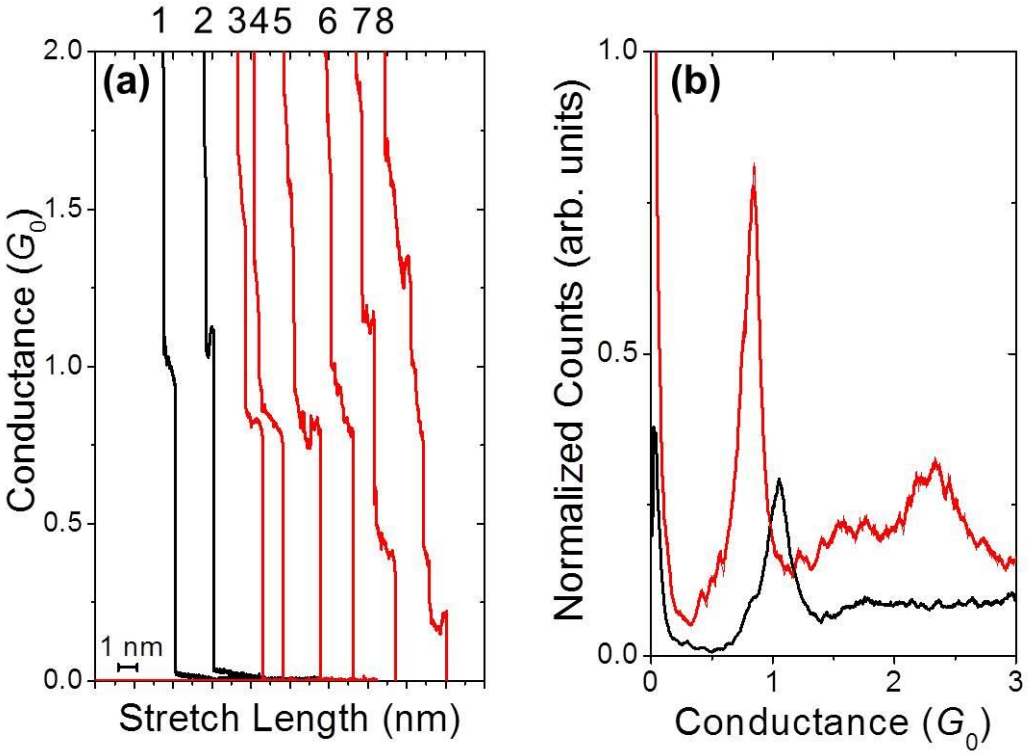

Figure 6.7: Conductance traces (a) and histograms (b) of Cu contacts before (black) and after (red) the introduction of N_2. Bias voltage: 50 mV.

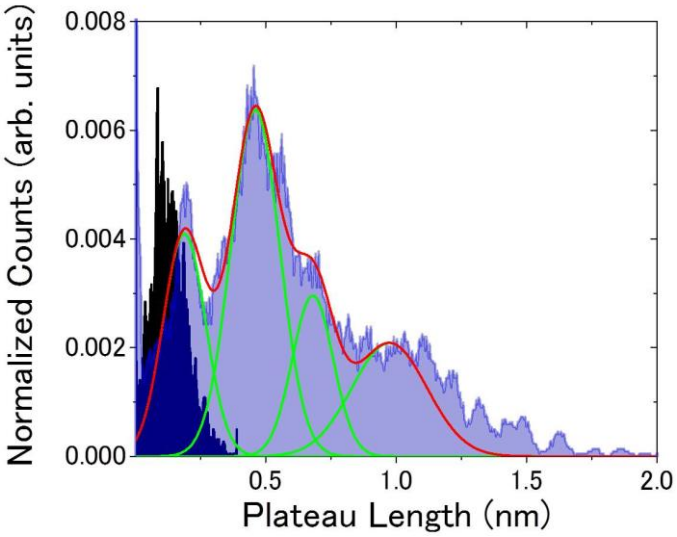

Figure 6.8: Plateau length histogram before (black) and after (blue) the introduction of N_2. Green and Red line: fitting by Gaussian function.

Next the formation of the linear Cu atomic chain was investigated. Figure 6.9 shows a schematic of the simulation, in which we used several groups of models to describe the possible structures appearing at different stages during the elongation of a Cu LAC in N_2 atmosphere. In the models, the left and right Cu electrodes were constructed from metal bulk oriented in the [111] direction, which was also used in conductance calculations. Tips were modeled as two opposite tetrahedrals, which represent the broken section of the nanowire. The N_2 molecule adhered to the broken section in two ways, i.e., parallel or vertical to the stretch direction. The models were stretched quasi-statically with the first-principle computer code Atomistix Toolkit (ATK) software.

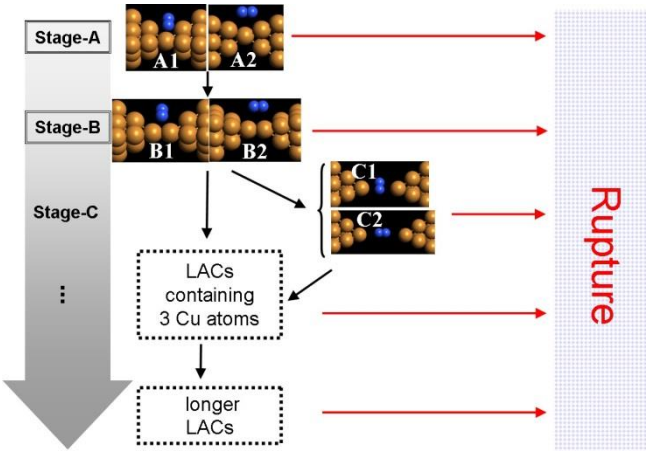

Figure 6.9: Schematic diagram for the simulation of a stretch of the Cu single atomic chain in N_2 atmosphere. The arrows show the possible routes.

The evolution of the energy and conductance of the models belonging to different stages are plotted in Figure 6.10. The stretch length is defined as the distance between electrodes. The total energy profile is presented by setting the lowest energy point as zero. As models A1 and A2 have one fewer Cu atoms than the others, neither of them is plotted in the figure. The V-shaped energy curves reflect the fact that there is an energy barrier between stages. If there is a weak connection in the LAC, it cannot be transformed to a new stage, and will rupture. By connecting three different stages, a typical conductance trace similar to those in Figure 6.7(a) was produced. The calculated trace has a plateau at 0.9 G_0, which agrees with the conductance measurement. The plateau in the cyan region contains a small portion of stage A and a large portion of stage B, which provides possible atomic structures corresponding to the conductance steps around 0.86 G_0, which was observed experimentally. In other words, the conductance peak at 0.86 G_0 in Figure 6.7(b) corresponds to the structure in which the Cu atomic junction is attached to the N_2 molecule, while clean LACs (atomic contacts) showed conductance values around 1.0 G_0. The conductance steps observed around 0.2–0.5 G_0 (the 7th and 8th traces in Figure 6.7) may be explained by structures such as C1 or C2, in which N_2 is inserted between Cu atoms; nevertheless, such a structure did not contribute to the peak in the conductance histogram of Figure 6.7.

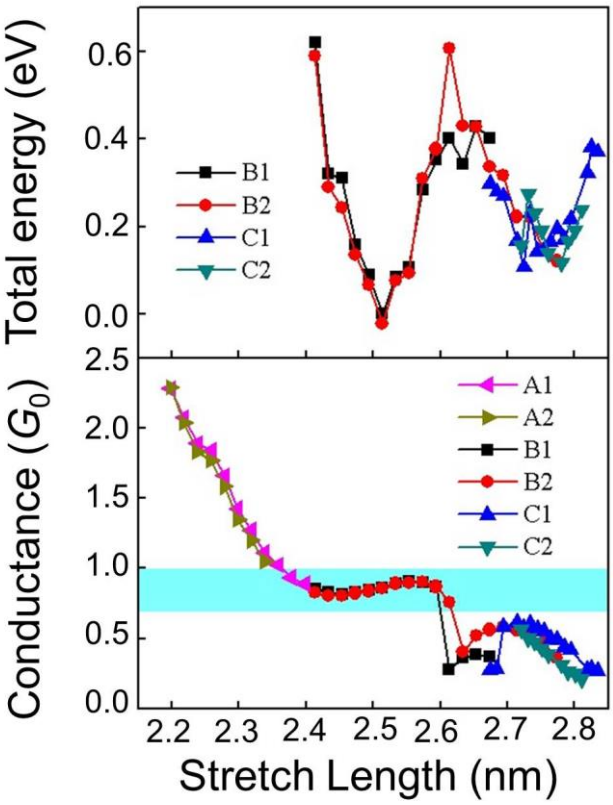

Figure 6.10: Evolution of total energy (upper panel) and differential conductance at zero bias (lower panel) during the quasi-static stretch.

Based on both the experimental and theoretical results, it was considered that the adsorption of the N_2 molecules contribute to strengthening the Cu–Cu bond and the formation of Cu LACs. A previous theoretical study showed that the adsorption of molecules stabilizes the high-energy state of a metal atomic junction (*29*). The presence of adsorbates on the LAC reduces the energy of the surface in low coordination states, which may enable us to form metal LACs. Another role of the N_2 molecule in the formation of LACs is the direct support of the Cu–Cu bond. On the other hand, there is another possible scenario for the formation of a Cu atomic chain. Figure 6.11 shows the strength of the interaction between N-Cu and Cu-Cu during the stretch. The strength of the Cu–Cu interaction (the binding energy of B0) decreases rapidly, while that of the N–Cu interaction (the binding energy of B2) remains small and constant until 2.61 nm, where the Cu–Cu distance is so great that the N_2 starts to be inserted between the atoms. The rapid decrease in the interaction between the Cu atoms at a certain separation indicates that Cu atomic junction is brittle without N_2 molecule. On the other hand, the presence of N_2 makes the connection more flexible and increases the junction's durability; this makes it easy to extract

another atom from the tip. In an experimental scenario, i.e., a dynamic process, the atoms do not have enough time to reach the most energetically stable configuration, such as C2. The Cu nanowire tends to rupture at some weak Cu–Cu connections where no N_2 molecules are attached.

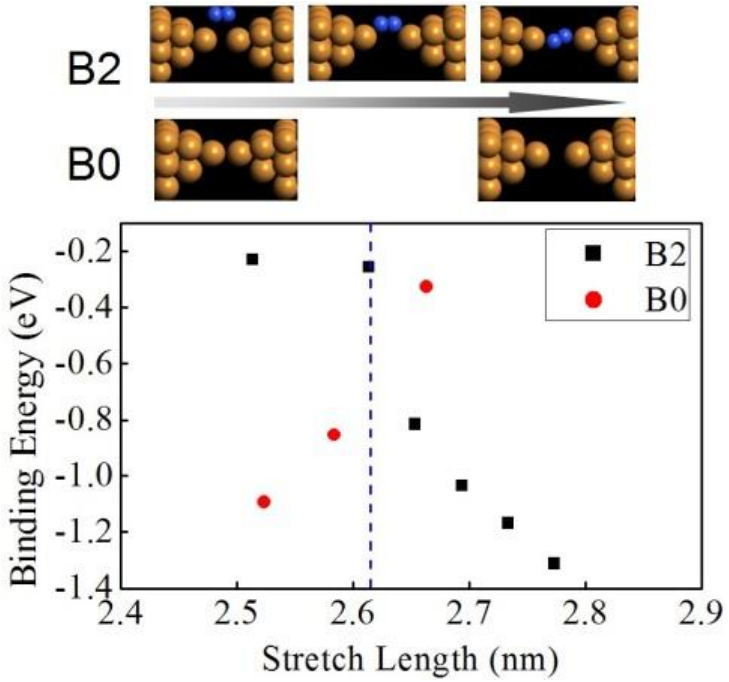

Figure 6.11: Comparison between N–Cu interaction (B2) and Cu–Cu interaction (B0).

6.4 Conclusions

The electronic conductance of the platinum-copper contact in nitrogen atmosphere has been investigated using both an experimental technique and theoretical calculations. A single N_2 molecule was placed between Pt electrodes in parallel. The conductance of the single N_2 molecular junction was 1 $G_{0,}$ which was close to that of the metal atomic contact. Two dominant channels originating from the coupling between the N_2 molecule and electrodes contribute to the electron transport. On the other hand, the N_2 molecule was not placed between copper electrodes. With the support of the N_2 molecule, the linear Cu atomic chain was formed, although Cu does not form a linear atomic chain without molecules. The lone pair in the nitrogen atom formed Pt-N_2 bonds, and successfully formed a Pt/N_2/Pt single molecular junction.

References

1. H. Ohnishi, Y. Kondo, K. Takayanagi, Quantized conductance through individual rows of suspended gold atoms. *Nature* **395**, 780-783 (1998).
2. S. R. Bahn, K. W. Jacobsen, Chain formation of metal atoms. *Phys. Rev. Lett.* **87**, 266101 (2001).
3. W. H. A. Thijssen, M. Strange, J. M. J. A. de Brugh, J. M. van Ruitenbeek, Formation and properties of metal-oxygen atomic chains. *New J. Phys.* **10**, 033005 (2008).
4. T. Nakazumi, M. Kiguchi, Formation of Co atomic wire in hydrogen atmosphere. *J. Phys. Chem. Lett.* **1**, 923-926 (2010).
5. R. H. M. Smit, Y. Noat, C. Untiedt, N. D. Lang, M. C. van Hemert *et al.*, Measurement of the conductance of a hydrogen molecule. *Nature* **419**, 906-909 (2002).
6. D. Djukic, J. M. van Ruitenbeek, Shot noise measurements on a single molecule. *Nano Lett.* **6**, 789-793 (2006).
7. K. Aika, A. Ohya, A. Ozaki, Y. Inoue, I. Yasumori, Support and promoter effect of ruthenium catalyst: II. ruthenium alkaline-earth catalyst for activation of dinitrogen. *J. Catal.* **92**, 305-311 (1985).
8. E. P. M. Amorim, E. Z. da Silva, Mechanochemistry in Cu nanowires: N and N-2 enhancing the atomic chain formation. *Phys. Rev. B* **82**, 153403 (2010).
9. E. P. M. Amorim, E. Z. da Silva, Effect of light impurities on the electronic structure of copper nanowires. *Phys. Rev. B* **85**, 155407 (2012).
10. M. Kiguchi, O. Tal, S. Wohlthat, F. Pauly, M. Krieger *et al.*, Highly conductive molecular junctions based on direct binding of benzene to platinum electrodes. *Phys. Rev. Lett.* **101**, 046801 (2008).
11. S. Kaneko, T. Nakazumi, M. Kiguchi, Fabrication of a well-defined single benzene molecule junction using Ag electrodes. *J. Phys. Chem. Lett.* **1**, 3520-3523 (2010).
12. M. Kiguchi, S. Miura, K. Hara, M. Sawamura, K. Murakoshi, Conductance of single 1,4-disubstituted benzene molecules anchored to Pt electrodes. *Appl. Phys. Lett.* **91**, 053110 (2007).
13. M. Kiguchi, H. Nakamura, Y. Takahashi, T. Takahashi, T. Ohto, Effect of anchoring group position on formation and conductance of a single disubstituted benzene molecule bBridging Au electrodes: Change of conductive molecular orbital and electron pathway. *J. Phys. Chem. C* **114**, 22254-22261 (2010).
14. M. Kiguchi, T. Nakazumi, K. Hashimoto, K. Murakoshi, Atomic motion in H-2 and D-2 single-molecule junctions induced by phonon excitation. *Phys. Rev. B* **81**, 045420 (2010).

15. R. H. M. Smit, C. Untiedt, A. I. Yanson, J. M. van Ruitenbeek, Common origin for surface reconstruction and the formation of chains of metal atoms. *Phys. Rev. Lett.* **87**, 266102 (2001).
16. N. Agrait, A. L. Yeyati, J. M. van Ruitenbeek, Quantum properties of atomic-sized conductors. *Phys. Rep.* **377**, 81-279 (2003).
17. B. C. Stipe, M. A. Rezaei, W. Ho, Single-molecule vibrational spectroscopy and microscopy. *Science* **280**, 1732-1735 (1998).
18. A. V. Khotkevich, Modern state of point contact spectroscopy of electron-phonon interaction in transition metals. *Physica B* **218**, 31-34 (1996).
19. K. P. Huber, G. Herzberg, *Molecular Spectra and Molecular Structure; Constants of Diatomic Molecules*. (van Nostrand Reinhold, New York, 1979).
20. M. Paulsson, T. Frederiksen, H. Ueba, N. Lorente, M. Brandbyge, Unified description of inelastic propensity rules for electron transport through nanoscale junctions. *Phys. Rev. Lett.* **100**, 226604 (2008).
21. O. Tal, M. Krieger, B. Leerink, J. M. van Ruitenbeek, Electron-vibration interaction in single-molecule junctions: from contact to tunneling regimes. *Phys. Rev. Lett.* **100**, 196804 (2008).
22. Y. Kim, T. Pietsch, A. Erbe, W. Belzig, E. Scheer, Benzenedithiol: A broad-range single-channel molecular conductor. *Nano Lett.* **11**, 3734-3738 (2011).
23. I. S. Kristensen, M. Paulsson, K. S. Thygesen, K. W. Jacobsen, Inelastic scattering in metal-H_2-metal junctions. *Phys. Rev. B* **79**, 235411 (2009).
24. M. Brandbyge, J. L. Mozos, P. Ordejon, J. Taylor, K. Stokbro, Density-functional method for nonequilibrium electron transport. *Phys. Rev. B* **65**, 165401 (2002).
25. J. Taylor, H. Guo, J. Wang, Ab initio modeling of quantum transport properties of molecular electronic devices. *Phys. Rev. B* **63**, 245407 (2001).
26. M. J. Frisch, G. W. Trucks, H. B. Schlegel, G. E. Scuseria, M. A. Robb *et al. Gaussian 09* (Gaussian, Inc., 2009.).
27. L. W. Bruch, R. P. Nabar, M. Mavrikakis, Weak molecular chemisorption of N_2/Pt(111). *J Phys-Condens Mat* **21**, 264009 (2009).
28. T. Nakazumi, S. Kaneko, M. Kiguchi, Electron transport properties of Au, Ag, and Cu atomic contacts in a hydrogen environment. *J. Phys. Chem. C* **118**, 7489-7493 (2014).
29. W. R. French, C. R. Iacovella, P. T. Cummings, The influence of molecular adsorption on elongating gold nanowires. *J. Phys. Chem. C* **115**, 18422-18433 (2011).

7 Controlling the electrical property of highly conductive single pyrazine molecular junction

A N_2 molecule was successfully placed between Pt electrodes. The lone pair of N_2 formed a single molecular junction with a high and well-defined conductance value. In this chapter, I investigate the application of a pyrazine molecule between the Pt electrode. Pyrazine molecules are expected to have two conductance states. One is the configuration where a π orbital is parallel to the bonding direction. The other is the configuration where a p orbital is vertical to the bonding direction. Here, bi-stable states were fabricated and their configurations were investigated in terms of their conductance and differential conductance, near edge X-ray fine structure, and theoretical calculations. Defined configurations were switched by an external force. The electric property of the single molecular junction was controlled by changing the interface structure.

The contents of this chapter have been published in: Satoshi Kaneko, Manabu Kiguchi, "Investigation on the pyrazine molecular junction studied by conductance measurement and near edge X-ray absorption fine structure" *Fullerenes, Nanotubes and Carbon Nanostructures* 22, 166-172 (2014), and Satoshi Kaneko, Carlo Motta, Gian Paolo Brivio, Manabu Kiguchi, "Mechanically controllable bi-stable states in highly conductive single pyrazine molecular junction" *Nanotechnology* 24, 315201 (2013).

7.1 Introduction

The utilization of bi-stable states in single molecular junctions as memory, switches, and other components is a key issue in the realization of molecular electronics. Molecular-based switches are advantageous because of their small energy consumption as slight structural changes are sufficient to control the conductance of the molecular junction, and such changes can be induced by tiny mechanical forces, electric fields, and photo irradiation, etc. (*1-5*). For example, the mechanophore molecule was proposed as a distortion sensor whose color is changed by the deformation of the molecule (*1, 2*). In addition, a high on/off ratio has been measured for logical circuits using rotaxane molecules (*3*) and suspended graphene by the application of voltage pulses (*4*). Recently, several single molecular switches showing bi-stable states have been reported using photochromic molecules, 1,6-hexanedithiol, 4,4'-bipyridine, and other molecules, thanks to the recent development of experimental techniques (e.g., scanning tunneling microscope (STM) break junction and mechanically controllable break junction (MCBJ)) (*6-8*). In particular, single bipyridine molecular switches have been extensively studied because Au-N bonds provide fixed conductance values (*8-14*), which is very important to obtaining reliable single molecular switches. However, there remain unresolved problems in this field. First, the conductance value of the on-state of the single molecule switch is too low, namely below 10^{-1}~10^{-2} G_0 ($G_0 = 2e^2/h$) (*7, 8*). Second, until the present, all of the evidence for the switching behavior has been obtained indirectly. The conductance measurements can only provide information on the conductance switching, and the mechanism at the base of the transition between bi-stable states is often not clear.

Because it was revealed that nitrogen in a π-conjugated system works well to fabricate single molecular junction with high and well-defined conductance values, the next target is to fabricate the bi-stable electric states and to control the bi-stable states utilizing the pyrazine molecule. In this chapter, I discuss the fabrication of highly conductive single molecular junctions showing bi-stable states, and I investigate the switching mechanism using a combination of experimental and theoretical techniques. In order to improve the conductance of the single molecular junctions, I first address the metal-molecule interface. Typically, in conventional single molecular junctions, the molecules are attached to the metal electrodes via anchoring groups (e.g., thiol, amine) (*15-20*). Although a stable single molecular junction can be prepared in this way, it has been reported that the anchoring group acts as a resistive spacer, leading to low conductivity, as mentioned in chapter 1. Recently, the direct binding of π-conjugated molecules to metal electrodes has been found to be a promising technique to improve the conductance of single molecular junctions (*21-29*). Indeed, an efficient overlap between π orbitals of the molecule and the metal states leads to high conductivity. In this chapter, the use of a pyrazine

single molecular junction is discussed. In this system, the π orbitals of pyrazine, including the *p* orbital of nitrogen, can directly bind to the metal electrodes. In addition, the presence of nitrogen atoms in the pyrazine molecular backbone can fix the binding site with metal electrodes, forming a non-directional σ bond between the lone pair of the nitrogen atom and the metal. This realizes the efficient coupling between the molecule and the tip, allowing for stable conductance values (*17*). Earlier theoretical calculations on jellium electrodes predicted the conductance of the pyrazine molecular junction as high as 1 G_0 (*10*). Next, I focus on the metal electrodes. In the simple tunneling model, the conductance of single molecular junction depends on the local density of states (LDOS) of the contact metal atoms at the Fermi level (*30*). Differently from Au, Pt displays a narrow 5*d* band located at E_F, and consequently, a larger density of states (DOS) occurs. Thus, molecular orbitals can effectively be hybridized with the *d* orbital of Pt. For this reason, single molecular junctions using Pt as metal electrodes are expected to have high conductivity. Actually, such increases in the conductance of single molecular junction have been reported for various molecules including benzenedithiol (*19*), benzene (*21, 22*), and H_2 (*31, 32*).

This chapter shows highly conductive pyrazine/Pt junctions using the MCBJ technique at 10 K. The conductance measurements display two distinct conductance states of 1.0 G_0 and 0.3 G_0, which are two orders of magnitude larger when compared to single molecular junctions with anchoring groups, including pyrazine-related molecular junctions. By combining the experimental conductance results, IETS measurements and theoretical calculation revealed that these two states are due to different geometrical configurations of pyrazine, which exhibit large and small coupling with the electrodes. I also demonstrated that the controlled torsion of the molecule is capable of switching between the two conducting regimes.

7.2 Experiments

Pyrazine was placed between Pt electrodes using the MCBJ technique at 10 K, following the method mentioned in chapter 3. Pyrazine (Wako 97%) was degassed by performing freezing and pumping cycles, as well as the thawing technique. Both before and after the introduction of the pyrazine, the conductance was measured with a bias voltage of 300 mV during the stretching process. The differential conductance was measured by a lock-in technique with an AC modulation with amplitude of 1 mV and a frequency of 7.777 kHz. The conductance was monitored for a fixed contact configuration during the sweep of the DC bias from -80 mV to +80 mV.

The NEXAFS (near edge X-ray absorption fine structure) spectra were measured at the soft

X-ray beam line BL-7A in the Photon Factory at the Institute of Materials Structure Science, Tsukuba, Japan. The photon energy was calibrated with respect to the C 1s to π* peak position of highly oriented pyrolytic graphite (HOPG) at 285.5 eV. After preparing the clean Pt(111) surface by repeated cycles of Ar sputtering and annealing, the multilayer of the pyrazine film was deposited on the Pt surface by the introduction of pyrazine gas at a substrate temperature below 240 K. The monolayer film was prepared by heating the sample up to 300 K.

7.3 Results and discussion

7.3.1 Conductance

Figure 7.1(a) displays typical conductance traces as a function of the stretch length, which is the displacement between the stem parts of the Pt electrodes that are fixed with epoxy adhesive. Before the introduction of pyrazine, the conductance decreases in a stepwise fashion with the stretching of the junction, showing the last plateaus around 1.5 G_0. The corresponding conductance histogram (Figure 7.1(b)) presents a peak around 1.5 G_0, which corresponds to clean Pt atomic contacts. After the introduction of pyrazine, steps appear around 1.0 G_0 and 0.3 G_0. Some steps have positive or negative slopes and display fluctuations in the conductance, which are caused by the small change in the atomic configuration of the junction. Note that the 0.3 G_0 step appears after the 1 G_0 step, as shown more clearly in the last two traces in Figure 7.1(a). The 1.5 G_0 peak, which is characteristic of the Pt atomic contacts (*21*), is suppressed in the conductance histogram (Figure 7.1(b)), and a larger weight is distributed in the entire range below that value. The new features, which are due to the introduction of pyrazine, signal the existence of two distinct conductance states. This indicates that the clean Pt atomic contacts are hardly formed, and that pyrazine molecules would bridge between Pt electrodes. Their conductance was determined to be 1.0 G_0 (high-conductance state, HC) and 0.27 G_0 (low-conductance state, LC) by numerically averaging the conductance values in the histograms that were measured for four distinct samples. Some features observed above 1.5 G_0 may have originated from a Pt atomic contact covered with pyrazine molecules.

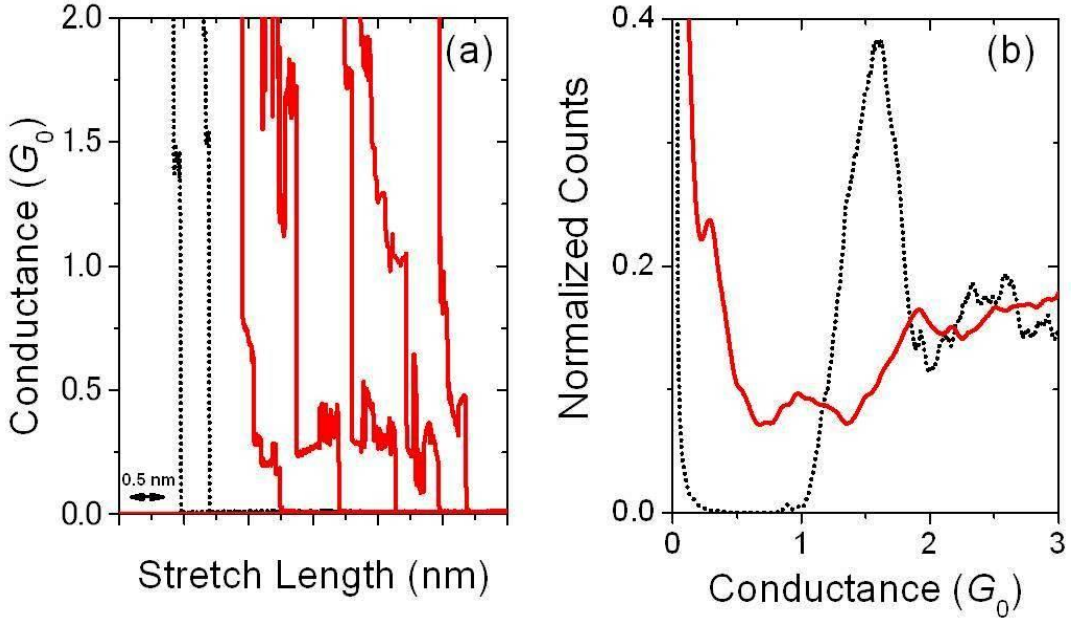

Figure 7.1: (a) Conductance traces. (b) Conductance histograms of the Pt contacts before (black dotted curve) and after (red curve) the introduction of pyrazine. The bias voltage is set to 300 mV. The conductance histogram is constructed without data selection from 1000 conductance traces of breaking metal contacts. The intensity of the conductance histograms is normalized by the number of conductance traces. The bin size was 0.004 G_0.

The measured conductance values were compared with those of other similar single molecular junctions, where π-conjugated molecules are directly bound to metal electrodes. The single Pt/benzene/Pt molecular junction showed conductance values of 1.0-0.2 G_0 depending on the atomic configuration of the benzene single molecular junctions (*21*). The single Ag/benzene/Ag molecular junction showed a fixed conductance value of 0.2 G_0, reflecting a weak benzene-Ag interaction compared with a strong benzene-Pt interaction (*22*). The conductance values of the single Au/C_{60}/Au, Ag/C_{60}/Ag, and Pt/C_{60}/Pt molecular junctions were 0.3 G_0, 0.5 G_0, and 0.7 G_0, respectively (*23, 24*). The direct-binding technique has also been applied to endohedral Ce@C_{82} metallofullerenes, ethylene and acetylene, and other molecules (*25, 26*). These single molecular junctions showed high conductance values around 1.0-0.2 G_0, while the pyrazine single molecular junction shows conductance values of 1.0 G_0 and 0.3 G_0. The latter are close to those of other single molecular junctions fabricated using the direct-binding technique.

7.3.2 *dI/dV* measurements and NEXAFS measurements

While conductance traces provide evidence of a bi-stable molecular junction, further insight into the conduction properties can be obtained by examining the IETS. Such measurements as a function of the voltage across the single molecular junction were performed for both HC and LC regimes, keeping the electrode separation fixed. Figure 7.2 displays the differential conductance and its derivative for HC and LC regimes. The arrows denote shallow symmetric upward features in the differential conductance around 30 mV for the LC state and 60 mV for that of the HC (Figure 7.2(a)). Note that there are clear peaks in the derivatives (Figure 7.2(b) and 7.2(c)). In addition, an asymmetric background in the differential conductance (Figure 7.2(a)) was observed. The asymmetric feature may be attributed to the interference of electrons scattered on defects in the leads (*33-35*), asymmetric coupling between the molecule and metal leads, and other effects. The conductance enhancement is explained by the opening of an additional tunneling channel for electrons that give energy to a vibration mode (*36, 37*), as previously mentioned. Because the phonon modes of Pt are below 20 meV (T mode: 6, 10 meV, L mode: 20 meV) (*38*), the two observed features correspond to vibration modes of the Pt-molecule bond or internal molecular ones, which confirms that pyrazine was placed between the Pt leads. The different bias voltages of HC and LC vibrations reflect two distinct configurations. Here, I discuss the shape of the IETS. In the present study, a peak appeared in d^2I/dV^2 curves even in the HC regime. Based on the theory of single molecular junctions, there should be a peak in the d^2I/dV^2 curves if the transmission probability is below 0.5, and a dip in the d^2I/dV^2 curves if the transmission probability is above 0.5 (*39*). In such a model, electron transport occurs through a single channel and the molecule-metal coupling is symmetric (*39*). The shape of the IETS is discussed in the latter theoretical part in terms of the number of channels.

Figure 7.3 shows the C-K and N-K edge NEXAFS spectra of the monolayer and multilayer pyrazine film on a Pt surface taken at X-ray incidence angles of 55° for the C-K edge, and 30° for the N-K edge to the Pt surface. The NEXAFS spectra were normalized with respect to the value of the edge jump, where the intensity was proportional to the number of carbon or nitrogen atoms. The C-K edge NEXAFS spectra of the multilayer pyrazine film showed peaks at 284 eV, 287 eV, and 304 eV, which correspond to the C 1s to π*, the C 1s to π*, and the C 1s to σ* transitions, respectively (*40, 41*) . The N-K edge NEXAFS spectra of the multilayer pyrazine film showed peaks at 397 eV and 407eV, which correspond to the N 1s to π* and the N 1s to σ* transitions, respectively (*40, 41*). While the C-K edge NEXAFS spectra of the monolayer film was similar to that of the multilayer film, the N-K edge NEXAFS spectra of the monolayer film changed from that of the multilayer film. The broadening of the π* peak was clear for the N-K edge NEXAFS spectra of the monolayer film. Because the π* peak of the N-K

edge NEXAFS spectra reflected the electronic structure of the *p* orbital of the N atoms of the pyrazine molecule, the broadening of the π* peak of the N-K edge NEXAFS spectra indicated that the pyrazine molecule was adsorbed on the Pt surface via the N atoms of pyrazine molecules.

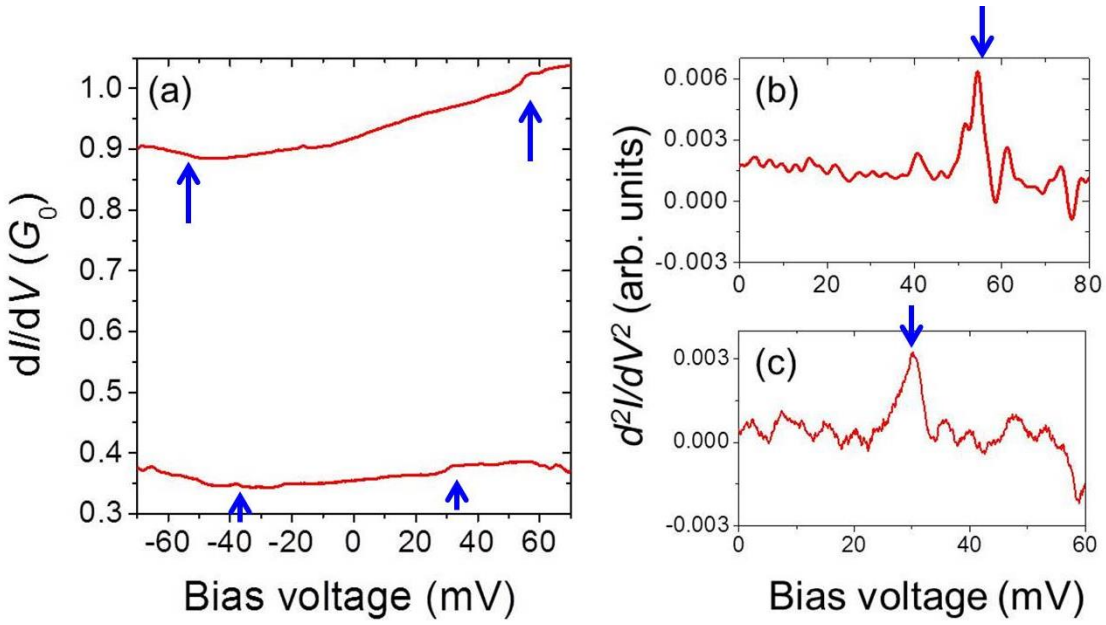

Figure 7.2: (a) Differential conductance spectra of single pyrazine molecular junctions and their derivatives taken at (b) high- and (c) low-conductance regimes.

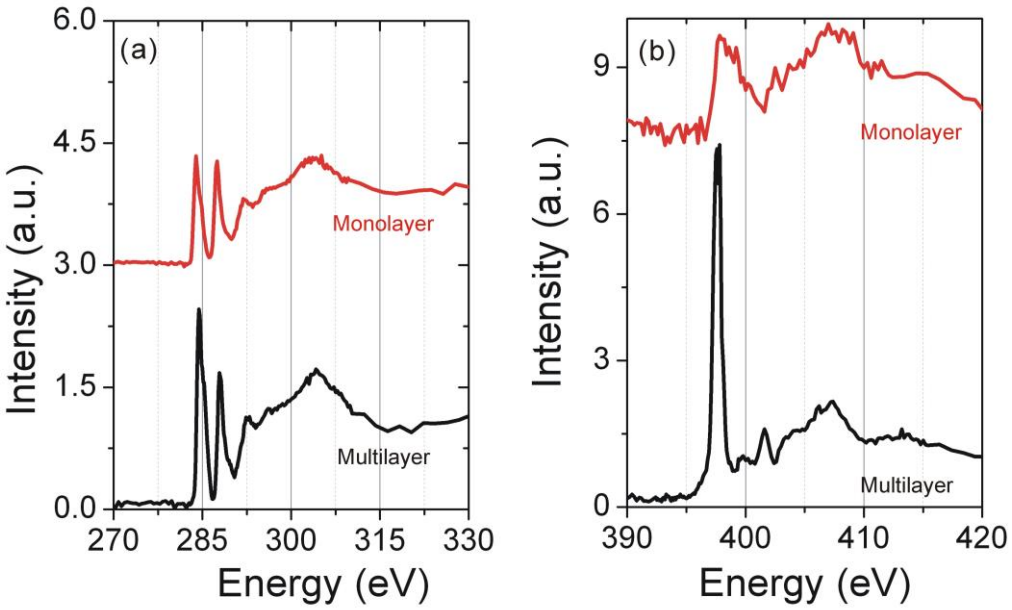

Figure 7.3: (a) C-K edge and (b) N-K edge NEXAFS spectra for pyrazine films grown on Pt(111) taken at X-ray incidence angles of 55° for the C-K edge, and 30° for the N-K edge to the Pt surface. The black and red curves are the result of the thick layer and monolayer, respectively.

7.4 Calculations

7.4.1 Methods

The electronic structure calculations were carried out using the first-principle self consistent method implemented in the SIESTA code (*42, 43*), which uses a basis set of numerical atomic orbitals. Conductance calculations were done within the formalism of the non-equilibrium Green's function combined with the DFT, as implemented in the TranSIESTA package (*44*). The exchange-correlation energy is described by the Perdew-Burke-Ernzerhof (PBE) generalized gradient approximation (GGA) (*45*). The potential used was Troullier-Martins, norm-conserving pseudopotentials in the fully separable Kleimann and Bylander form with channels having core radii of 2.60, 1.25, 1.48, and 1.25 Bohr for Pt, C, N, and H, respectively. A single-ζ polarized basis set of numerical atomic orbitals was used, with cut-off radii that have been determined by imposing confinement energy of 0.01 Ry. The energy cutoff for a real-space mesh was set to 200 Ry. These values have been tested both for bulk Pt and isolated pyrazine.

7.4.2 Structure and conductance

Ab-initio calculations were performed to analyze the switching mechanism of pyrazine/Pt single molecular junctions. In order to determine the most suitable contact configuration to be adopted, the adsorption energies for different structures were calculated. Several adsorption sites were considered, namely, the adsorption on top of a pyramidal Pt_4 cluster, on the hollow and bridge sites of a Pt_3 cluster, and on the hollow and top sites of the clean Pt(111) surface. In Figure 7.4, the relaxed structures as well as the adsorption energies for all five configurations are reported. The most stable contact configuration is the pyramidal Pt_4 electrode, which is placed on the top of Pt(111). The surface top adsorption is unfavorable compared to the Pt_4 top one because of the steric repulsion between the molecule and the surface Pt atoms. The calculations also suggest that pyrazine adsorbed on a hollow site is unstable, and that N selectively forms a bond on the top of a Pt atom. The NEXAFS study for the pyrazine molecules on the Pt surface supports the formation of N-Pt bonds, as mentioned in the previous section.

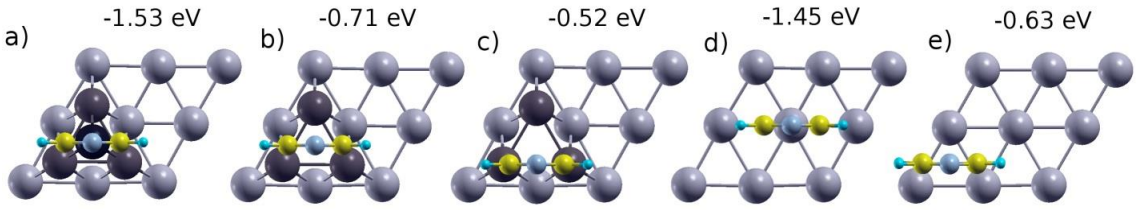

Figure 7.4: Adsorption energies of pyrazine on different electrode geometries: (a) on top of Pt_4 cluster, on (b) hollow site and (c) bridge site of a Pt_3 cluster, on the (d) top site, and (e) hollow site of the clean Pt(111) surface.

According to these results, the tips were modeled as composed by two Pt_4 pyramids placed on top of a 3 × 3 Pt(111) surface. In order to describe the pyrazine junction, a periodic supercell was considered, as shown in Figure 7.5(e) and (f). The density matrices were calculated using a 3 × 3 **k**-mesh in the plane orthogonal to the junction axis (i.e., the longest cell dimension in Figure 7.5(f)), while the transmission spectra were instead computed using a 5 × 5 **k**-mesh. Preliminary results indicate that the transmission functions converged with respect to the lateral cell size. The slab contains 10 atomic layers. First, the single electrode containing the tip is relaxed, and then I used the obtained geometry to build the junction. All the subsequent relaxations were performed by keeping all of the electrodes' atomic positions fixed, and allowing the Pt pyramidal atoms as well as the pyrazine ones to relax until the residual forces

are smaller than 0.04 eV/Å.

The configuration dependency of the properties was measured, as shown in Figure 7.5. In Figure 7.5, the distance D is defined as the distance between the two outermost Pt surfaces. Here, d_{Tips} is the distance between the apical Pt atoms, and $\alpha_{1,2}$ are defined as the angles between the straight line of the N-N molecular backbone and that defined by the N-Pt bonds (as shown in the inset). E_{form} is the junction formation energy, which is calculated as $E_{form} = E_{Pt\text{-}molecule\text{-}Pt}\text{-}2E_{Pt}\text{-}E_{molecule}$, and $T(E_F)$ is the transmission function at the Fermi level. By observing Figure 7.5(a), two regimes can be distinguished. An HC regime is observed for distances D lower than 14.5 Å, where the conductance is within the range of 1.3 G_0 and 1.5 G_0. In this regime, the tilt angles $\alpha_{1,2}$ are lower than 120°, meaning that the molecule sits in a tilted configuration with respect to the junction axis. The electronic coupling between the molecule orbitals and the *d* orbitals of the Pt tip is favored due to the orientation of the molecule, and correspondingly the transmission function increases inversely with $\alpha_{1,2}$. The transmission does not change within the range between D = 13.0 Å and 14.5 Å, and it shows an HC plateau. In the range between 14.3 Å and 14.7 Å, a rapid rotation of the molecule is assisted, which overcomes the energy barrier (Figure 7.5(b)) to reach the local energy minimum corresponding to the LC state.

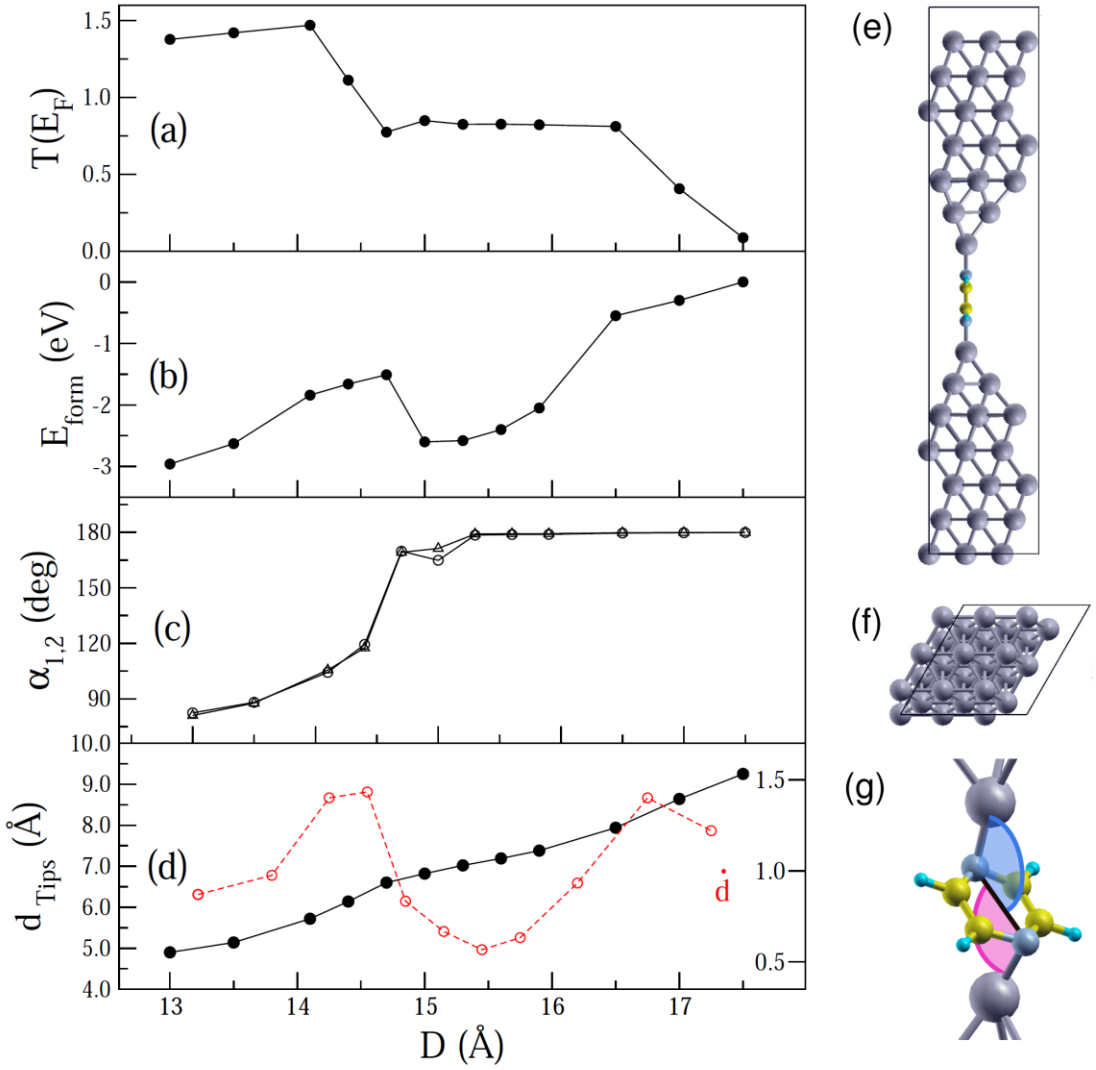

Figure 7.5: Left (a-d): Pyrazine/Pt junction properties plotted against the surface distance D, (a) transmission function $T(E_F)$, (b): junction formation energy E_{form}, (c): bending angles $\alpha_{1,2}$, (d): distance d_{Tips} between the outermost Pt atoms and its derivative d'. Right (e-f): geometry of the Pyrazine/Pt junction for the calculation. Top (e) and front (f) view of supercell used for theoretical calculation. (g): geometry of the central part of the junction during the stretching process. The $\alpha_{1,2}$ is highlighted by blue and red. The following atomic color scheme was used : grey = Pt, yellow = C, cyan = H, light blue = N.

In this regime, the pyrazine is aligned with the junction axis, i.e., $\alpha_{1,2}$ are equal to 180°; this is reflected in a lower coupling between the molecule orbitals and those of Pt. As a consequence, it was revealed that the transmission $T(E_F)$ assumes fractional values, and its intensity is fairly constant and equal to 0.7 G_0 for a range of about 2 Å. This is in agreement with the appearance of the LC feature in the conductance histogram (Figure 7.1(b)). When D is larger than 16.5 Å, the Pt-N bond is broken, causing an abrupt decay from $T(E_F)$ to zero, while the binding energy also tends to zero. During the junction elongation, d_{Tips} increases almost linearly (Figure 7.5(d)), while the peaks in its derivative signal transitions between different regimes. The two experimental conductance states of the HC and LC states were assigned to the two regimes, as highlighted by first-principles calculations. In agreement with the conductance traces, the LC plateau appears after the HC one and extends for a longer range. Note that the distance D between the two plateaus is comparable to the experimental ones in Figure 7.1(a). The differences between theory and experiments regarding the conductance intensities are due to the intrinsic limitations of the ground-state DFT applied to electronic transport, as the underestimation of the HOMO-LUMO gap and the self-interaction error (*46*). In fact, even with the prototypical case of the Au/benzenedithiol/Au junction, the DFT-NEGF approach overestimates any experimental conductance by at least one order of magnitude (*47*). In this case, no significant discrepancies were found because the system shows a strong metal-molecule coupling. It was found that the molecule stretching along the minimum-energy path obtained a bi-stable junction where conductance results are in fairly good agreement with the experimental ones. For this reason, an average over several molecular configurations was not performed.

In order to obtain a more comprehensive view of the electronic properties, in Figure 7.6, calculations were performed to show the projected density of the states' (PDOS) onto the basis orbitals associated with the N and C species and the 5*d* orbitals of Pt for a representative state in each conductance regime (D = 13.5 Å for the solid line and D = 15.3 Å for the dashed line). Calculations reveal that in both cases, the pyrazine HOMO orbital is highly hybridized with the Pt states, and it provides the main contribution for the conductance at E_F. At the same time, the D = 15.3 Å junction shows more pronounced peaks, which indicates a lower hybridization of the molecular orbitals with respect to the D = 13.5 Å case. As mentioned previously, this is because of the different bending angles that are formed by the pyrazine with the junction. Accordingly, in the upper panel, one can see that the overall conductance for D = 13.5 Å is larger not only near E_F, but also over a broader energy range. In fact, the transmission coefficient depends on the metal-molecule coupling. For the bent structure, the coupling is larger because of a higher hybridization of the pyrazine orbitals, which are polarized

orthogonally to the molecular plane, and the metal *d* orbitals, which stem from the under-coordination of the surface Pt atoms. The result of the bending is a higher overlap between the respective wave functions, which leads to larger hybridization and conductance.

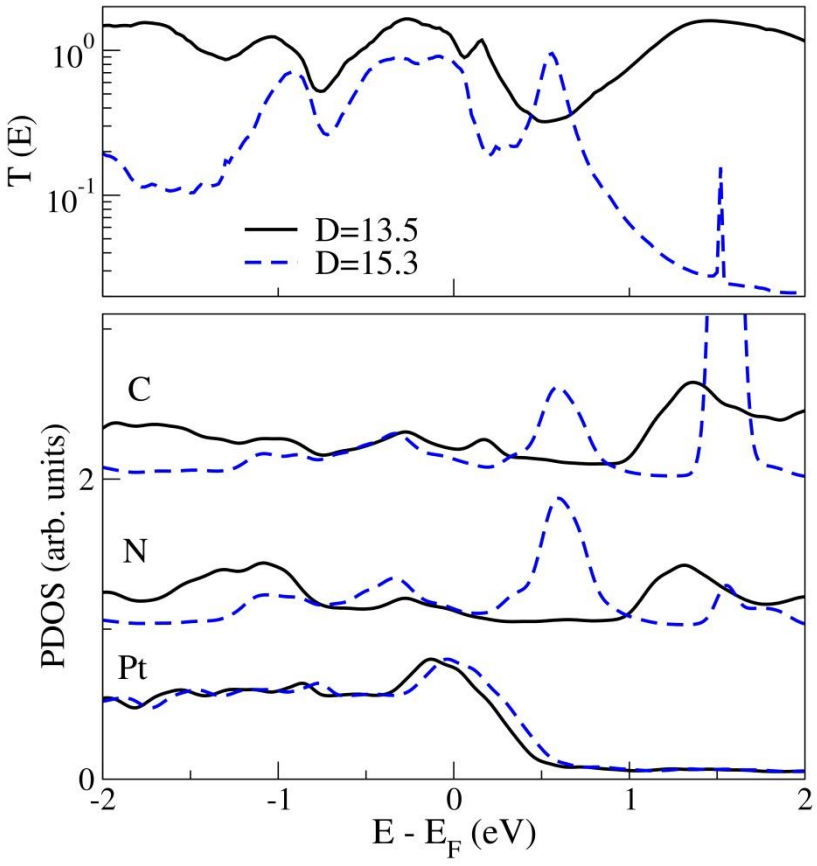

Figure 7.6: Upper panel: transmission function T(E) of Pt/pyrazine junctions for high- and low-conductance structures calculated for two representative distances D, namely 13.5 Å (black solid line: HC) and 15.3 Å (blue dashed line: LC). Lower panel: PDOS of the same structures on the C and N orbitals and on the Pt 5d orbital.

To obtain information about the individual channel contributions to the conduction, the eigenchannels were calculated (*48*) for these two reference configurations. From the results, in the HC regime, two channels are open and equally contribute to the charge transport, while only one is present in the LC regime. In Figure 7.7, such transport channels are depicted to provide an intuitive picture of transport. For D = 15.3 Å, the symmetry and the spatial distribution of the channel has the same character of the π-type HOMO pyrazine, while for D = 13.5 Å, the two channels display a stronger interaction between the states of the Pt atoms and those of the molecule.

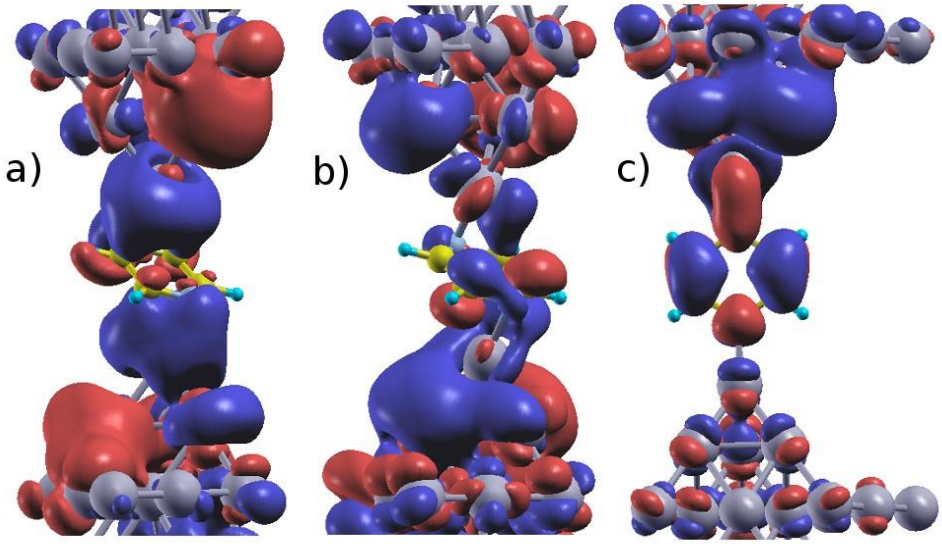

Figure 7.7: Isosurface plots of most of the transmitting eigenchannels of the high- and low-conductance structures at two representative distances D. (a) and (b) first and second eigenchannel for D = 13.5 Å (HC). (c) single eigenchannel for D = 15.3 Å (LC). The real part of the scattering state is shown.

7.4.3 Vibrations

In this section, the shape of the IETS is discussed. In the present study, a peak appears in the d^2I/dV^2 curves even for the HC regime, as similarly discussed in chapter 6. It was verified that more than one channel contributes to the electron transport through the single pyrazine molecule bridging Pt electrodes at the HC regime (see above), and this may explain the appearance of the peak in the d^2I/dV^2 curves, even for the HC regime (1 G_0). The number of conductance channels can be experimentally determined by multi-Andreev reflection or shot-noise measurement (*49, 50*).

Theoretical calculations can help to identify the vibrational modes, which are activated in the IETS. The DFT calculations were performed in order to calculate the vibrational modes of the pyrazine/Pt junctions for the geometries obtained at different D. The finite Pt clusters were considered to represent the electrodes and all the Pt atoms were fixed, which was justified by the large difference between the mass of Pt and that of the other species involved. Figure 7.8 shows the stretching dependence of the relevant vibration modes. The lowest three modes involve rigid vibrations of the entire molecule with respect to the Pt junction. As a consequence, their energy is strongly affected by stretching (D). At distances D > 15 Å, two possible

candidates for the LC mode were observed with IETS. Namely, these modes involve a shuffling of the molecule in the axial direction, and in the frustrated rotation of the molecule with respect to the axis of its plane. Unlike the third rigid mode (light blue on line) shown in Figure 7.8, their energy dependence on D is the same. Their vibrational energy increases while the molecule is progressively rotated, and slowly decreases once it is coaxial with the junction. On the other hand, the possible candidates for the HC mode are two internal vibrations of the pyrazine.

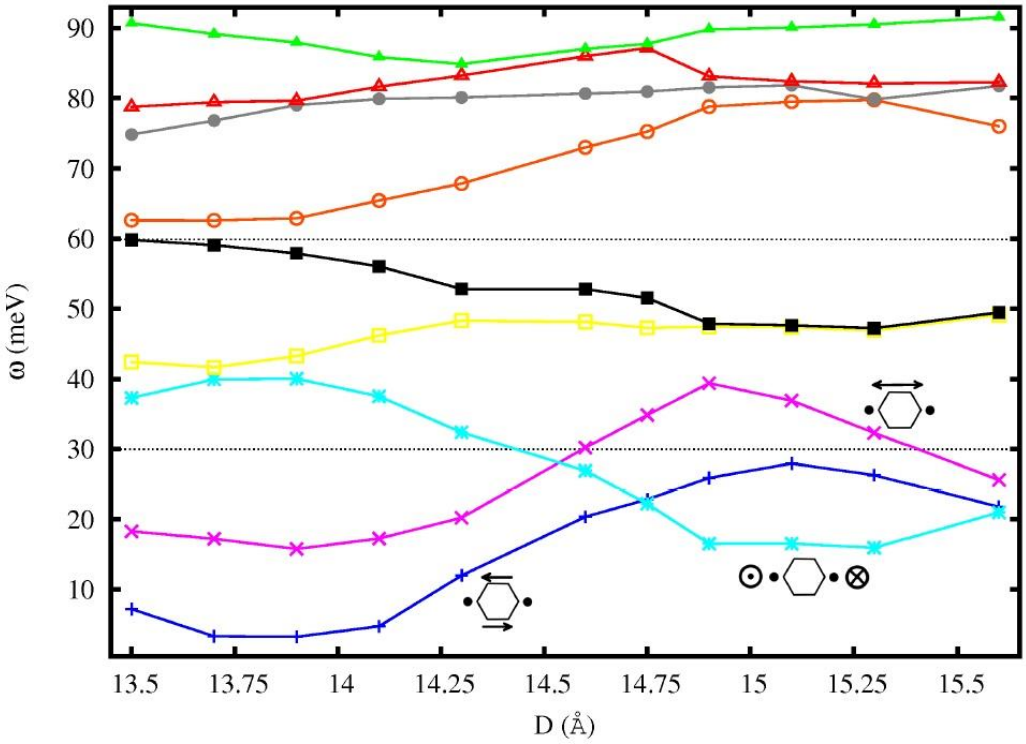

Figure 7.8: Stretching dependence of the relevant vibrational modes of pyrazine/Pt junctions involved in experiments. The insets represent the characteristics of the three lower energy modes, which involve a collective vibration of the molecule with respect to the Pt junction. The two dotted lines correspond to the experimental vibrational energies for HC and LC configurations.

7.5 Control of the electric conductance

It should be noted that pyrazine can be anchored to the Pt tips in two ways, namely by its N atom and by its two C atoms. The N-anchoring approach found in this study is always energetically favored. However, at a low D, the bending of the molecule also enables the

realization of the C-anchoring with an energy cost of less than 0.1 eV. On the other hand, for larger tip separations (D > 14.5 Å), the molecule sits coaxially with the junction and the C-linking is unfavorable, as the steric repulsion between the H and Pt would cost more than 1 eV. From the calculations, in the case of C-anchoring for D = 13.2 Å, the transmission $T(E_F)$ is approximately 1.5 G_0. This further confirms the presence of two regimes associated with the geometrical features of the pyrazine.

After showing the application of pyrazine single molecular junction on Pt leads, the existence of bi-stable structures, and characterizing their atomic configurations, a mechanically controlled conductance switching was demonstrated. Mechanical elongation/compression was repeated by applying an AC voltage (triangle wave) to the piezo element. The resulting displacement amounts to 1.0 nm at a modulation frequency of 0.4~0.8 Hz. Figure 7.9 displays two examples of conductance switching of the pyrazine single molecular junction. The curve (a) shows the transition between the HC and LC states and breaking the junction, while curve (b) shows the transition only between the HC and LC states. The conductance changes from high to low in a discrete manner in response to the smooth triangle-wave perturbation. This confirms that conductance switching indeed occurs via transitions between two specific metal-molecule contact configurations following mechanical controllable modulation.

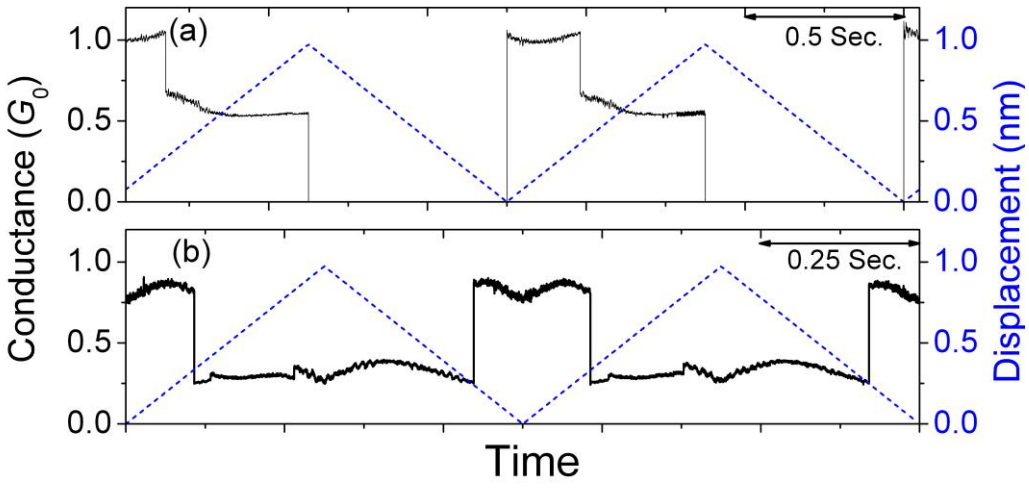

Figure 7.9: Sample pyrazine switching conductance traces, collected while applying the linear ramps (dashed black line) measured at a 100 mV applied bias. The displacement is 1.0 nm, and the modulation frequency is (a) 0.8 and (b) 0.4 Hz.

7. 6 Conclusions

In this chapter, I investigated the electron transport of a pyrazine molecule using Pt electrodes. Break-junction experiments suggest the existence of two distinct stable states that exhibit high (1.0 G_0) and low (0.3 G_0) conductance values, the latter appearing at larger stretching. The experimental results of the conductance versus stretch length show two plateaus, which are signatures of the formation of two different molecule-Pt states. In addition, the conducting traces highlight the existence of bi-stable states that display two high conductivities, the lower one at about 0.3 G_0 and the higher one at about 1.0 G_0. Mechanical manipulation of the junction by the application of an AC voltage to the piezo element shows that the switch can be reversibly moved from one state to the other, and that lower conductance is displayed at larger distances. The effect of the vibration mode on the conductance of such junctions has been measured by IETS. In the spectra, two peaks were found at 30 meV and 60 meV, and their vibrational origin was proven by the measured relatively linear temperature dependence of the width of the IETS derivative of the peak at 30 meV. It is interesting to note that there are two eigenchannels of the transmission matrix with the largest eigenvalues, whose magnitude is just below 0.5. This may explain why peaks were observed in the IETS derivatives, and not dips. In support of the experiments, I also performed DFT first-principle calculations of both the junction geometry and of the conductance to simulate the junction elongation. To do this, I followed the minimum energy path. By optimizing the configuration of the system, I found that pyrazine was coupled to a Pt_4 cluster. Then, by controlled torsion of the molecule from a bent shape in which the N-Pt axis forms and angle of about 90 degrees with the molecular one to one in which such angle is 180 degrees, the two configurations corresponding to the two bi-stable states were obtained. The calculated conductance value was 1.3 G_0 at the shorter distance and 0.7 G_0 at the longer distance. The DFT calculations revealed that the two stable states can be ascribed to different geometrical configurations in which the pyrazine axis is bent and coaxial with the junction, which correspond with high and low couplings of the molecular orbitals with the electrodes, respectively. The lowest energy configuration successfully provided a good qualitative estimate of the variation of the system geometry due to stretching of the molecule-electrode coordinate, and of the formation of the bi-stable states. In conclusion, the highly conductive bi-stable molecular junction was constructed. The Pt/pyrazine/Pt molecular junction exhibited well-defined structures, where the Pt electrodes are covalently bonded directly to the C backbone without an intervening link group.

References

1. C. R. Hickenboth, J. S. Moore, S. R. White, N. R. Sottos, J. Baudry *et al.*, Biasing reaction pathways with mechanical force. *Nature* **446**, 423-427 (2007).
2. D. A. Davis, A. Hamilton, J. L. Yang, L. D. Cremar, D. Van Gough *et al.*, Force-induced activation of covalent bonds in mechanoresponsive polymeric materials. *Nature* **459**, 68-72 (2009).
3. C. P. Collier, E. W. Wong, M. Belohradsky, F. M. Raymo, J. F. Stoddart *et al.*, Electronically configurable molecular-based logic gates. *Science* **285**, 391-394 (1999).
4. H. Zhang, W. Z. Bao, Z. Zhao, J. W. Huang, B. Standley *et al.*, Visualizing electrical breakdown and ON/OFF states in electrically switchable suspended graphene break junctions. *Nano Lett.* **12**, 1772-1775 (2012).
5. S. J. van der Molen, P. Liljeroth, Charge transport through molecular switches. *J Phys-Condens Mat* **22**, 133001 (2010).
6. D. Dulic, S. J. van der Molen, T. Kudernac, H. T. Jonkman, J. J. D. de Jong *et al.*, One-way optoelectronic switching of photochromic molecules on gold. *Phys. Rev. Lett.* **91**, 207402 (2003).
7. M. Taniguchi, M. Tsutsui, K. Yokota, T. Kawai, Mechanically-controllable single molecule switch based on configuration specific electrical conductivity of metal-molecule-metal junctions. *Chem Sci* **1**, 247-253 (2010).
8. S. Y. Quek, M. Kamenetska, M. L. Steigerwald, H. J. Choi, S. G. Louie *et al.*, Mechanically controlled binary conductance switching of a single-molecule junction. *Nat. Nanotechnol.* **4**, 230-234 (2009).
9. B. Q. Xu, N. J. J. Tao, Measurement of single-molecule resistance by repeated formation of molecular junctions. *Science* **301**, 1221-1223 (2003).
10. N. D. Lang, P. Avouris, Electrical conductance of individual molecules. *Phys. Rev. B* **64** , 125323 (2001).
11. M. Kamenetska, S. Y. Quek, A. C. Whalley, M. L. Steigerwald, H. J. Choi *et al.*, Conductance and geometry of pyridine-linked single-molecule junctions. *J. Am. Chem. Soc.* **132**, 6817-6821 (2010).
12. E. S. Tam, J. J. Parks, W. W. Shum, Y. W. Zhong, M. B. Santiago-Berrios *et al.*, Single-molecule conductance of pyridine-terminated dithienylethene switch molecules. *Acs Nano* **5**, 5115-5123 (2011).
13. K. Hashimoto, M. Kiguchi, T. Konishi, K. Murakoshi, Conductance of single 4,4 '-bipyridine molecule anchored on Au electrodes under electrochemical potential control.

T Mrs Jap **33**, 181-184 (2008).

14. K. Horiguchi, S. Kurokawa, A. Sakai, Conductance and I-V characteristics of Au/BPY/Au single molecule junctions. *J. Chem. Phys.* **131**, 104703 (2009).
15. F. Chen, X. L. Li, J. Hihath, Z. F. Huang, N. J. Tao, Effect of anchoring groups on single-molecule conductance: Comparative study of thiol-, amine-, and carboxylic-acid-terminated molecules. *J. Am. Chem. Soc.* **128**, 15874-15881 (2006).
16. A. Mishchenko, L. A. Zotti, D. Vonlanthen, M. Burkle, F. Pauly *et al.*, Single-molecule junctions based on nitrile-terminated biphenyls: A promising new anchoring group. *J. Am. Chem. Soc.* **133**, 184-187 (2011).
17. L. Venkataraman, J. E. Klare, I. W. Tam, C. Nuckolls, M. S. Hybertsen *et al.*, Single-molecule circuits with well-defined molecular conductance. *Nano Lett.* **6**, 458-462 (2006).
18. W. Haiss, C. S. Wang, I. Grace, A. S. Batsanov, D. J. Schiffrin *et al.*, Precision control of single-molecule electrical junctions. *Nat. Mater.* **5**, 995-1002 (2006).
19. M. Kiguchi, S. Miura, K. Hara, M. Sawamura, K. Murakoshi, Conductance of single 1,4-disubstituted benzene molecules anchored to Pt electrodes. *Appl. Phys. Lett.* **91**, 053110 (2007).
20. J. M. Seminario, C. E. De la Cruz, P. A. Derosa, A theoretical analysis of metal-molecule contacts. *J. Am. Chem. Soc.* **123**, 5616-5617 (2001).
21. M. Kiguchi, O. Tal, S. Wohlthat, F. Pauly, M. Krieger *et al.*, Highly conductive molecular junctions based on direct binding of benzene to platinum electrodes. *Phys. Rev. Lett.* **101**, 046801 (2008).
22. S. Kaneko, T. Nakazumi, M. Kiguchi, Fabrication of a well-defined single benzene molecule junction using Ag electrodes. *J. Phys. Chem. Lett.* **1**, 3520-3523 (2010).
23. M. Kiguchi, Electrical conductance of single C_{60} and benzene molecules bridging between Pt electrode. *Appl. Phys. Lett.* **95**, 073301 (2009).
24. M. Kiguchi, K. Murakoshi, Conductance of single C_{60} molecule bridging metal electrodes. *J. Phys. Chem. C* **112**, 8140-8143 (2008).
25. S. Kaneko, L. Wang, G. F. Luo, J. Lu, S. Nagase *et al.*, Electron transport through single endohedral Ce@C_{82} metallofullerenes. *Phys. Rev. B* **86**, 155406 (2012).
26. T. Nakazumi, S. Kaneko, R. Matsushita, M. Kiguchi, Electric conductance of single ethylene and acetylene molecules bridging between Pt electrodes. *J. Phys. Chem. C* **116**, 18250-18255 (2012).
27. C. A. Martin, D. Ding, J. K. Sorensen, T. Bjornholm, J. M. van Ruitenbeek *et al.*, Fullerene-based anchoring groups for molecular electronics. *J. Am. Chem. Soc.* **130**, 13198-13199 (2008).

28. Z. L. Cheng, R. Skouta, H. Vazquez, J. R. Widawsky, S. Schneebeli *et al.*, In situ formation of highly conducting covalent Au-C contacts for single-molecule junctions. *Nat. Nanotechnol.* **6**, 353-357 (2011).
29. M. Kiguchi, T. Takahashi, Y. Takahashi, Y. Yamauchi, T. Murase *et al.*, Electron transport through single molecules comprising aromatic stacks enclosed in self-assembled cages. *Angew. Chem. Int. Ed.* **50**, 5707-5710 (2011).
30. J. C. Cuevas, E. Scheer, *Molecular Electronics: An Introduction to Theory and Experiment* World Scientific Series in Nanotechnology and Nanoscience (World Scientific Publishing Co. Pte. Ltd., Singapore, 2010).
31. R. H. M. Smit, Y. Noat, C. Untiedt, N. D. Lang, M. C. van Hemert *et al.*, Measurement of the conductance of a hydrogen molecule. *Nature* **419**, 906-909 (2002).
32. M. Kiguchi, T. Nakazumi, K. Hashimoto, K. Murakoshi, Atomic motion in H_2 and D_2 single-molecule junctions induced by phonon excitation. *Phys. Rev. B* **81**, 045420 (2010).
33. M. Kumar, R. Avriller, A. L. Yeyati, J. M. van Ruitenbeek, Detection of vibration-mode scattering in electronic shot noise. *Phys. Rev. Lett.* **108**, 146602 (2012).
34. C. Untiedt, G. R. Bollinger, S. Vieira, N. Agrait, Quantum interference in atomic-sized point contacts. *Phys. Rev. B* **62**, 9962-9965 (2000).
35. B. Ludoph, M. H. Devoret, D. Esteve, C. Urbina, J. M. van Ruitenbeek, Evidence for saturation of channel transmission from conductance fluctuations in atomic-size point contacts. *Phys. Rev. Lett.* **82**, 1530-1533 (1999).
36. N. Agrait, A. L. Yeyati, J. M. van Ruitenbeek, Quantum properties of atomic-sized conductors. *Phys. Rep.* **377**, 81-279 (2003).
37. W. Y. Wang, T. Lee, I. Kretzschmar, M. A. Reed, Inelastic electron tunneling spectroscopy of an alkanedithiol self-assembled monolayer. *Nano Lett.* **4**, 643-646 (2004).
38. A. V. Khotkevich, Modern state of point contact spectroscopy of electron-phonon interaction in transition metals. *Physica B* **218**, 31-34 (1996).
39. M. Paulsson, T. Frederiksen, H. Ueba, N. Lorente, M. Brandbyge, Unified description of inelastic propensity rules for electron transport through nanoscale junctions. *Phys. Rev. Lett.* **100**, 226604 (2008).
40. A. L. Johnson, E. L. Muetterties, J. Stohr, F. Sette, Chemisorption geometry of pyridine on Pt(111) by NEXAFS. *J. Phys. Chem.* **89**, 4071-4075 (1985).
41. J. A. Horsley, J. Stohr, A. P. Hitchcock, D. C. Newbury, A. L. Johnson *et al.*, Resonances in the K-Shell excitation-spectra of benzene and pyridine - gas-phase, solid, and chemisorbed states. *J. Chem. Phys.* **83**, 6099-6107 (1985).

42. J. M. Soler, E. Artacho, J. D. Gale, A. Garcia, J. Junquera *et al.*, The SIESTA method for ab initio order-N materials simulation. *J Phys-Condens Mat* **14**, 2745-2779 (2002).
43. E. Artacho, E. Anglada, O. Dieguez, J. D. Gale, A. Garcia *et al.*, The SIESTA method; developments and applicability. *J Phys-Condens Mat* **20**, 064208, (2008).
44. M. Brandbyge, J. L. Mozos, P. Ordejon, J. Taylor, K. Stokbro, Density-functional method for nonequilibrium electron transport. *Phys. Rev. B* **65**, 165401 (2002).
45. J. P. Perdew, K. Burke, M. Ernzerhof, Generalized gradient approximation made simple. *Phys. Rev. Lett.* **77**, 3865-3868 (1996).
46. C. Toher, A. Filippetti, S. Sanvito, K. Burke, Self-interaction errors in density-functional calculations of electronic transport. *Phys. Rev. Lett.* **95**, 146402 (2005).
47. C. Toher, S. Sanvito, Effects of self-interaction corrections on the transport properties of phenyl-based molecular junctions. *Phys. Rev. B* **77**, 155402 (2008).
48. M. Paulsson, M. Brandbyge, Transmission eigenchannels from nonequilibrium Green's functions. *Phys. Rev. B* **76**, 115117 (2007).
49. D. Djukic, J. Van Ruitenbeek, Shot noise measurements on a single molecule. *Nano Lett.* **6**, 789-793 (2006).
50. E. Scheer, P. Joyez, D. Esteve, C. Urbina, M. H. Devoret, Conduction channel transmissions of atomic-size aluminum contacts. *Phys. Rev. Lett.* **78**, 3535-3538 (1997).

8 General conclusions

In this thesis, I addressed the fabrication of single molecular junctions showing high and well-defined conductance values, and dealt with problems regarding the uncertainty and uncontrollable property of the interface between the molecule and metal in single molecular junctions. Electric conductance measurement systems that are based on the mechanically controllable break junction (MCBJ) technique enabled us to investigate the electron transport property of single molecular junctions. The fabricated single molecular junctions were characterized not only in terms of their conductance, but also in terms of their *I-V* response or *dI/dV* spectrum. These measurements enabled us to discuss the energy alignment or the interface structure of the single molecular junctions.

In this thesis, I focused on a single molecular junction with a π-conjugated molecule without anchoring groups such as thiol or amine. In chapter 4, a benzene single molecular junction was fabricated using Ag electrodes considering the strength of the interaction between the metal and molecule. The proper interaction between benzene and Ag enables us to fabricate the benzene molecular junction with a well-defined conductance value of 0.24 G_0. The conductance value improved by a factor of ten compared with that of a typical single molecular junction with anchoring groups. The interface structure of the single molecular junction was determined by the *dI/dV* spectrum, which detected the vibration mode between benzene and Ag. The conductance measurements, together with the *dI/dV* spectrum, revealed that an Ag/benzene/Ag single molecular junction was formed only with the most stable configuration. In this configuration, the benzene molecule binds to Ag electrodes with its *p* orbital parallel to the bonding direction. The proper interaction between the molecule and electrodes enabled us to form a single molecular junction with a well-defined conductance value. Then, in chapter5, I focused on the fullerene molecule in order to fabricate a single molecular junction that shows a high and well-defined conductance value. The spherical shape of the Ce@C_{82} molecule successfully formed a single molecular junction with a well-defined conductance value using Ag electrodes. The *I-V* characteristics revealed the presence of a narrow energy gap between the Fermi level of Ag and the fullerene molecular orbital, which results in a high conductivity of the fullerene molecule. The enclosed Ce atom reduced the conductance value by localizing the orbital of the fullerene cage compared with C_{60}. It should be noted that Au did not form single molecular junctions for both benzene and Ce@C_{82}. This was explained by the formation of the metal linear atomic chain of the Au. The linear atomic chain formed a larger nanogap, which prevented the formation of the single molecular junction. These studies with different electrodes

have revealed not only the strength of the interaction, but also that the stability of the low-coordination states of metal plays an important role in the formation of single molecular junctions.

After fabricating a single molecular junction with a high and well-defined conductance value by properly designing the interface structure, I focused on controlling the electrical conductivity of the single molecular junction. In order to control the interface structure without reducing the conductivity, the use of a nitrogen atom in the π-conjugated system was considered. First, in chapter 6, the nitrogen molecule was investigated as the smallest π-conjugated system enclosed the nitrogen atom using Cu and Pt electrodes. The single N_2 molecular junction was formed with Pt electrodes having a conductance value of 1 G_0, which is comparable to the conductance of metal atomic contacts. The high and well-defined conductance value of the N_2 molecular junction with Pt electrodes showed the possibility that the nitrogen atom works as an anchoring point in highly conductive π-conjugated molecules with Pt electrodes. On the other hand, the single molecular junction was not formed with Cu electrodes. It should be noted that a linear Cu atomic chain was formed with a few atomic lengths, although Cu does not form a linear atomic chain without molecules. From these results, I observe that N_2, which is inert in isolated states, showed high conductivity and helped the formation of the linear atomic chain.

In chapter 7, I demonstrated the fabrication and control of bi-stable states for a Pt/pyrazine/Pt molecular junction. First, the conductance was investigated during the breaking process. Statistical analysis showed that the Pt/pyrazine/Pt single molecular junction had two conductance states: 1.0 G_0 and 0.3 G_0. Then, the *dI/dV* spectrum detected vibration energies of 30 meV and 60 meV for each conductance state. The *dI/dV* spectrum combined with the theoretical calculation revealed the configurations of the two conductance states. Finally, the two conductance states were switched by changing the distance between the two electrodes. The two conductance states were successfully switched in the high-conductance region by an external force. This result is unique for nano-sized systems because in bulk states, it is difficult to change the electrical property with a mechanical force.

The findings in this thesis revealed that the electron transport property of a single molecular junction can be controlled by designing a proper metal molecule interface. This finding pertaining to the controllable electric transport in a highly conductive single molecular junction results in the single molecular junction being the next stage in the development of nano-sized electronic components. Moreover, because the molecular orbital in highly conductive single molecular junction is significantly hybridized with a metal orbital, it is considered that such a

single molecular junction is a unique nano-sized system. We may activate the inert molecule by sandwiching the molecule between a metal nanogap such as the $Pt/N_2/Pt$ junction, and induce a novel reaction by applying proper stimuli such as light, electric pulses, and mechanical force for a single molecular junction. In particular, because electromagnetic waves can be significantly magnified at the nanogap, it is expected that a novel optical reaction will be observed in a single molecular junction. In conclusion, the highly conductive single molecular junctions studied in this thesis are expected to open the door to a new science field related to novel nano-sized metal- molecule systems.

Acknowledgements

This thesis would not have been possible without the involvement of people who I met during the PhD course. The many interactions provide me with valuable knowledge, and motivated me towards carrying out further investigations. I would therefore like to express my sincere gratitude to everyone here.

I am grateful for the opportunity to have pursued the PhD course under the supervision of Prof. Manabu Kiguchi (Tokyo Institute of Technology), who introduced me to the science world with great passion. His valuable advice and encouragement were a tremendous support. I would therefore like to express my deep appreciation to Prof. Kiguchi.

I would also like to express my gratitude to all of the collaborators in this investigation. They are Prof. Takeshi Akasaka (University of Tsukuba), Dr. Michio Yamada (Tokyo Gakugei University), and Dr. Zdenek Slanina (University of Tsukuba), who provided me with the wonderful molecule Ce@C_{82}. Prof. Shigeru Nagase (Institute for Molecular Science), Dr. Guangfu Luo (University of Wisconsin-Madison), Mr. Lu Wang, and Dr. Jing Lu (Peking University) helped me with the theoretical calculations regarding the electron transport of Ce@C_{82}. Prof. Jianwei Zhao, Mr. Jinjiang Zhang, and Mr. Xiongbo Yang gave me the theoretical support related to the formation and electron transport of the nitrogen single molecular junction. Prof. Gian Paolo Brivio (University of Milano-Bicocca) and Dr. Carlo Motta (Trinity College Dublin) provided me with theoretical insight about the electron transport of the pyrazine molecule.

Next, I appreciate the input by Prof. Toshiaki Enoki (Tokyo Institute of Technology), who shared several suggestions and discussions about fundamental physics. I also thank Dr. Shintaro Fujii (Tokyo Institute of Technology) for the discussions about single molecular junctions. Dr. Kazuhito Tsukagoshi (National Institute for Materials Science, Japan) encouraged me and shared a lot of knowledge about nanotechnology techniques.

Special thanks also to Prof. Jan van Ruitenbeek (Leiden University), Dr. Manohar Kumer (Aalto University), Dr. Tadashi Shiota, and members of the AMC group at Leiden University. My experience at Leiden University and the continuous fruitful discussion with them gave me a lot of valuable information about atomic-sized conductors, and they were a great encouragement.

The NEXAFS measurements presented in chapter 7 were performed at the Photon Factory in the Institute of Materials Structure Science High Energy Accelerator Research Organization. I appreciate the assistance by Prof. Amemiya and the faculty members in the Photon factory for their kind help.

Heartfelt thanks to the members and alumni of the Kiguchi-Nishino Laboratory at the Tokyo Institute of Technology, especially Dr. Tomoaki Nishino, Dr. Santiago Marques-Gonzalez, Mr. Rjuuji Matsushita, Mr. Ryoji Takahashi, Ms. Yu Li, Mr. Sho Suzuki, Ms. Akira Aiba, Dr. Tomoka Nakazumi, Mr. Daigo Murai, Mr. Yuuga Nakamura, Chenyang Liu, and Ms. Tomoko Kuroiwa for sharing their experiences with different scientific activities.

Finally, I would like to express my deep appreciation to my family for their unceasing support.

Achievements

List of Publications

1. **Satoshi Kaneko**, Daigo Murai, Santiago Marques-Gonzalez, Hisao Nakamura, Yuki Komoto, Shintaro Fujii, Tomoaki Nishino, Katsuyoshi Ikeda, Kazuhito Tsukagoshi, Managu Kiguchi, "Site selection in single-molecule junction for highly reproducible molecular electronics" *Journal of the American Chemical Society* in press.
2. Yu Li, Firuz Demir, **Satoshi Kaneko**, Shintaro Fujii, Tomoaki Nishino, Alireza Saffarzadeh, George Kirczenow, Manabu Kiguchi, "Electrical conductance and structure of copper atomic junctions in the presence of water molecules" *Physical Chemistry Chemical Physics* **17**, 32436-32442 (2015).
3. **Satoshi Kaneko**, Yuuga Nakamura, Ryuuji Matsushita, Santiago Marques-Gonzalez, Manabu Kiguchi, "Simultaneous measurement of electrical conductance and thermopower of single benzeneditiol molecular junctions" *Applied Physics Express* **8**, 065201 (2015).
4. **Satoshi Kaneko**, Yuuga Nakamura, Jingiang Zhang, Xiongbo Yang, Jianwei Zhao, Manabu Kiguchi, "Formation of single Cu atomic chain in nitrogen atmosphere" *The Journal of Physical Chemistry C* **119**, 862–866 (2015).
5. Yu Li, **Satoshi Kaneko**, Shintaro Fujii, Manabu Kiguchi, "Symmetry of single hydrogen molecular junction with Au, Ag and Cu Electrodes" *The Journal of Physical Chemistry C* **119**, 19452-19457 (2015).
6. Ryoji Takahashi, **Satoshi Kaneko**, Shintaro Fujii, Manabu Kiguchi, "Photochromic reaction of the diarylethene derivative on Au nanoparticles" *Advances in Natural Sciences: Nanoscience and Nanotechnology* **6**, 015006 (2015).
7. Ryuuji Matsushita, **Satoshi Kaneko**, Shintaro Fujii, Hisao Nakamura, Manabu Kiguchi, "Temperature dependence of the thermopower and its variation of the Au Atomic contact" *Nanotechnology* **26**, 045709 (2015).
8. Ryoji Takahashi, **Satoshi Kaneko**, Shintaro Fujii, Manabu Kiguchi, "Extension of photopolymerization region from the nanoscale to the macroscopic scale using a chemically amplified photoresist" *Bulletin of the Chemical Society of Japan* **88**, 277–282 (2015).
9. Chenyang Liu, **Satoshi Kaneko**, Yuki Komoto, Shintaro Fujii, Manabu Kiguchi, "Highly conductive single naphthalene and anthracene molecular junction with well-defined conductance" *Applied Physics Letters* **106**, 103103 (2015).

10. Shintaro Fujii, **Satoshi Kaneko**, Liu Chenyang, Manabu Kiguchi, “Single naphthalene and anthracene molecular junctions using Ag and Cu electrodes in ultra high vacuum” *Applied Surface Science* **354**, 362-366 (2015).
11. **Satoshi Kaneko**, Manabu Kiguchi, “Investigation on the pyrazine molecular junction studied by conductance measurement and near edge X-ray absorption fine structure” *Fullerenes, Nanotubes and Carbon Nanostructures* **22**, 166-172 (2014).
12. Chenyang Liu, **Satoshi Kaneko**, Yuki Komoto, Shintaro Fujii, Manabu Kiguchi, “Fabrication of single linear aromatic molecule junction with high formation probability” *Applied Physics Express* **7**, 105201 (2014).
13. Tomoka Nakazumi, **Satoshi Kaneko**, Manabu Kiguchi, “Electron transport properties of Au, Ag, and Cu atomic contacts in a hydrogen environment” *The Journal of Physical Chemistry C* **118**, 7489-7493 (2014).
14. Si-Jia Hao, Vazhappilly Lona Joseph Joly, **Satoshi Kaneko**, Jun-ichi Takashiro, Kazuyuki Takai, Hitoshi Hayashi, Toshiaki Enoki, Manabu Kiguchi, “Magnetic edge-states in nanographene, HNO_3-doped nanographene and its residue compounds of nanographene-based nanoporous carbon” *Physical Chemistry Chemical Physics* **16**, 6273-6282 (2014).
15. Jun-ichi Takashiro, Yuki Kudo, **Satoshi Kaneko**, Kazuyuki Takai, Takafumi Ishii, Takashi Kyotani, Toshiaki Enoki, Manabu Kiguchi, “Heat treatment effect on the electronic and magnetic structures of nanographene sheets investigated through electron spectroscopy and conductance measurements” *Physical Chemistry Chemical Physics* **16**, 7280-7289 (2014).
16. **Satoshi Kaneko**, Carlo Motta, Gian Paolo Brivio, Manabu Kiguchi, “Mechanically controllable bi-stable states in highly conductive single pyrazine molecular junction” *Nanotechnology* **24**, 315201 (2013).
17. **Satoshi Kaneko**, Jinjiang Zhang, Jianwei Zhao, Manabu Kiguchi, “Electronic conductance of platinum atomic contact in a nitrogen atmosphere” *The Journal of Physical Chemistry C* **117**, 9903-9907 (2013).
18. Manabu Kiguchi, **Satoshi Kaneko**, “Single molecule bridging between metal electrodes” *Physical Chemistry Chemical Physics* **15**, 2253-2267 (2013).
19. 木口学, 松下龍二, **金子哲**, 中住友香, “単一分子接合の作製およびその物性評価” *日本画像学会誌* **52**, 26-33 (2013).
20. **Satoshi Kaneko**, Lu Wang, G.uangful Luo, Jing Lu, Shigeru Nagase, Satoru Sato, Michio Yamada, Zdenek Slanina, Takechi Akasaka, Manabu Kiguchi, “Electron transport through

single endohedral Ce@C_{82} metallofullerenes" *Physical Review B* **86**, 155406 (2012).

21. Tomoka Nakazumi, **Satoshi Kaneko**, Ryuuji Matsushita, Manabu Kiguchi, "Electric conductance of single ethylene and acetylene molecules bridging between Pt electrodes" *The Journal of Physical Chemistry C* **116**, 18250-0855 (2012).
22. Manabu Kiguchi, **Satoshi Kaneko**, "Electron transport through single π-conjugated molecules bridging between metal electrodes" *ChemPhysChem* **13**, 1116 -1126 (2012).
23. Ryuuji Matsushita, **Satoshi Kaneko**, Tomoka Nakazumi, Manabu Kiguchi, "Effect of metal-molecule contact on electron-vibration interaction in single hydrogen molecule junction" *Physical Review B* **84**, 245412 (2011).
24. 木口学，**金子哲**，中住友香，Oren Tal, Jan van Ruitenbeek, Juan Carlos Cuevas, "金属電極に架橋したベンゼン，C_{60} 単分子接合の構造および伝導特性の解明" *表面科学* **32**, 331-336 (2011).
25. **Satoshi Kaneko**, Tomoka Nakazumi, Manabu Kiguchi, "Fabrication of the well-defined single benzene molecule junction using Ag electrodes" *The Journal of Physical Chemistry Letters* **1**, 3520–3523 (2010).

International conference

1. **Satoshi Kaneko**, Manabu Kiguchi, Yuki Komoto, Daigo Murai, Kazuhito Tsukagoshi "Electron transport and surface enhanced Raman scattering at structurally well-defined single 1,4-benzenedithiol" 31st European Conference on Surface Science, Barcelona, oral, August, 2015.
2. **Satoshi Kaneko**, Manabu Kiguchi, Satoru Sato, Michio. Yamada, N. Mizorogi, Takeshi Akasaka, Wang Lu, Shigeru Nagase, "Electrical conductance of single Ce@C_{82} molecule bridging between metal electrodes" International School and Symposium on Molecular Materials, Tokyo, poster, November, 2013, **poster award.**
3. **Satoshi Kaneko**, Manabu Kiguchi, Carlo Motta "Highly conductive pyrazine molecular junction showing bi-stable states" International School and Symposium on Molecular Materials and Devices, Durham, poster, September, 2012. **poster award.**
4. **Satoshi Kaneko**, Manabu Kiguchi, Tomoka Nakazumi, "Fabrication of the well defined single benzene molecule junction using Ag electrodes" European Conference on Surface Science, Wrocłow, August, 2011.

5. **Satoshi Kaneko**, Manabu Kiguchi, Satoru Sato, Michio Yamada, Naomi Mizorogi, Takeshi Akasaka, Wang Lu, Shigeru Nagase "Electrical conductance of single Ce@C_{82} molecule bridging between metal electrodes " International Conference on Core Research and Engineering Science of Advanced Materials, Osaka, June, 2010.

Domestic Conference

1. 金子哲, 村井大午, 小本祐貴, 塚越一仁, 木口学 "表面増強ラマンスペクトル・電流-電圧特性同時計測による単分子接合の原子・電子構造解析" 2015 年真空・表面科学合同講演会, つくば, 2015 年 12 月.
2. 金子哲, 鈴木翔, 木口学, "金ナノ構造体を用いたベンゼン誘導体の表面増強ラマン散乱の界面構造依存性" 分子科学会, 東京, 2015 年 9 月.
3. 金子哲, 村井大午, 小本祐貴, 塚越一仁, 木口学 "表面増強ラマン分光法を活用した 1,4-ベンゼンジチオール単分子接合の電子輸送特性の解明" 応用物理学会, 神奈川, 2015 年 3 月.
4. 金子哲, 中村優雅, Jinjiang Zhang, Jianwei Zhao, 木口学 "窒素分子を利用した銅単原子ワイヤーの安定形成" 徳島, 日本物理学会, 2013 年 9 月.
5. 金子哲, 木口学, Lu Wang, Guangfu Luo, 永瀬茂, 佐藤悟, 山田道夫, Zdenek, Slanina, Jing Lu, 赤阪健 "金属内包フラーレン Ce@C82 単一分子の電子輸送特性" ナノスケール分子デバイスセミナー, 東京, 2013 年 3 月.
6. 金子哲, 木口学, Carlo Motta "ピラジンを用いた高機能単分子スイッチの開発" CSJ 化学フェスタ, 東京, 2012 年 10 月.
7. 金子哲, Carlo Motta, 木口学 "Pt 電極間に架橋されたピラジン単一分子接合の研究" 日本物理学会, 横浜, 2012 年 9 月.
8. 金子哲, 木口 学, "Pt 電極間に架橋された窒素単分子接合の研究" 日本物理学会, 2012 年, 3 月.
9. 金子哲 "窒素を含んだ単一分子の電子輸送特性の解明" ナノスケール分子デバイスセミナー, 東京, 2012 年 3 月.

10. 金子哲，中住友香，木口学“規定された電気伝導度を示すπ共役単分子接合の探索” 日本物理学会， 秋季大会，富山，2011 年 9 月.

11. 金子哲，木口学，佐藤悟，山田道夫，溝呂木直美，赤阪健，永瀬茂， “金属電間に架橋した Ce@C82 単分子の電気伝導度特性”, 日本物理学会第 65 回年次大会, 岡山, 2010 年 3 月.